Turbulence and warm rain formation in clouds

Szymon P. Malinowski

University of Warsaw,
Institute of Geophysics

International School
Fluctuations and Turbulence in the Microphysics and Dynamics of Clouds
Porquerolles, Sep. 2-10, 2010

Draft of contents

Clouds and Turbulence – overview.

Cloud topped boundary layer:
- – turbulence in Stratocumulus clouds;
- – turbulence in cumulus convection.

Condensation in convective motions.
- a) a sketch of Koehler's theory;
- b) availability of water substance for process condensation and droplet growth;
- c) collisions and coalescence and a „bottleneck" problem.

Experimental evidence of warm rain formation
- a) drizzle in Stratocumulus;
- b) warm rain in cumulus clouds;
  - similarities and differences.

Cloud-scale and small-scale turbulence

Entrainment and mixing:
- Cumulus
- Stratocumulus
- Mechanisms for entrainment in clouds

Turbulence and cloud microphysics: droplet size distribution
- Condensational growth and turbulence
- Collisions, coalescence and turbulence
  - Droplet relative velocity
  - Droplet clustering (preferential concentration)
  - Preferential sweeping
- The effect of entrainment on the droplet size distribution
  - Homogeneous and inhomogeneous mixing

Clouds and Turbulence – overview.

Cloud topped boundary layer:

– turbulence in Stratocumulus clouds;

– turbulence in cumulus convection.

Condensation in convective motions.

a) a sketch of Koehler's theory;

b) availability of water substance for process condensation and droplet growth;

c) collisions and coalescence and a „bottleneck” problem.

Experimental evidence of warm rain formation

a) drizzle in Stratocumulus;

b) warm rain in cumulus clouds;

- similarities and differences.

What is turbulence?

turbulence —
1. Irregular fluctuations occurring in fluid motions. It is characteristic of turbulence that the fluctuations occur in all three velocity components and are unpredictable in detail; however, statistically distinct properties of the turbulence can be identified and profitably analyzed. Turbulence exhibits a broad range of spatial and temporal scales resulting in efficient mixing of fluid properties.
2. Random and continuously changing air motions that are superposed on the mean motion of the air.

Glossary of Meteorology, American Meteorological Society

turbulence — In fluid mechanics, a flow condition (see turbulent flow) in which local speed and pressure change unpredictably as an average flow is maintained.

atmospheric turbulence — small-scale, irregular air motions characterized by winds that vary in speed and direction. Turbulence is important because it mixes and churns the atmosphere and causes water vapour, smoke, and other substances, as well as energy, to become distributed both vertically and horizontally.

Britannica Online

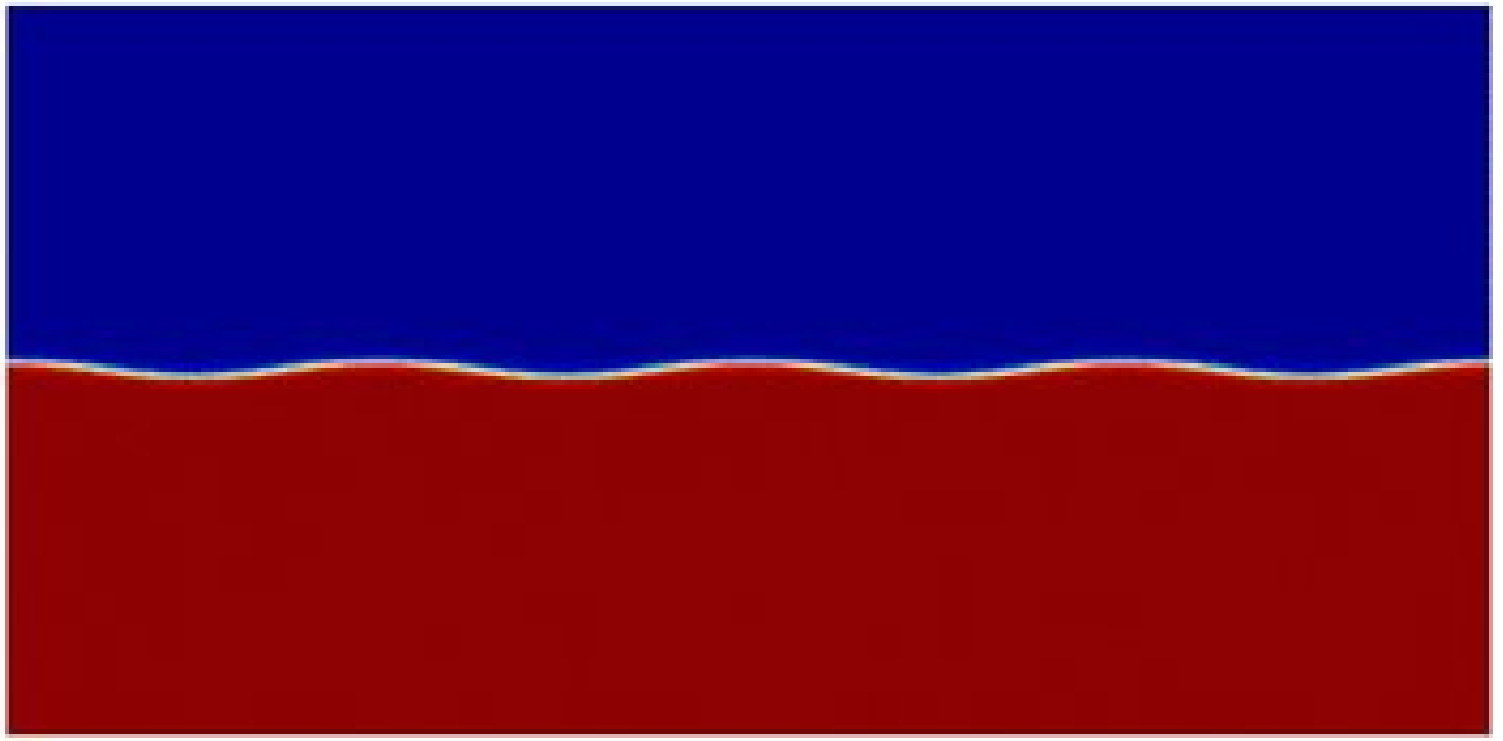

Kelvin-Helmholtz instability with Ri=.038, Re=5000

The **Reynolds number** is the ratio of inertia and friction,

$$Re \equiv \frac{UL}{\nu}$$

Buoyancy and inertia

$$Ri \equiv \frac{\partial b/\partial z}{|\partial \mathbf{u}/\partial z|^2}$$

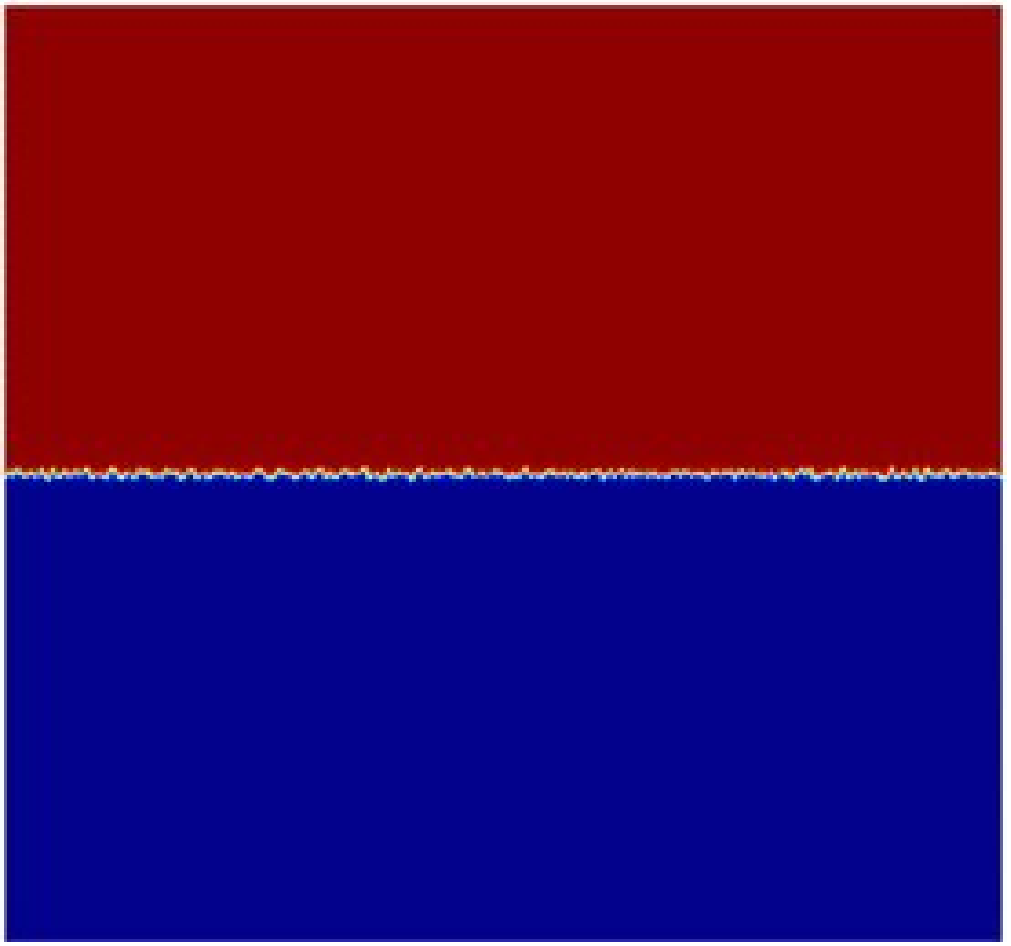

Rayleigh-Taylor instability with Ri=infinity, Ra=6000000, Re=300

Buoyancy and diffusion

$$Ra \equiv \frac{\Delta b L^3}{\kappa \nu}$$

Dominant shear instability with Ri=-0.038, Ra=3400000, Re=3600

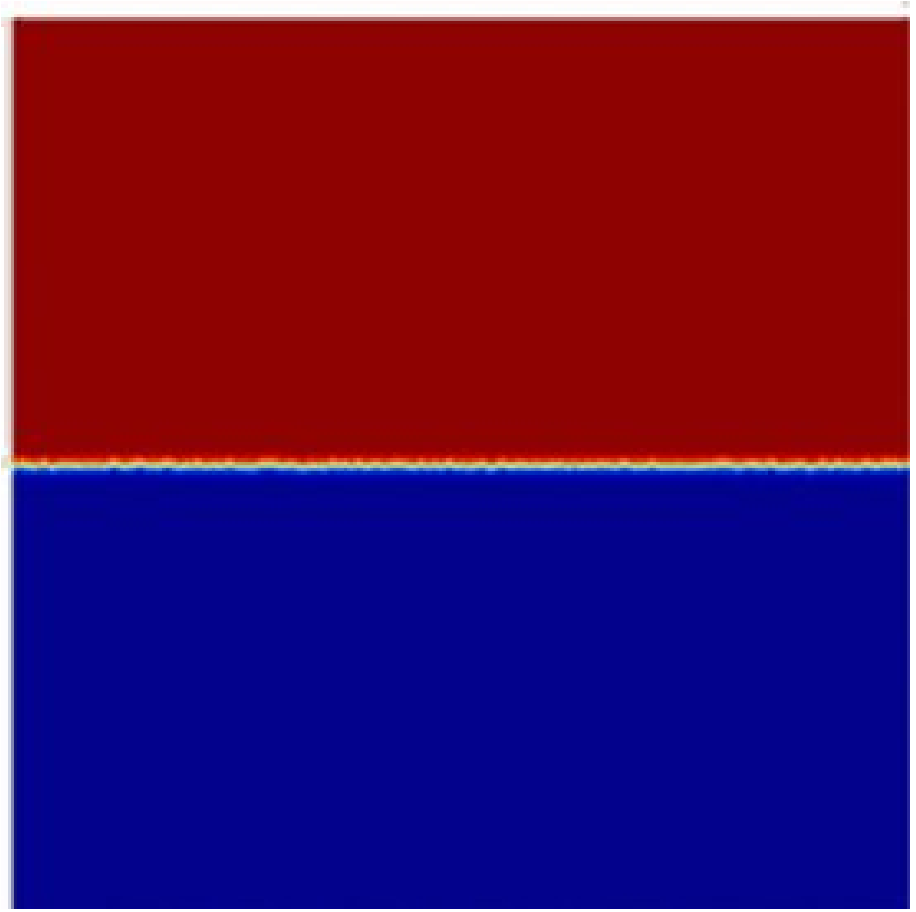

Dominant convective instability with Ri=-1.34, Ra=31000000, Re=1800

What is cloud?

Cloud – A visible aggregate of minute water droplets and/or ice particles in the atmosphere above the earth's surface

Glossary of Meteorology, American Meteorological Society

Cloud – any visible mass of water droplets, or ice crystals, or a mixture of both that is suspended in the air, usually at a considerable height

Britannica Online

What is the typical size of aerosol and cloud particles ?

From a few nanometers: a few molecules condensed

To a few centimeters: hailstones

Measurable parameters from in-situ observations

Particle size…….µm, mm, cm……$1\mu m<D<10cm$

Number Concentration……..cm^{-3}; l^{-1}; m^{-3}…….$1000cm^{-3}<N<1m^{-3}$

Extinction Coefficient…….km^{-1}……$100km^{-1}<\beta<0.01\ km^{-1}$

Water Content…….g/m^3……$10g/m^3<W<0.0001g/m^3$

Cloud formation processes:

Condensation of water vapour into small droplets

adiabatic expansion (e.g. ascending motions);

isobaric cooling (radiative, conductive);

isobaric mixing.

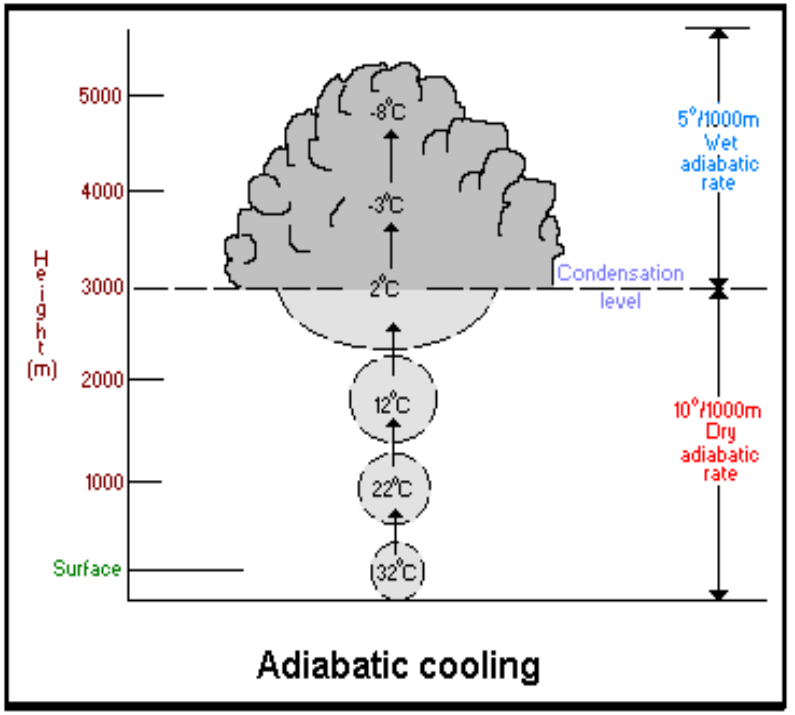

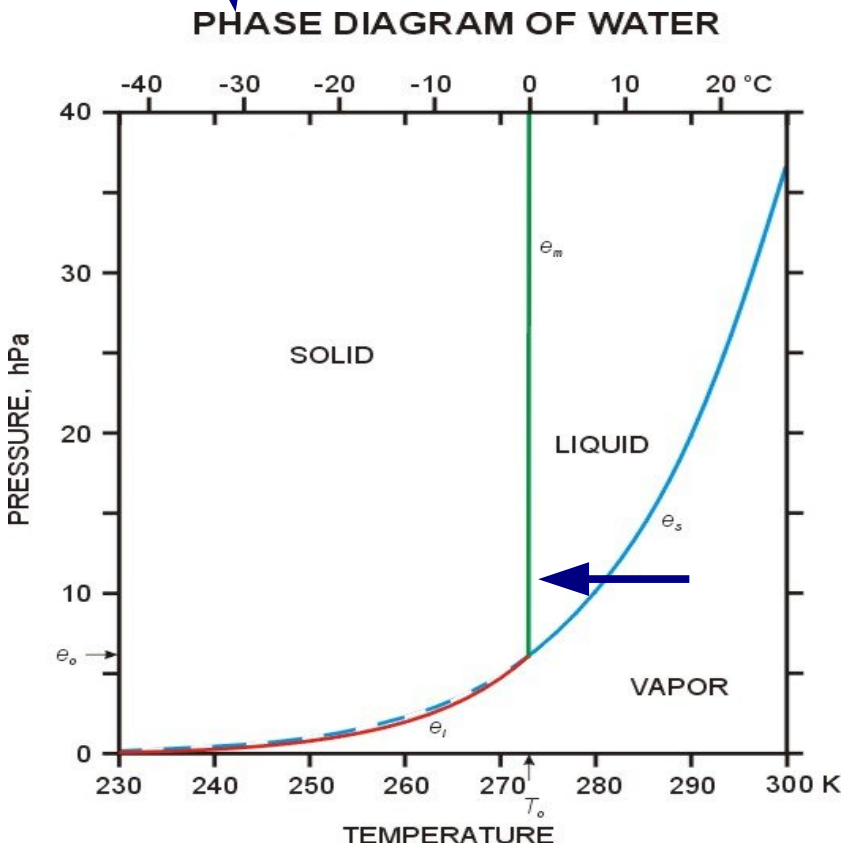

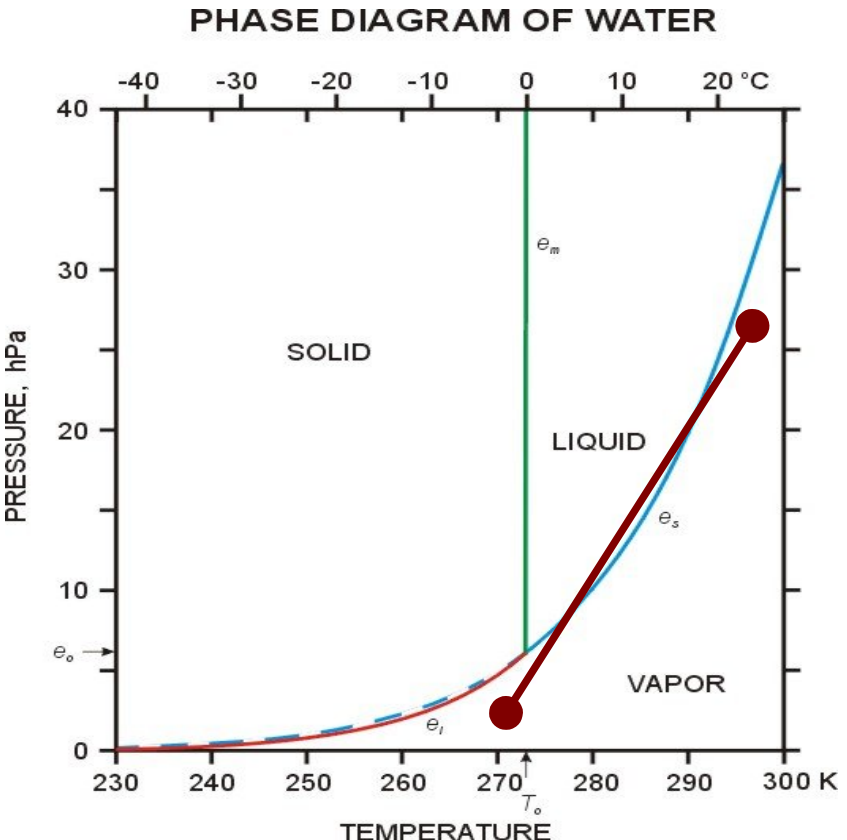

Examples of condensation (formation of clouds) due to adiabatic expansion.

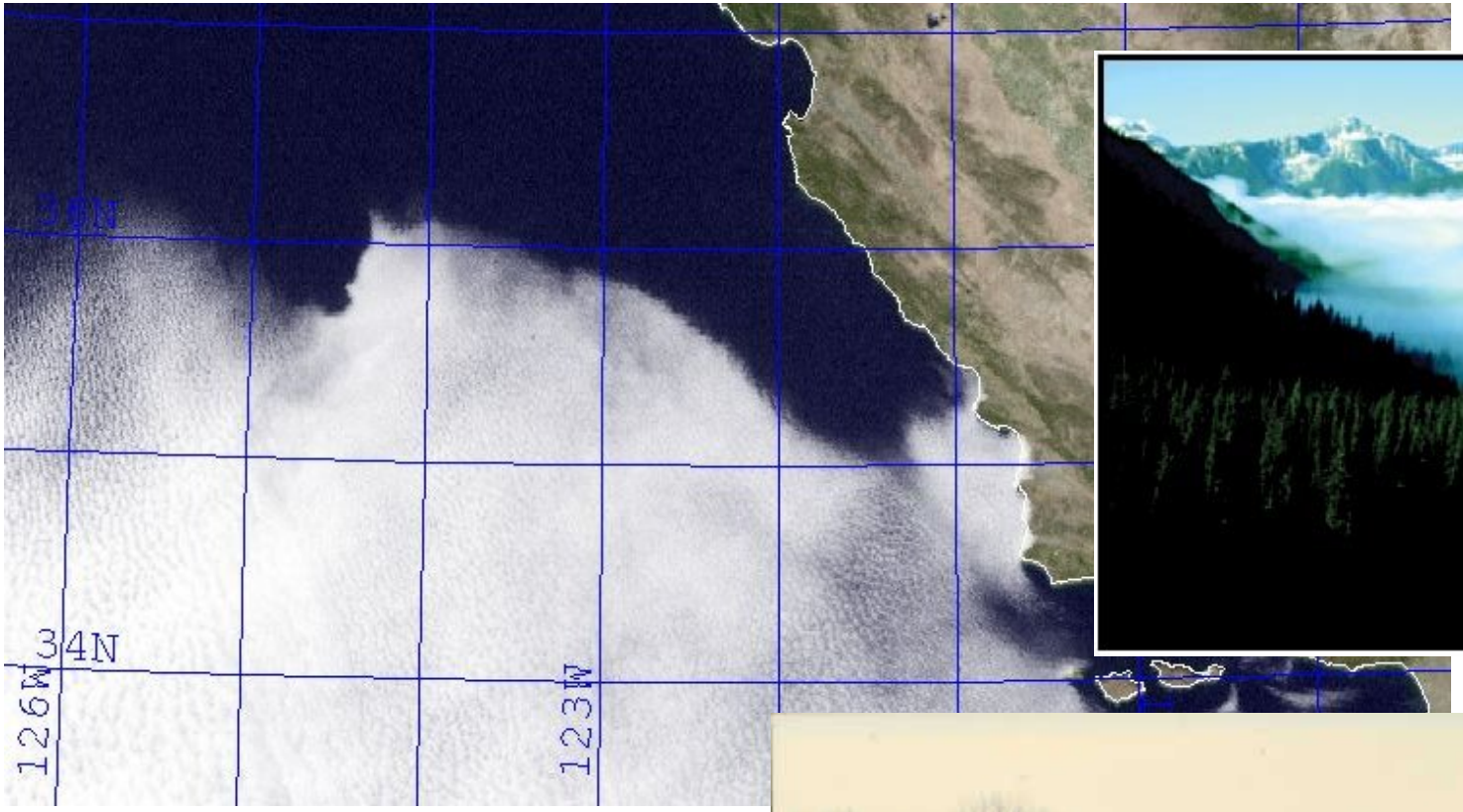

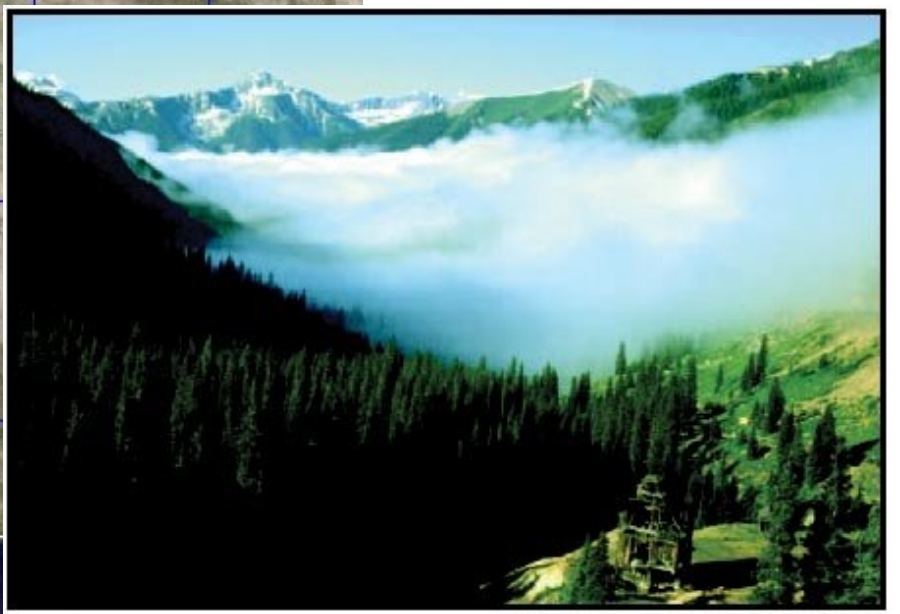

Examples of condensation
(formation of clouds)
due to isobaric cooling.

Examples of condensation (formation of clouds) due to isobaric mixing of two humid unsaturated airmasses.

Clouds and Turbulence – overview.

Cloud topped boundary layer:
– turbulence in Stratocumulus clouds;
– turbulence in cumulus convection.

Condensation in convective motions.
a) a sketch of Koehler's theory;
b) availability of water substance for process condensation and droplet growth;
c) collisions and coalescence and a „bottleneck” problem.

Experimental evidence of warm rain formation
a) drizzle in Stratocumulus;
b) warm rain in cumulus clouds;
- similarities and differences.

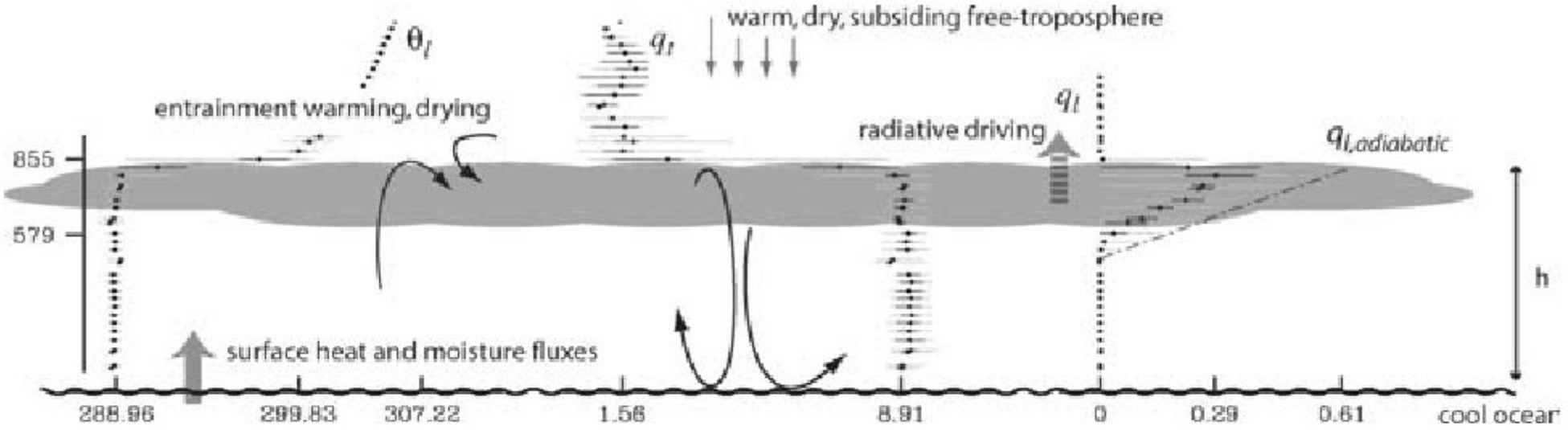

Figure 4 Cartoon of well-mixed, nonprecipitating, stratocumulus layer, overlaid with data from research flight 1 of DYCOMS-II. Plotted are the full range, middle quartile, and mean of θ_l, q_t, and q_l from all the data over the target region binned in 30-m intervals. Heights of cloud base and top are indicated, as are mixed layer values and values just above the top of the boundary layer of various thermodynamic quantities. The adiabatic liquid water content is indicated by the dash-dot line.

Stevens, 2005

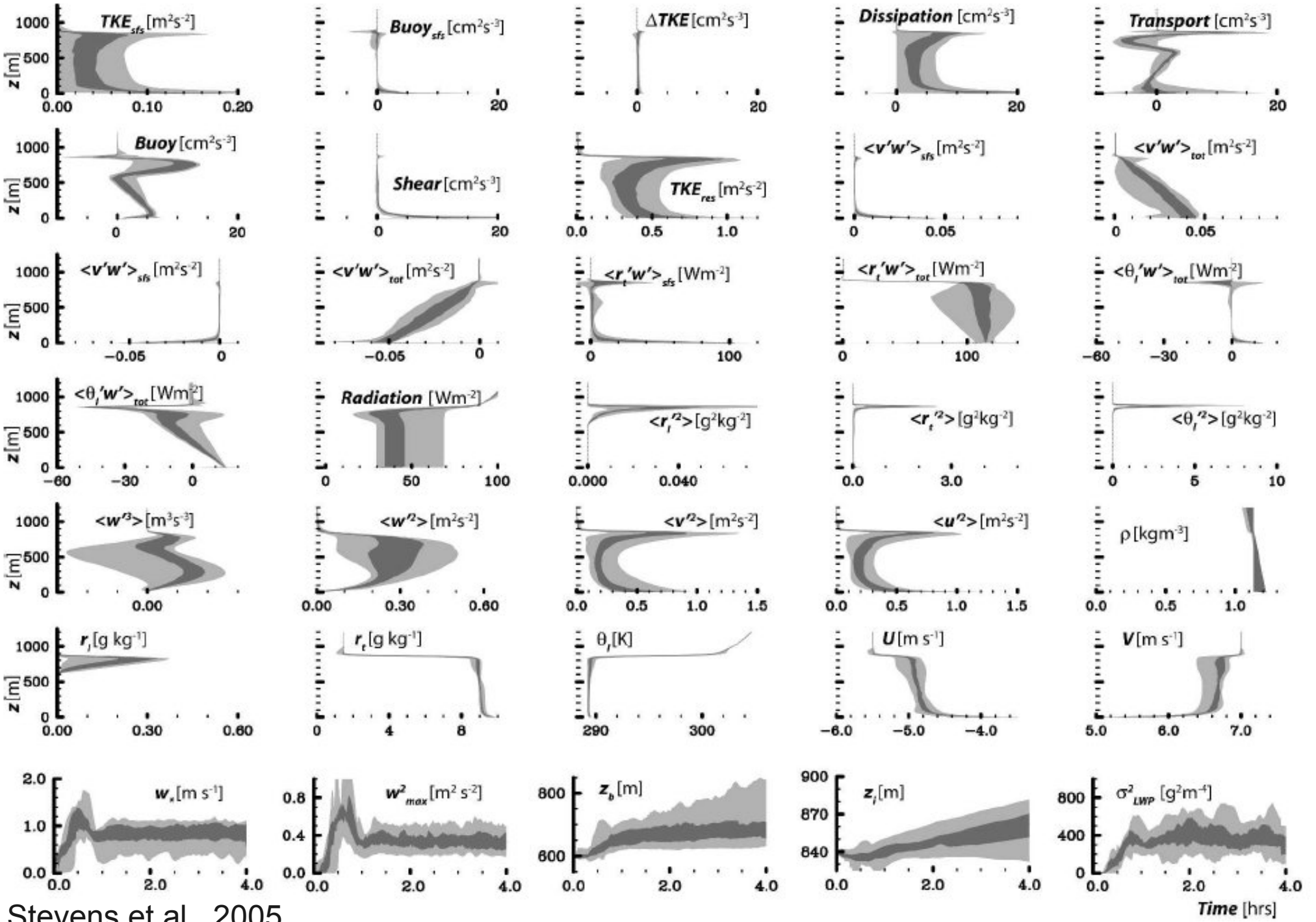

Stevens et al., 2005

FIG. C1. (upper six rows) Thumbnails of profile and (last row) time series statistics for the master ensemble.

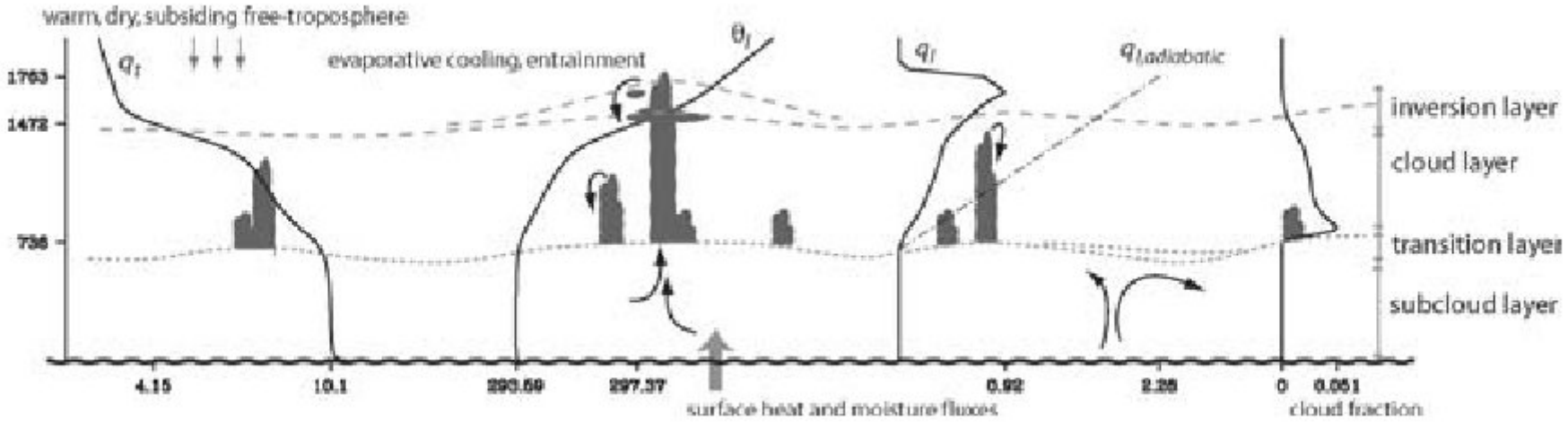

Figure 6 Cartoon of trade-wind boundary layer from large-eddy simulation. Heights of cloud base, level of maximum θ_l gradient (inversion height), and maximum cloud penetration depth are indicated, as are subcloud layer and inversion-level values of thermodynamic quantities. Cloud water contents are averaged over cloudy points only, with adiabatic liquid water contents indicated by the dash-dot line. The far right panel shows cloud fraction, which maximizes near cloud base at just over 5%.

Stevens, 2005

Courtesy B.Stevens

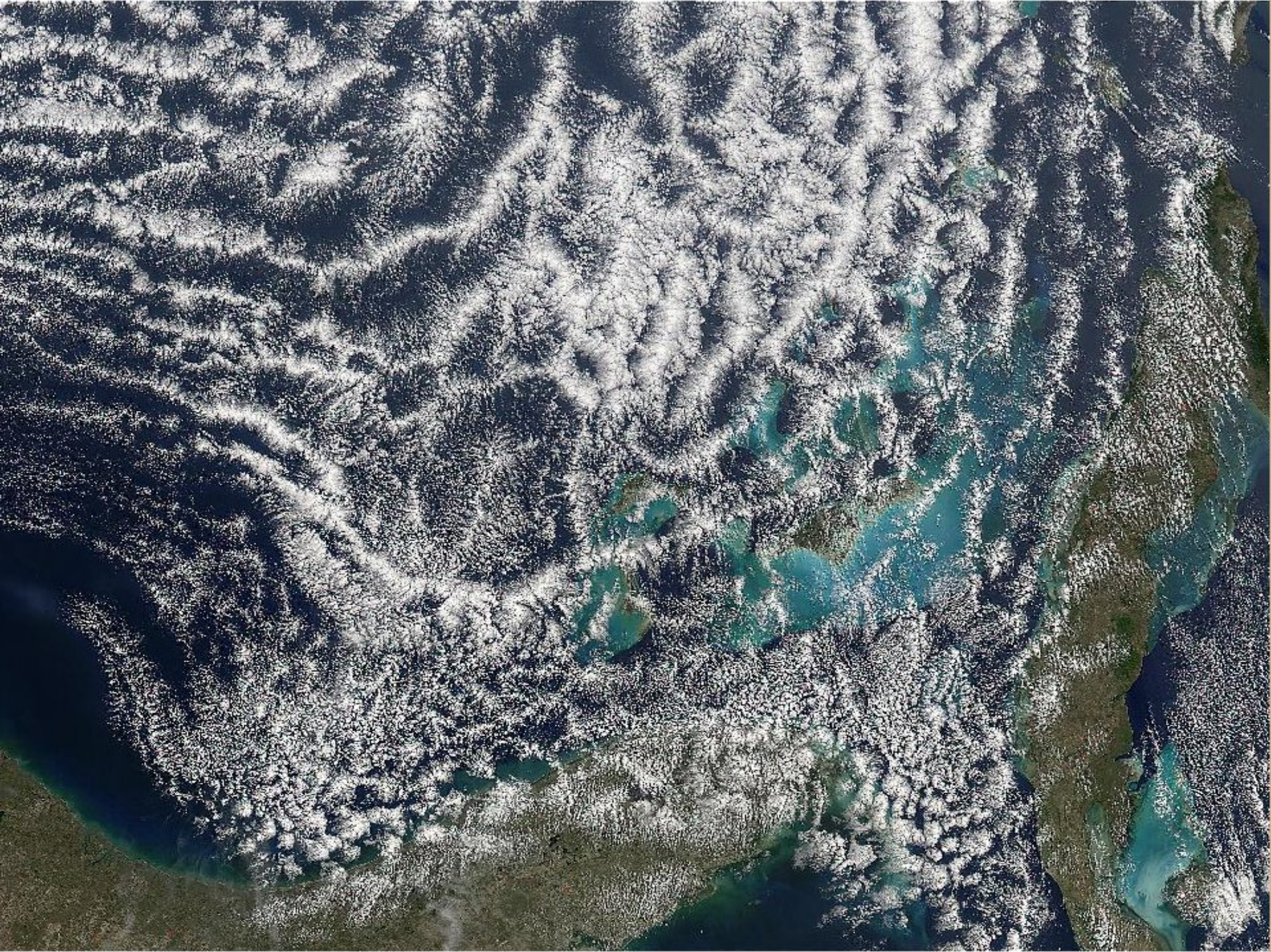

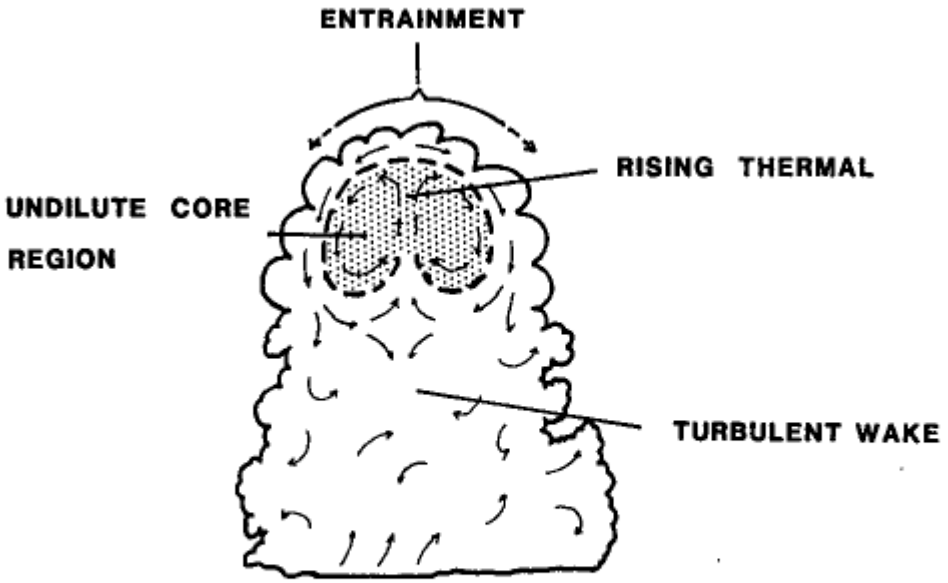

FIG. 14. Schematic model of a cumulus cloud showing a shedding thermal that has ascended from cloud base. Continuous entrainment into the surface of the thermal erodes the core, and the remaining undiluted core region continues its ascent, leaving a turbulent wake of mixed air behind it. See text for further discussion.

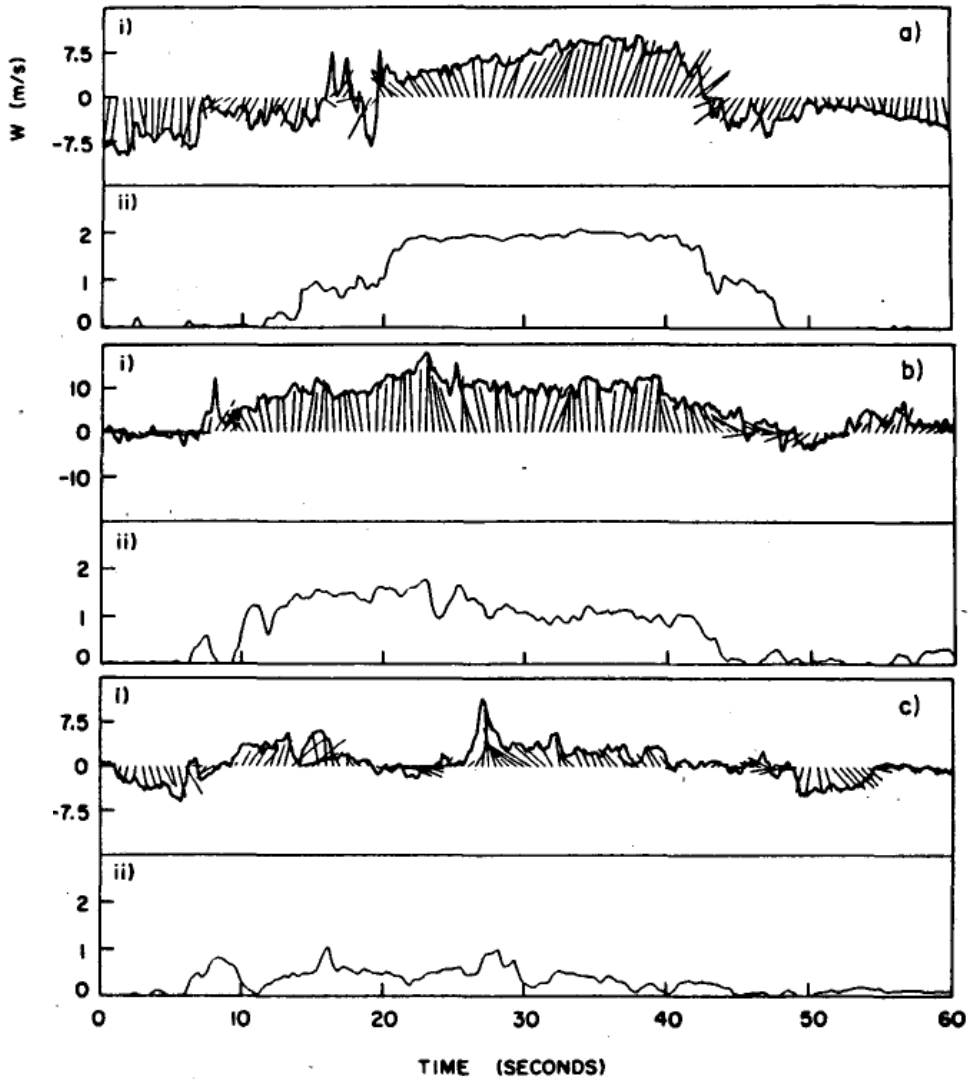

FIG. 17. Wind velocity (i) and liquid water content (ii) for three KA penetrations from 1625 to 1633 MDT in the 19 July 1981 cloud: (a) 472 mb, (b) 514 mb and (c) 527 mb. The wind vectors are formed from the vertical wind and the wind along the flight path and are drawn to scale.

Blyth et al., 1988

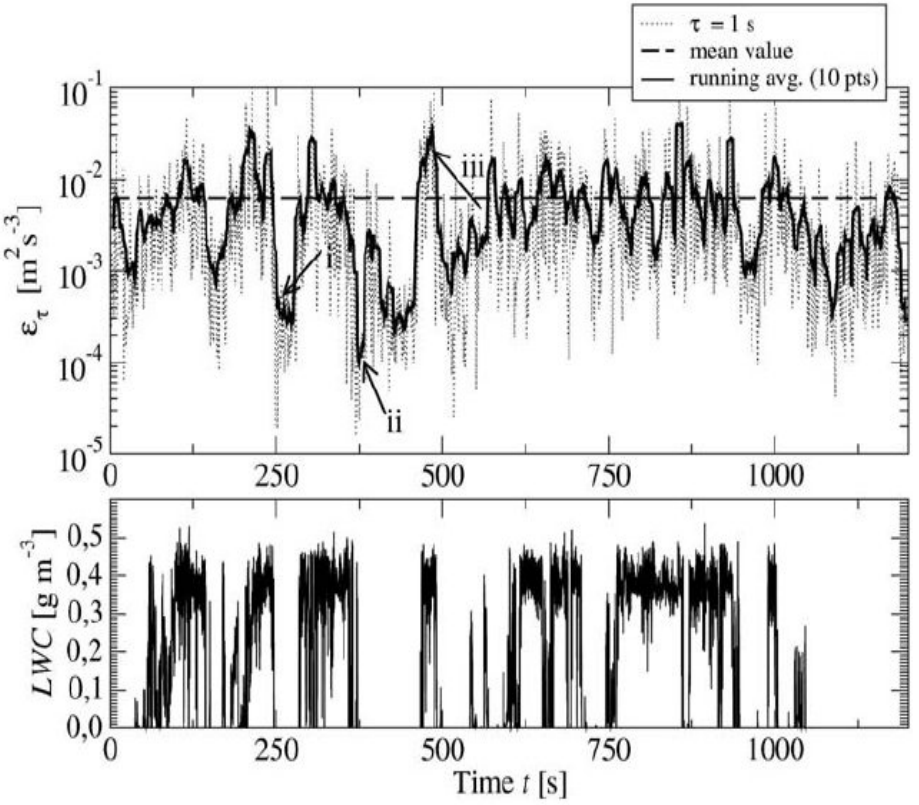

FIG. 8. (top) Time series of local energy dissipation rate ε_τ and (bottom) LWC of BBC2 data. The integration time τ for ε_τ is 1 s; a running average over 10 points is included.

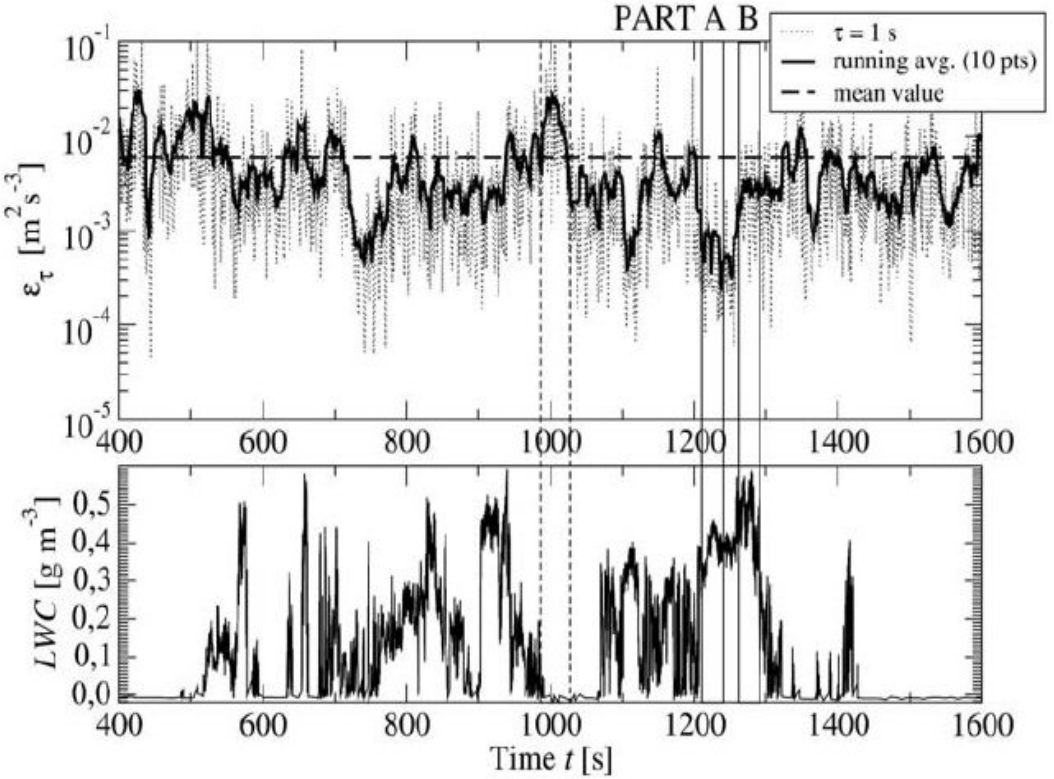

FIG. 9. (top) Time series of local energy dissipation rate ε_τ and (bottom) LWC of INSPECTRO2 data. The integration time τ for ε_τ is 1 s; a running average over 10 points is included.

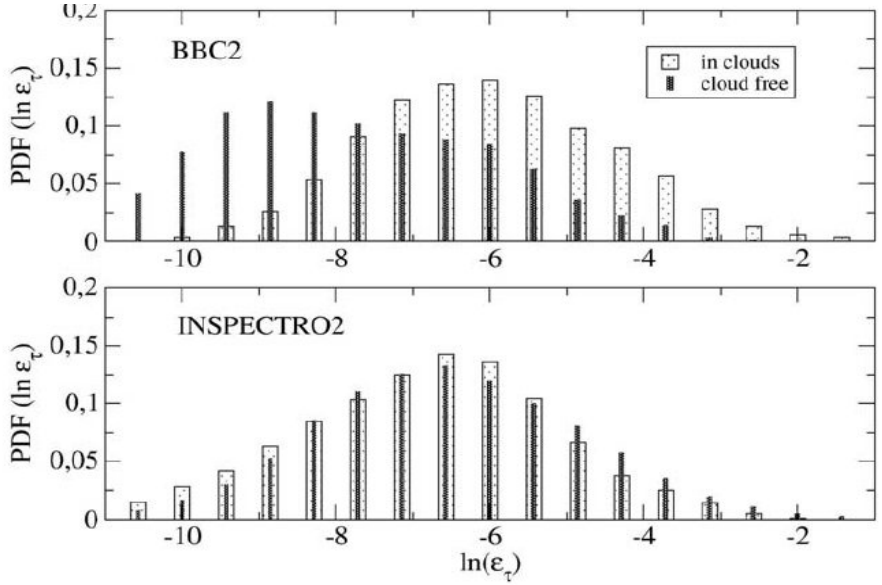

FIG. 12. PDF of natural logarithm of energy dissipation rates of the (top) BBC2 data and (bottom) INSPECTRO2 data inside of clouds and outside of clouds. The energy dissipation rates are conditionally sampled on the LWC.

Siebert, Lehmann and Wendisch, 2006.

The following parameters characterise warm turbulent clouds and give some indication of their variability.

Mean turbulent kinetic energy dissipation rates, ε, can vary from approximately 10 cm^2s^{-3} in stratiform clouds to 20010 cm^2s^{-3} in cumulus clouds (e.g. Caughey et al., 1982; MacPherson and Isaac, 1977).

The Taylor-scale Reynolds number, R_λ, varies from approximately 5000 in stratiform clouds to 20,000 in strong deep convective clouds (e.g. Shaw, 2003; Khain et al., 2007); recent measurements show that $\varepsilon \sim 3$ cm^2s^{-3} and $R_\lambda \sim 5000$ for stratocumulus (Siebert et al., 2010) and $\varepsilon \approx 20 - 30$ cm^2s^{-3} and $R_\lambda \sim 3 - 4 \times 10^4$ for small cumulus clouds (Siebert et al., 2006).

The maximum liquid water concentrations are observed in convective clouds with very strong updraughts and are not larger than 4–5 g m^{-3}; values more typical of cumulus clouds vary from 0.1–1 g m^{-3} depending on the stage of development (Pruppacher and Klett, 1997, §2.1.3).

It should be noted that most estimates of cloud parameters come from a limited number of measurements at low resolution; only recently (Siebert et al., 2006; Siebert et al., 2010) have higher-resolution (~20cm) measurements of turbulence in clouds been possible. Devenish et al., 2010

Clouds and Turbulence – overview.

Cloud topped boundary layer:

– turbulence in Stratocumulus clouds;

– turbulence in cumulus convection.

Condensation in convective motions.

a) a sketch of Koehler's theory;

b) availability of water substance for process condensation and droplet growth;

c) collisions and coalescence and a „bottleneck” problem.

Experimental evidence of warm rain formation

a) drizzle in Stratocumulus;

b) warm rain in cumulus clouds;

- similarities and differences.

$$S = \frac{e}{e_s} \approx 1 + \frac{A}{r} - \frac{B}{r^3} \qquad (2)$$

where $A = \frac{2M_w\sigma_{w/v}}{RT\rho_w}$ and $B = \frac{\nu m_s M_w}{M_s(4/3\pi\rho_w)}$, where ν is the number of dissociated ions per solute molecule, m_s is the the solute mass and subscripts s and w relate to solute and water properties, respectively. The term in A is denoted the Kelvin or curvature term, and that in B, the Raoult or solute term.

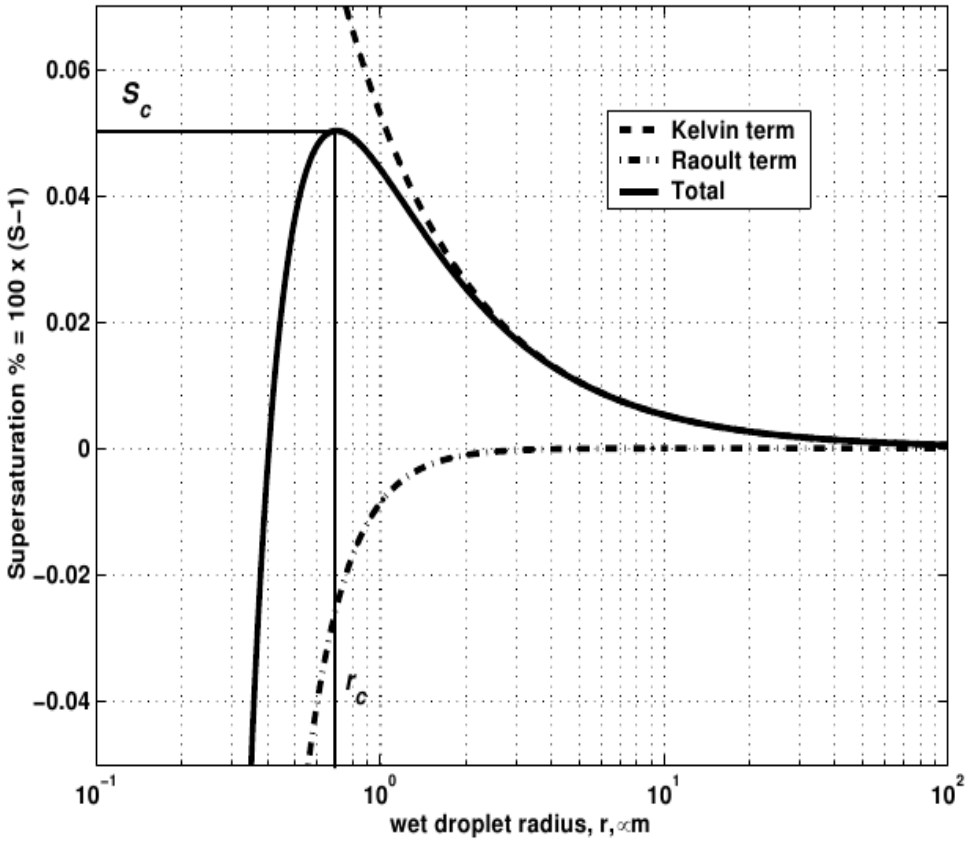

Fig. 1. The Kohler equation can be envisaged as the competition between the curvature (Kelvin) and solute (Raoult) terms.

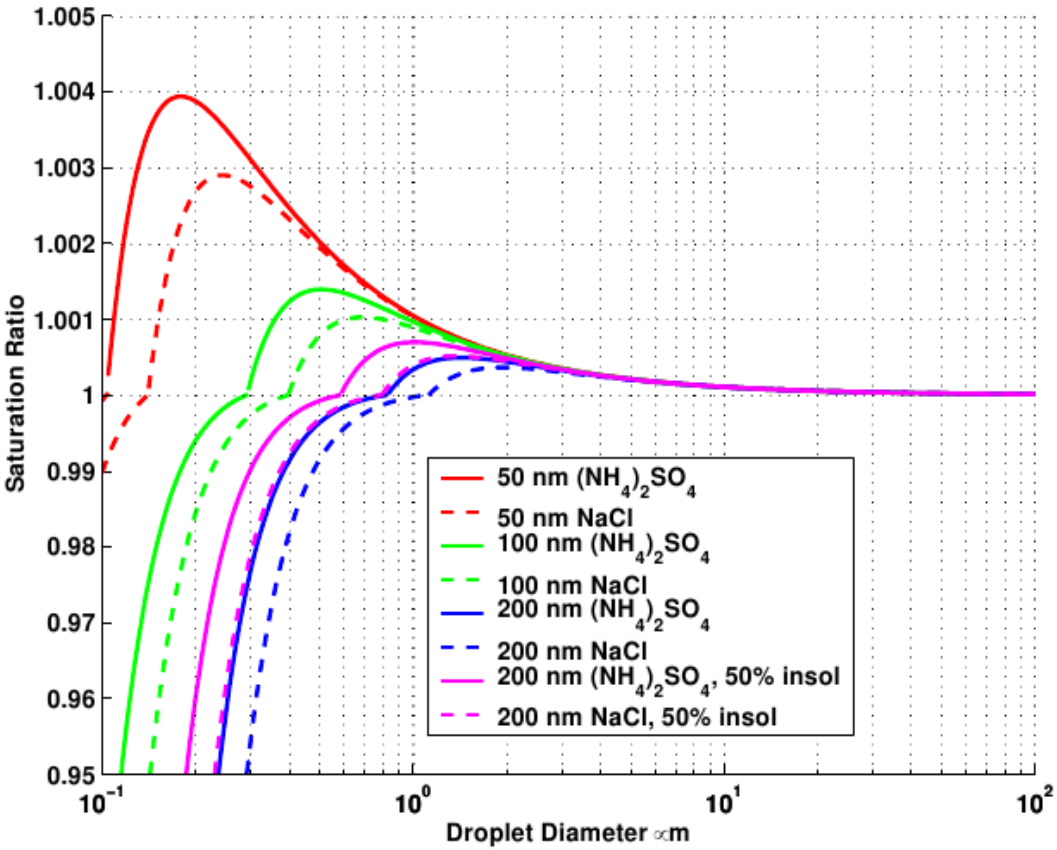

Fig. 3. Activation curves for a range of dry diameter of salt ((NH4)2 SO4 – solid, NaCl – dashed) particles (red, green and blue curves) and for 200 nm particles containing 50% by mass insoluble core (magenta).

McFiggans et al., 2006 www.atmos-chem-phys.net/6/2593/2006/

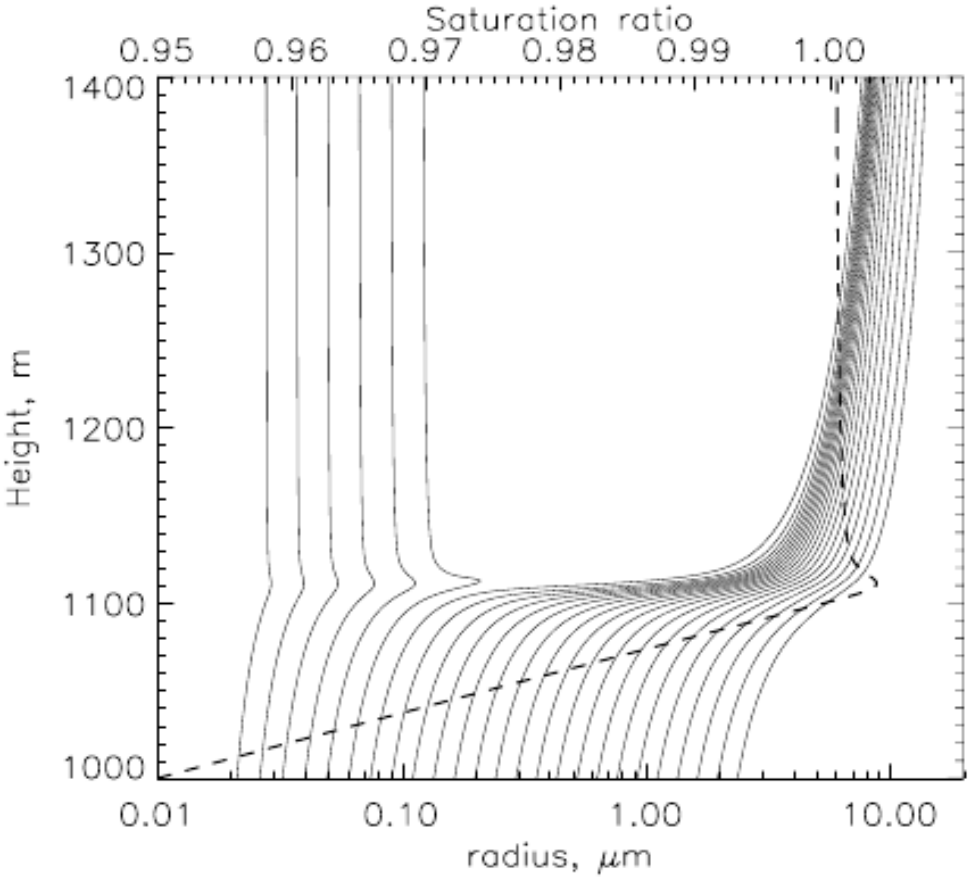

Fig. 4. Simulation showing the change in droplet radius with height in a simulation initialised with an ammonium sulphate aerosol with a geometric mean diameter of 140nm, a geometric standard deviation, σ of 1.7 and aerosol number concentration of 300 cm^{-3} (corresponding to a total mass loading of 0.76μgm^{-3}). The simulation was started at an RH of 95% at 1000 m. Solid lines represent selected aerosol size classes. The dashed line is the saturation ratio.

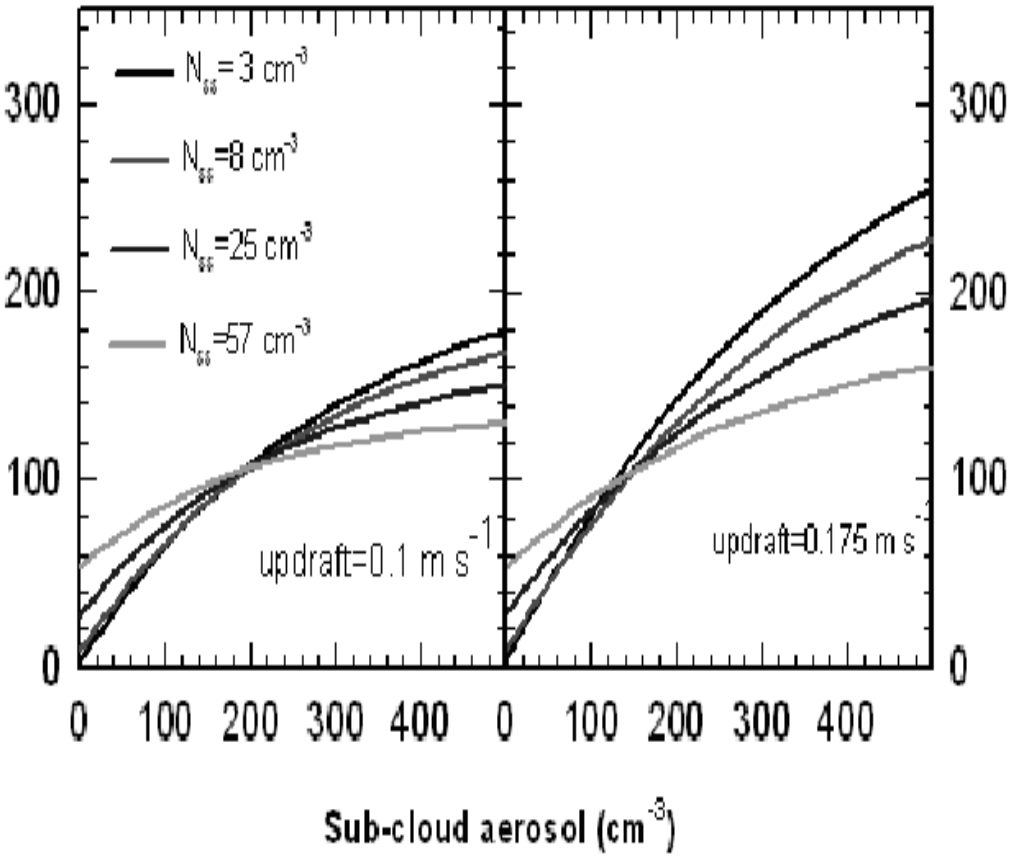

Fig. 5. Cloud droplet concentration as a function of sub-cloud aerosol where the sub-cloud aerosol comprises an external mix of sulphate and sea-salt CCN.

McFiggans et al., 2006 www.atmos-chem-phys.net/6/2593/2006/

What is rain?

rain — Precipitation in the form of liquid water drops that have diameters greater than 0.5 mm, or, if widely scattered, the drops may be smaller.

The only other form of liquid precipitation, drizzle, is to be distinguished from rain in that drizzle drops are generally less than 0.5 mm in diameter, are very much more numerous, and reduce visibility much more than does light rain.

warm rain — Rain formed from a cloud having temperatures at all levels above 0°C (32°F), and resulting from the droplet coalescence process.

Glossary of Meteorology, American Meteorological Society

rain — Precipitation of liquid water drops with diameters greater than 0.5 mm (0.02 inch). When the drops are smaller, the precipitation is usually called drizzle. See also precipitation.

Britannica Online

Aerosol, cloud and rain droplets:

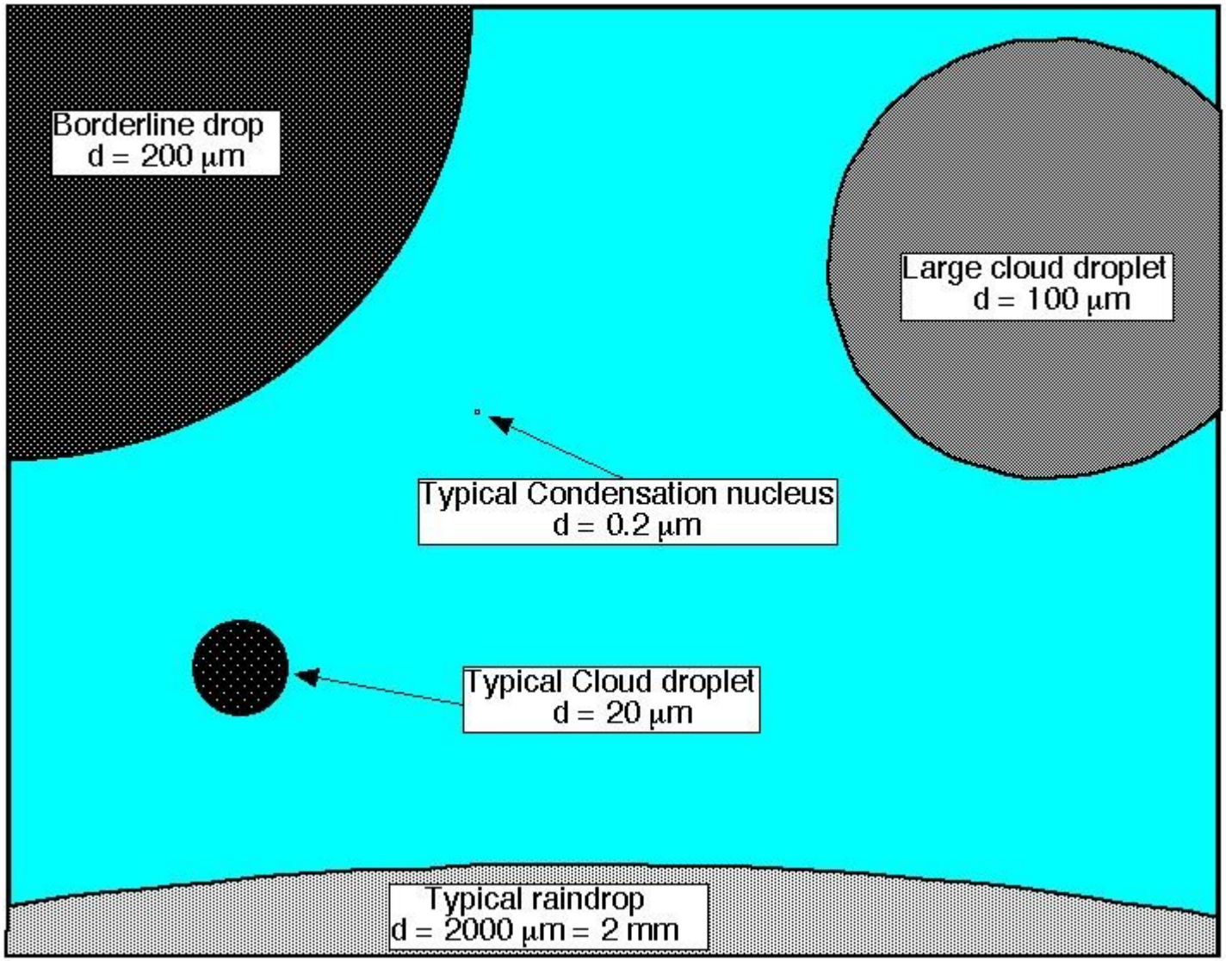

From: What about weather modification? By Chuck Doswell, http://www.flame.org/~cdoswell/wxmod/wxmod.html
After: McDonald, J.E., 1958: The physics of cloud modification. Adv. Geophys., 5, 223-303.

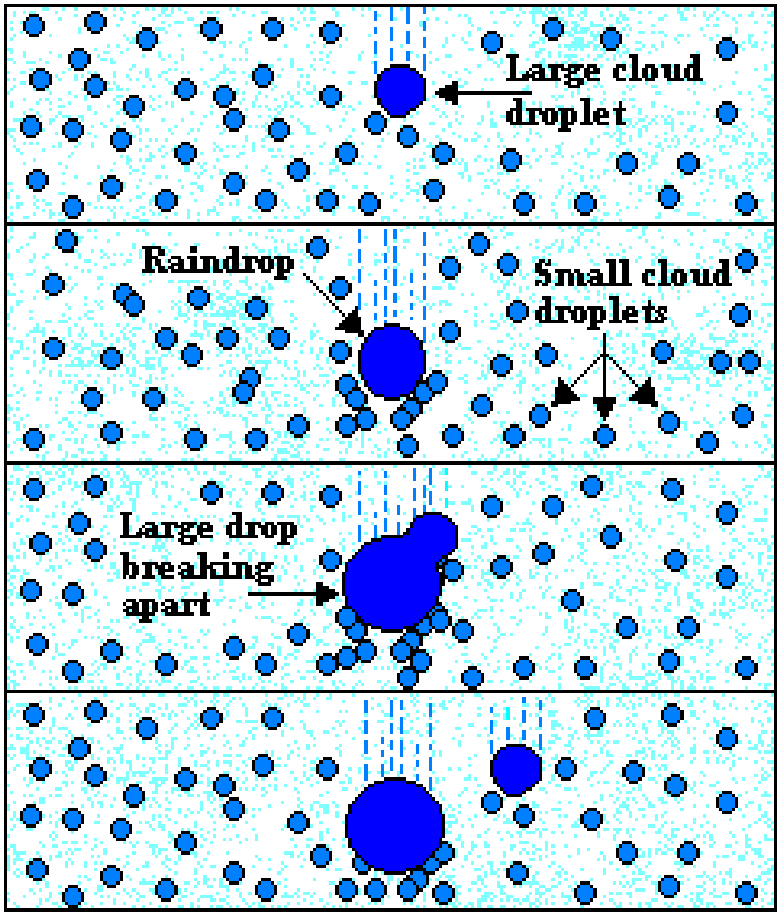

Collision-coalescence process

Mass of typical raindrop is is MILLION (10^6) times larger than mass of typical cloud droplet.

Liquid water mixing ratio in cloud after condensation ~0.1g/kg, in Ss ~1g/kg typical water vapour mixing ratio 10g/kg, factor 10^2-10^3

Large droplets are formed due to collision-coalescence:

substantially different terminal velocities required!

CLOUD-PARTICLE FALLSPEEDS

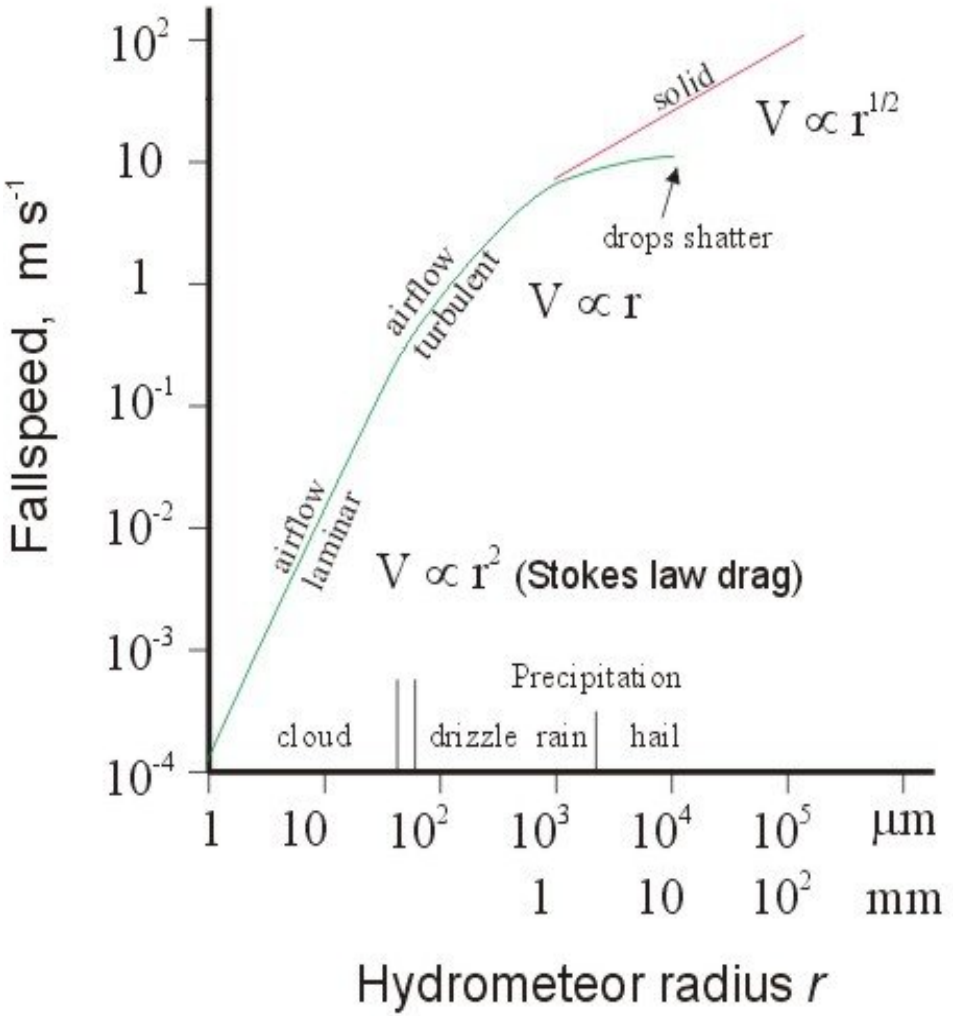

Adapted from McIlveen (1992)

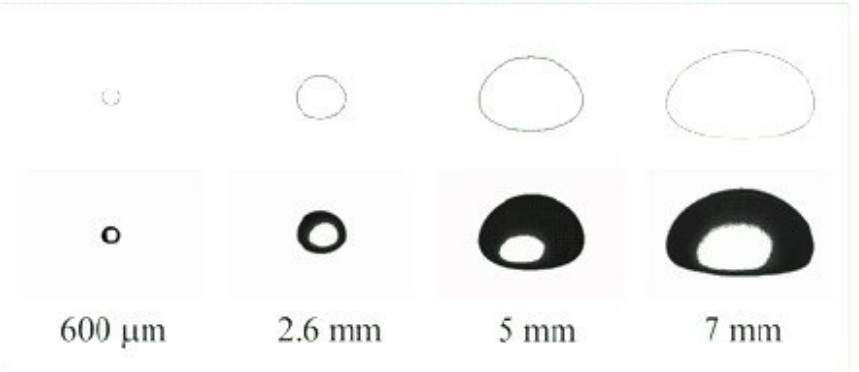

Fig. 1. Calculated drop shapes and real images of drops with different sizes floated in the Mainz vertical wind tunnel

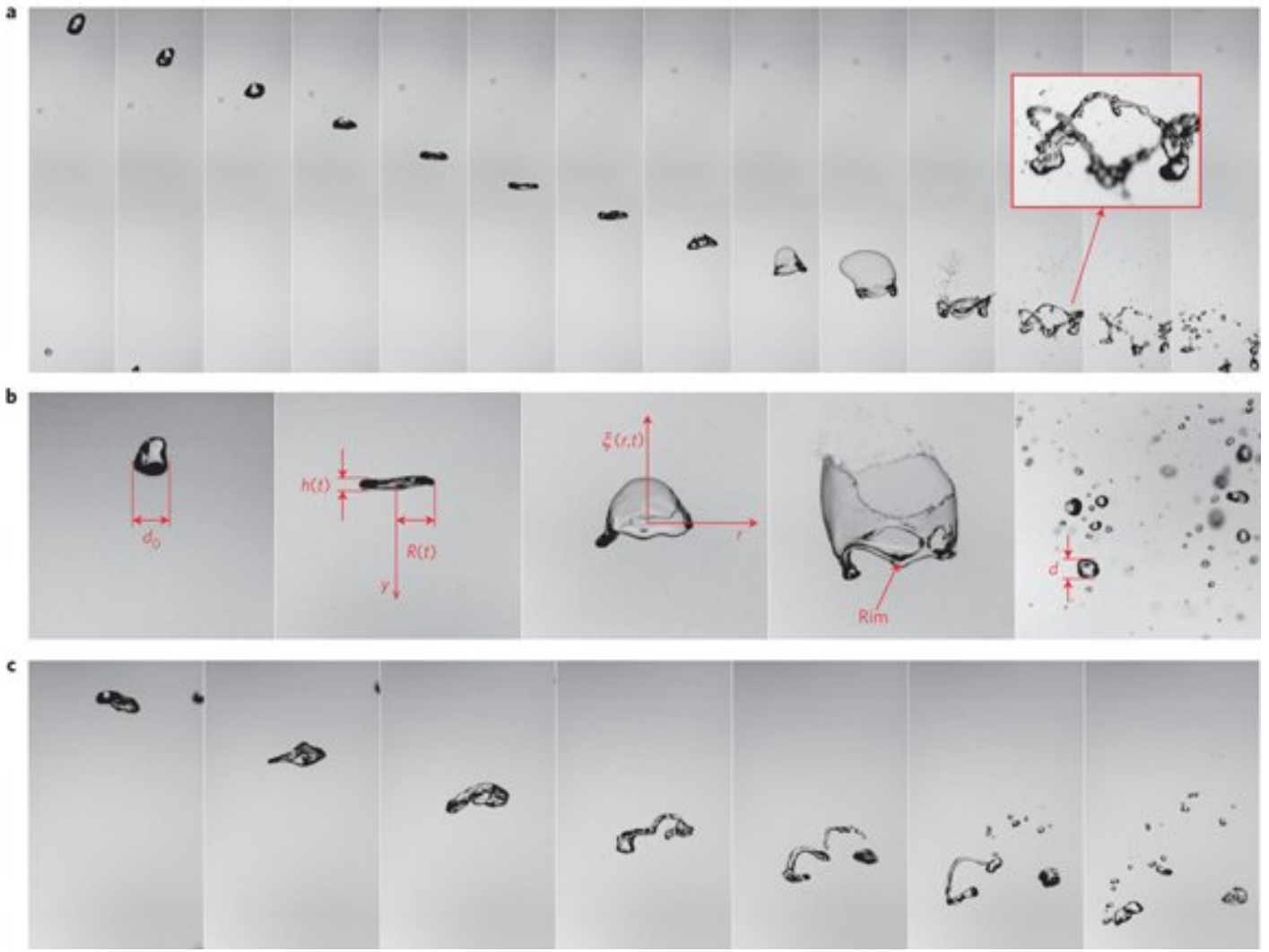

Top row: series of events of the fragmentation of a d_0=6 mm water drop falling in an ascending stream of air. The time interval between each image is Δt=4.7 ms. The sequence shows first the flattening of the drop into a pancake shape, the inflation of a bag bordered by a thicker corrugated rim, its break-up and the destabilization of the rim itself (highlighted in the inset), leading to disjointed drops distributed in size.
Middle row: a similar series defining the initial diameter d_0, the bag thickness h(t), its radius R(t) and shape x_i(r,t), and the final drop size d. Bottom row: the formation of a bag is not mandatory for the initial drop to break up. However, its fragmentation is always preceded by a change of topology into a ligament shape, which often occurs without bag inflation. The sequence is for d_0=6 mm and Δt=7.9 ms.

Emmanuel Villermaux & Benjamin Bossa, 2009

Concept of rain formation

HOW droplets large enough to start collision/coalescence cascade may appear in clouds???

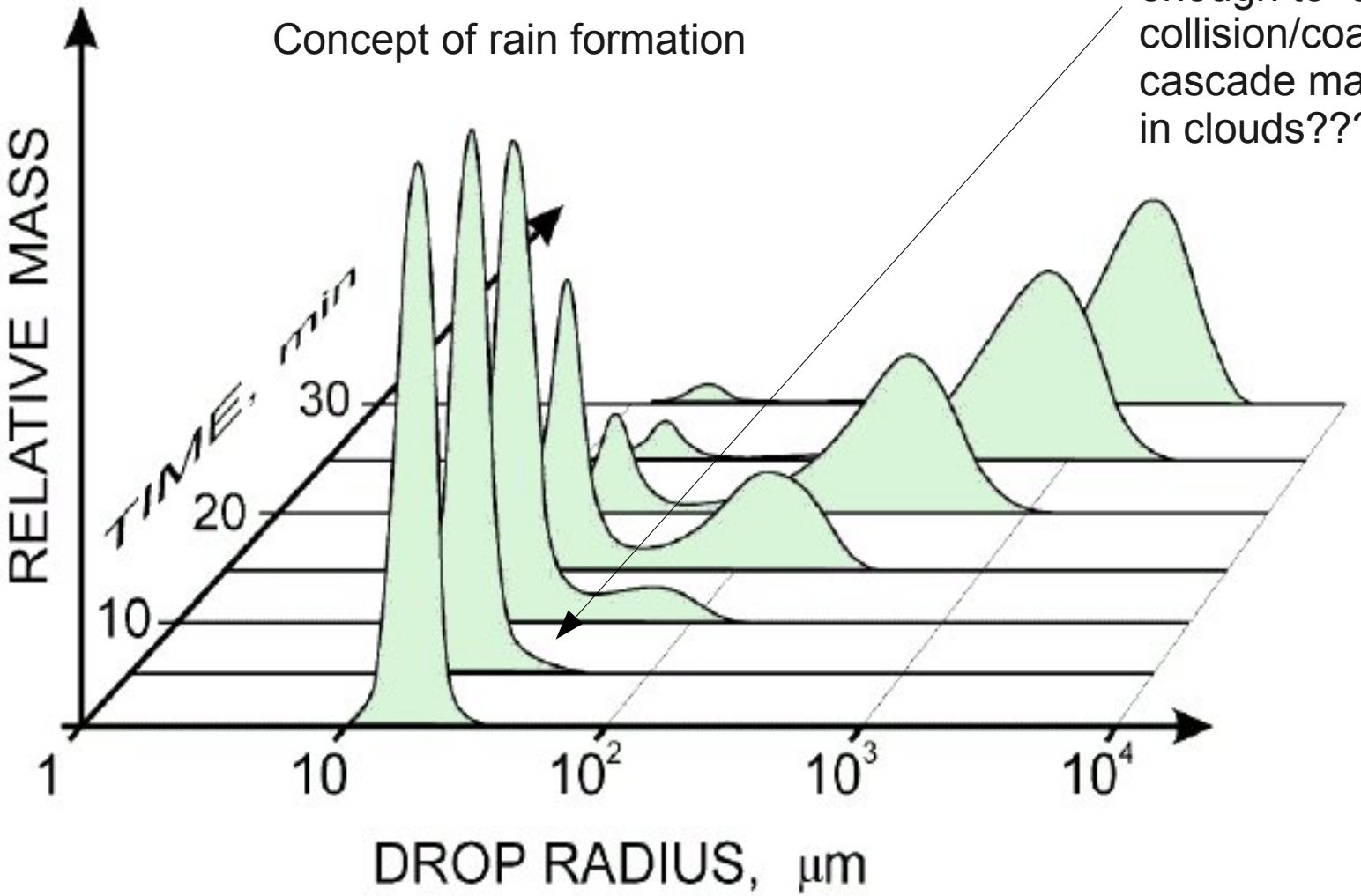

Figure 3 Illustration of the evolution of a droplet size distribution during the onset of the collision-coalescence process. Figure adapted from Berry & Reinhardt (1974) and Lamb (2001), courtesy of D. Lamb, Penn State University.

After Shaw, 2003.

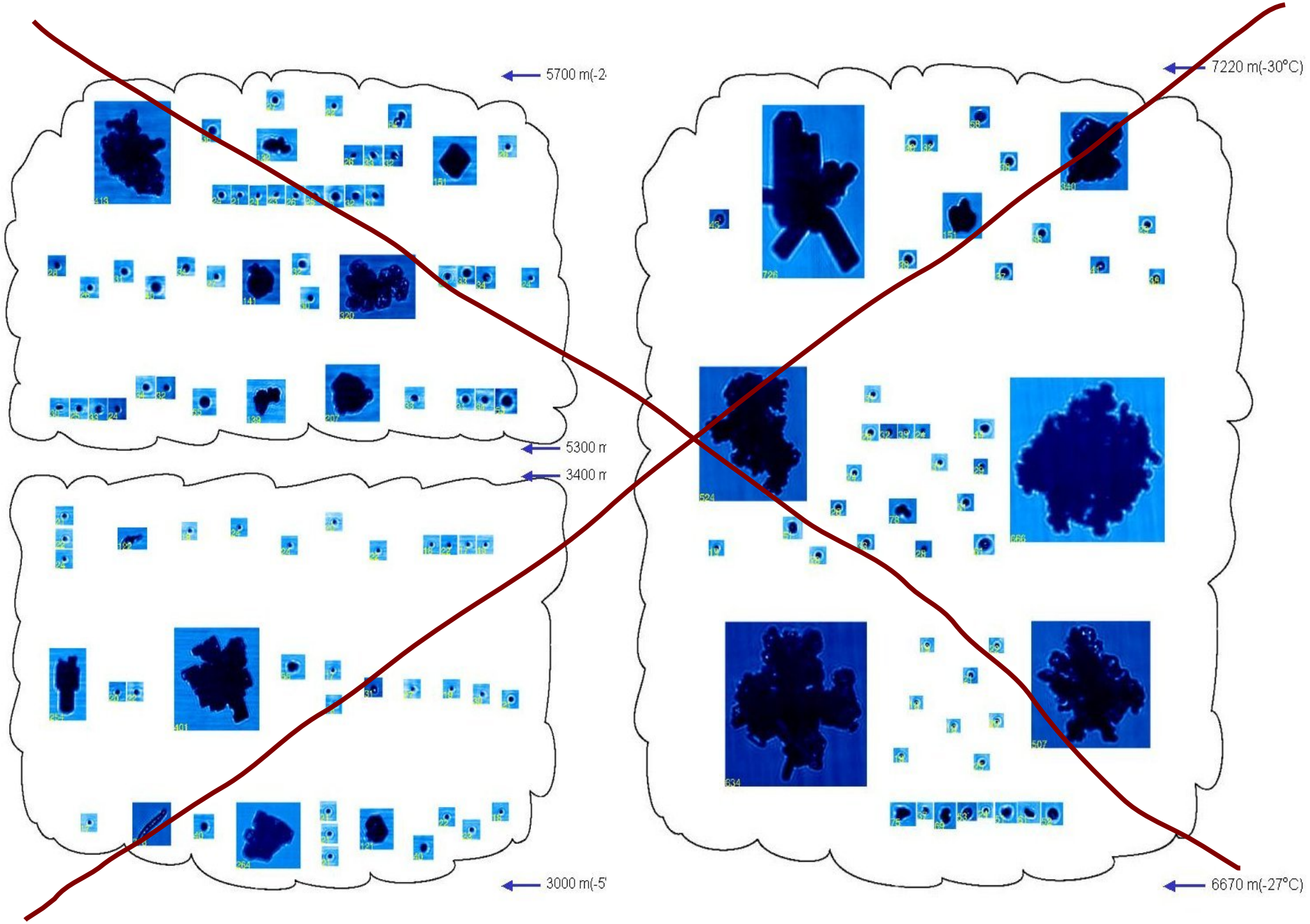

Cold cloud particles at various heights (temperatures) imaged by CPI (SPEC Inc.)

Concepts:

1. Giant Condensation nuclei

2. Entrainment and secondary activation

3. “Something to do with turbulence”

Clouds and Turbulence – overview.

Cloud topped boundary layer:
- turbulence in Stratocumulus clouds;
- turbulence in cumulus convection.

Condensation in convective motions.
a) a sketch of Koehler's theory;
b) availability of water substance for process condensation and droplet growth;
c) collisions and coalescence and a „bottleneck" problem.

Experimental evidence of warm rain formation
a) drizzle in Stratocumulus;
b) warm rain in cumulus clouds;
- similarities and differences.

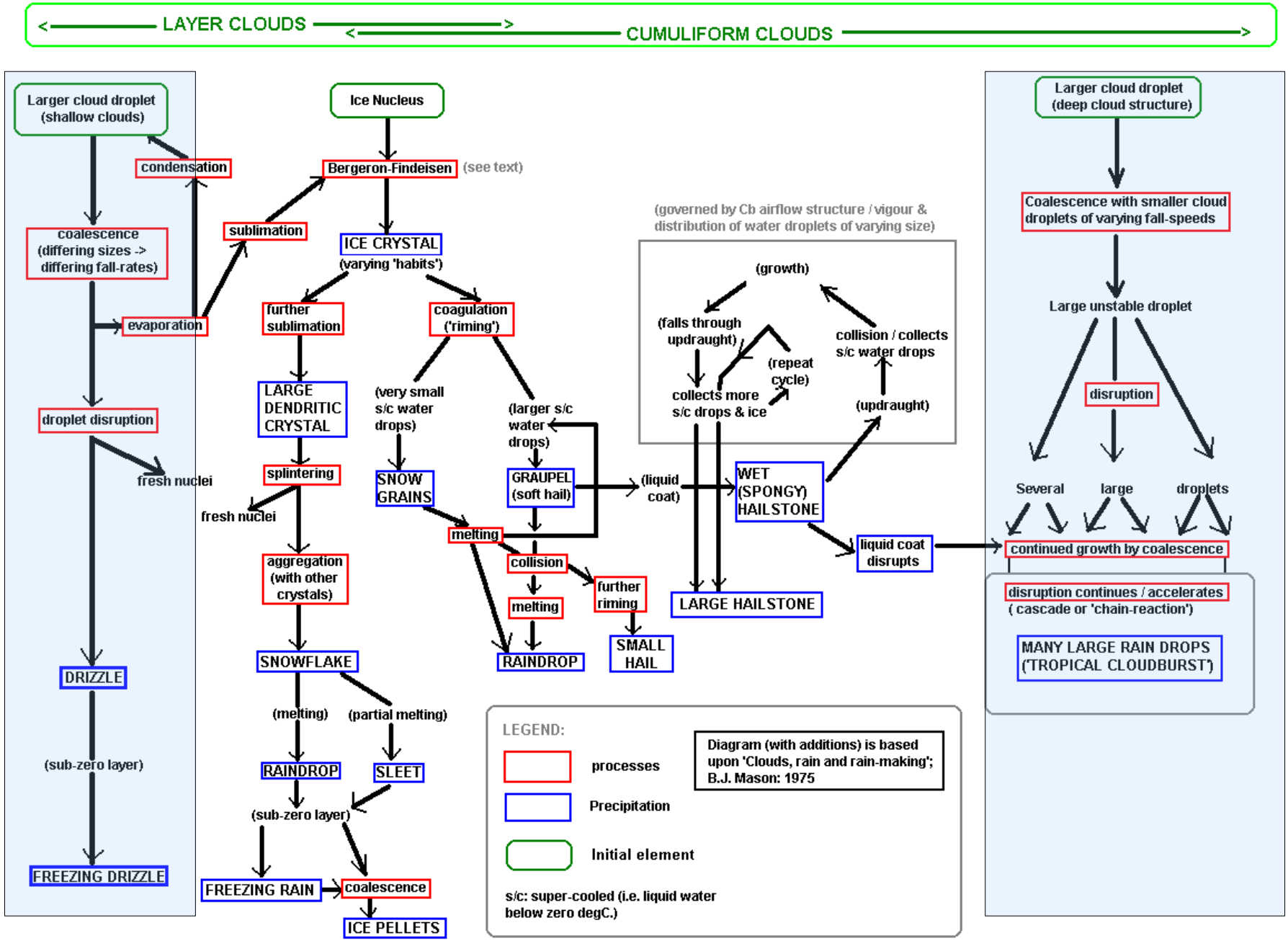

http://weatherfaqs.org.uk/node/160

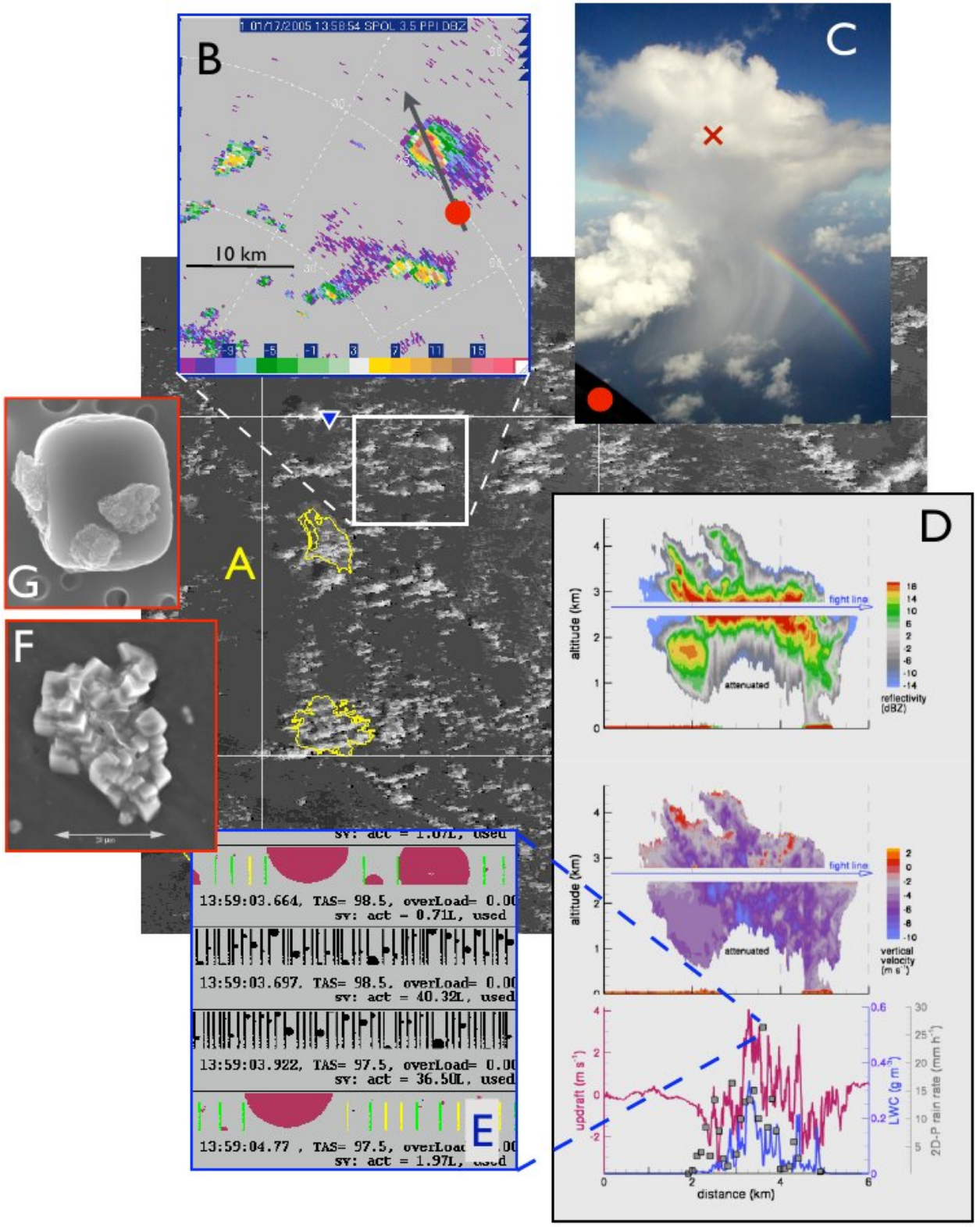

Figure 3: Observations on many scales of a precipitating small cumulus (17 January, 13:59 UTC). A: Satellite image from DMSP recorded 10 minutes before penetration by the Wyoming King Air. B: SPol radar image at 3.5◦ elevation; the cloud is about 46 km from the radar. C: Photograph taken from a position marked with the red dot in B. The cross marks the approximate location of the aircraft penetration at 2630 m altitude. D: Vertical sections of radar reflectivity and of Doppler velocity from the Wyoming Cloud Radar and plots of the in situ updraft, liquid water content and rain rate measurements. Note that the high rain rates and large drops are within the updraft. E: Millimeter sized drops seen at two different magnifications from imaging probes on the King Air. Also shown in F/G are scanning electron microscope images such as were made from data collected on NSF/NCAR C130 sub-cloud circles: 2 μm sea-salt particle collected by the total aerosol sampler (F); giant sea-salt particle (20 μm scale) collected with the giant nuclei sampler (G). The location of the Research Vessel Seward Johnson is marked with a blue triangle in A.

Rauber et al., 2007

Courtesy H.Siebert

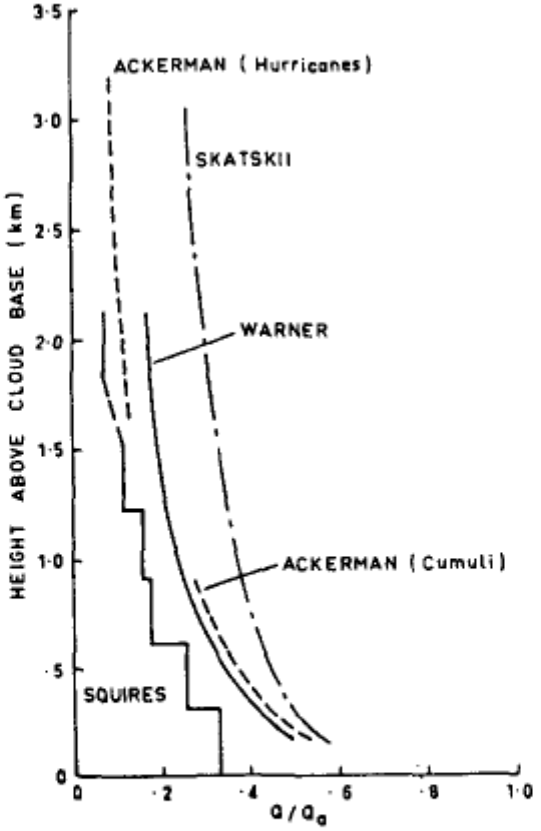

FIG. 1. The ratio of the observed mean liquid water content at a given height above cloud base to the adiabatic value. The values attributed to Skatskii were obtained from his published results assuming that the cloud base was at a height of 1 km and at a temperature of 8C.

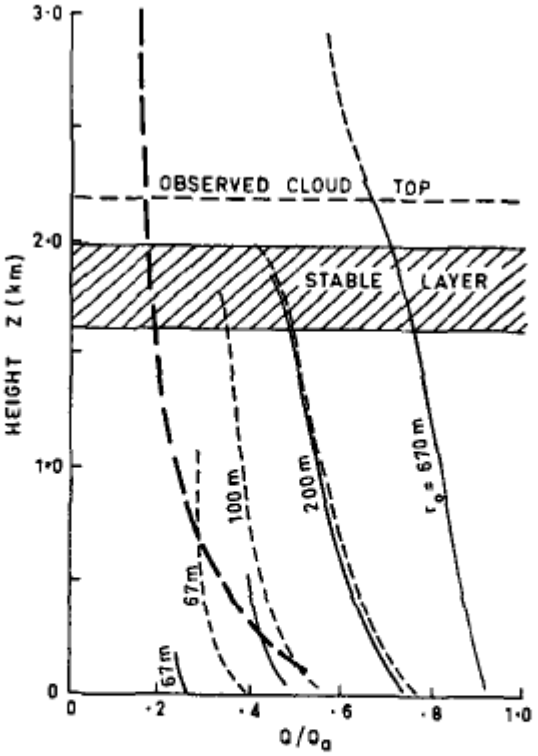

FIG. 2. Predicted ratio of liquid water content to its adiabatic value as a function of height for plumes of different initial radii obeying Eqs. (1)–(4) and growing in the environment listed in Table 2. Full lines are for zero initial updraft and temperature excess, dotted lines for initial values of 1 m sec^{-1} and 1C. The lines terminate at the maximum heights reached by the plumes. The heavy dashed line represents observed values of Q/Q_a.

Warner 1970

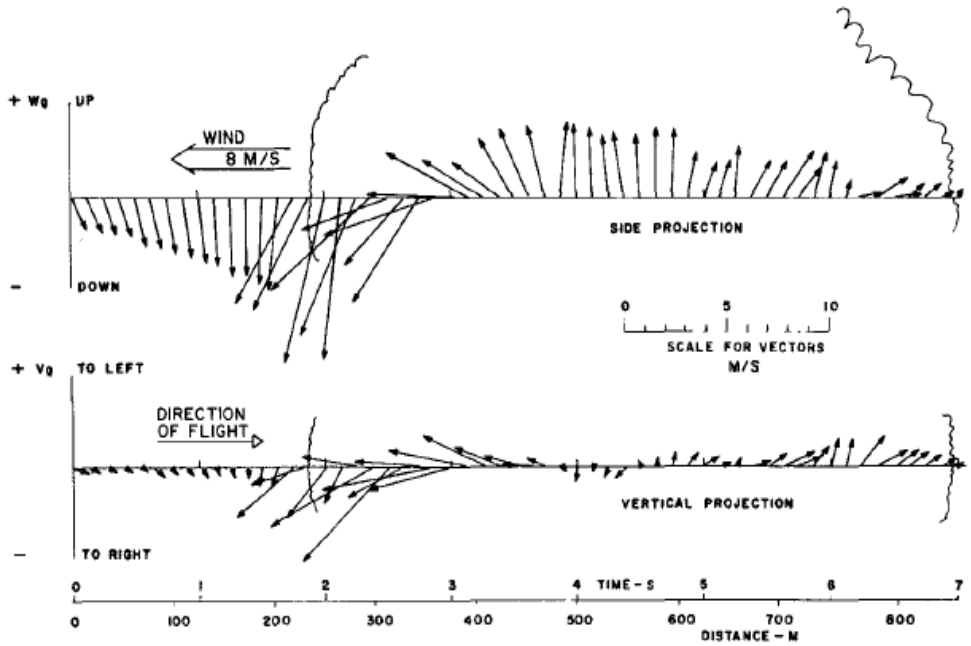

FIG. 5. Side and vertical projections of gust vectors for first cloud element penetrated in run 20–5 (Fig. 4).

McPherson and Isaac, 1977

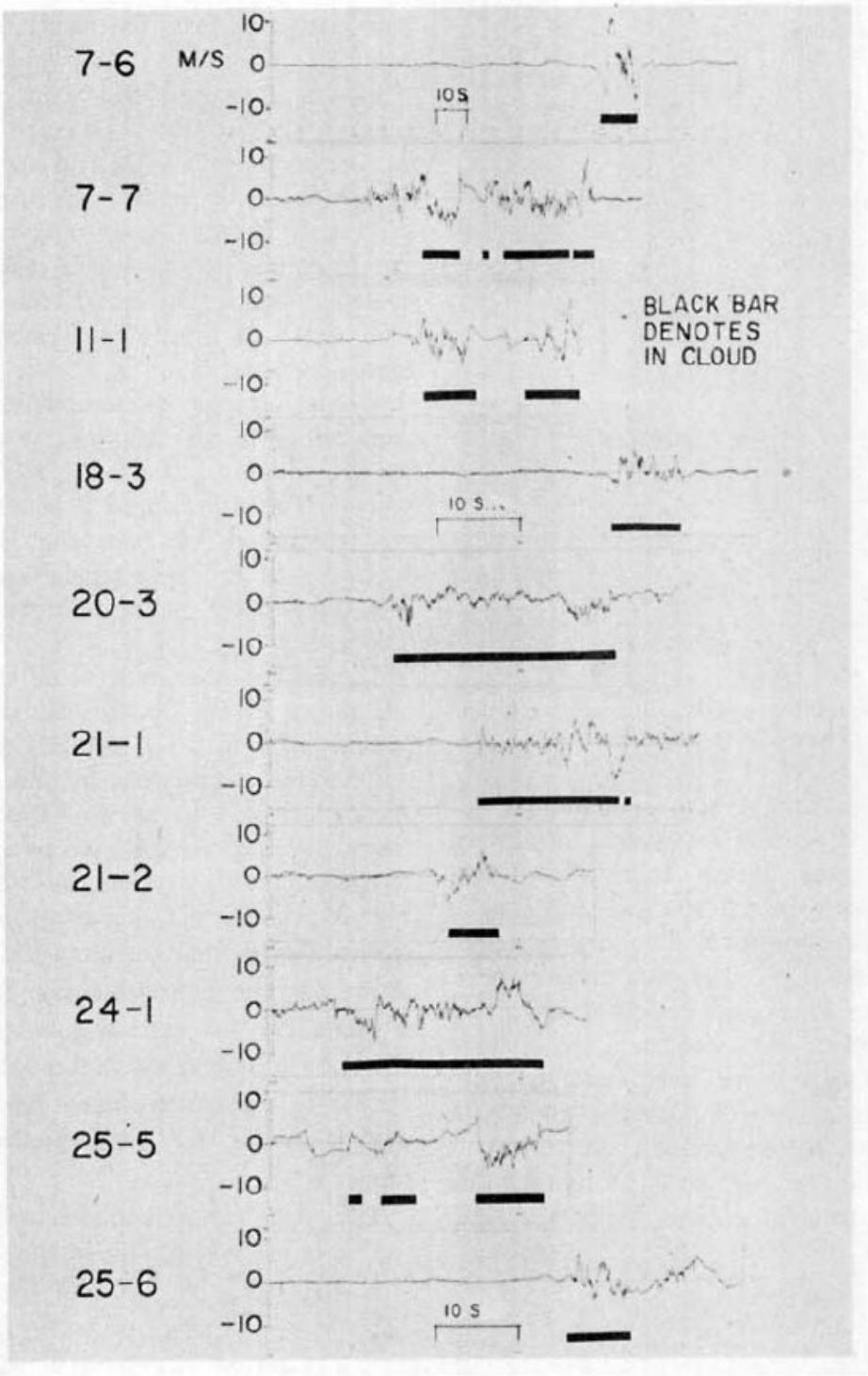

FIG. 6. Time histories of the vertical gust velocity for 10 of the cloud-top penetrations. Time scales vary as shown.

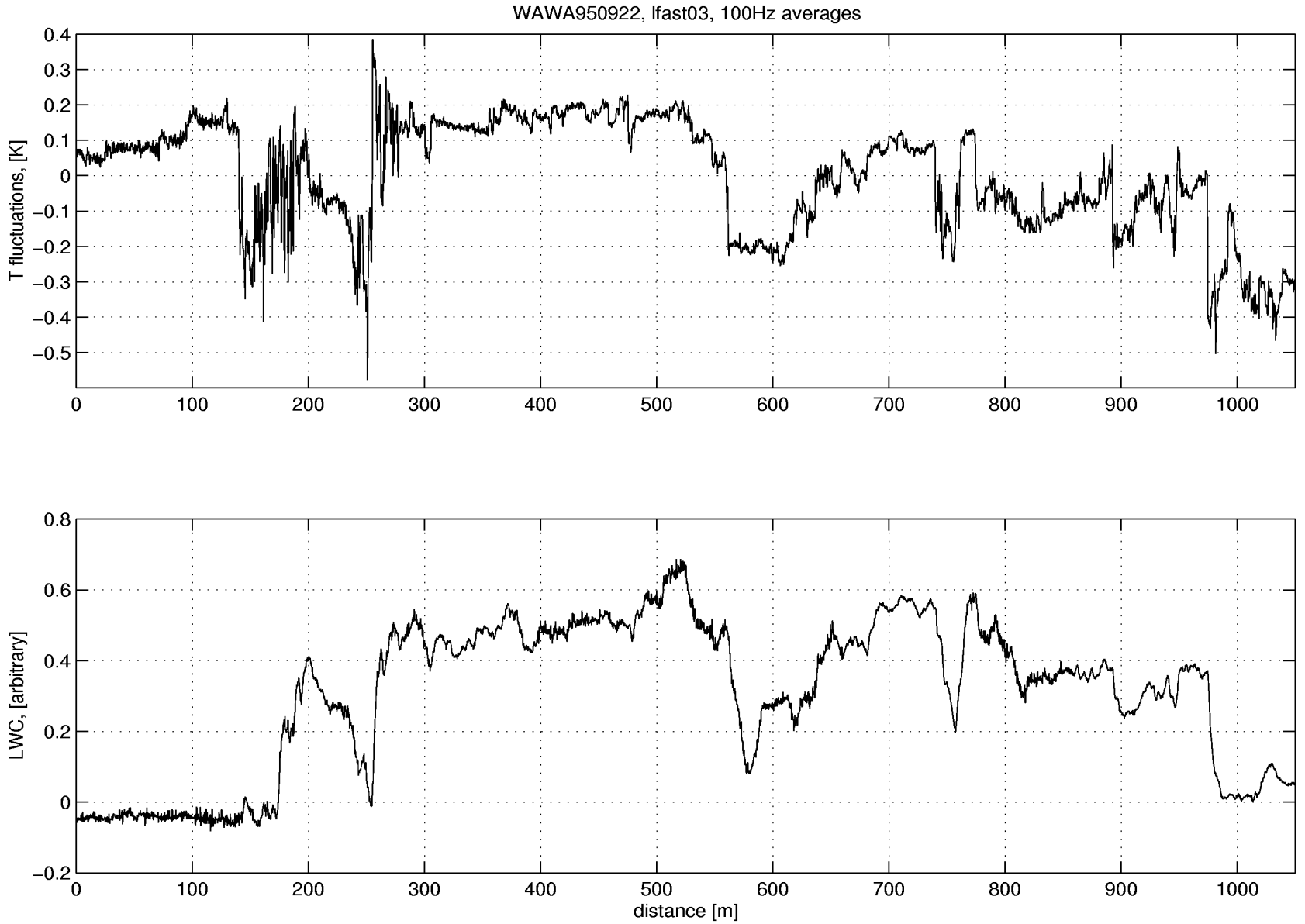

Haman and Malinowski 1996

SMALL-SCALE TURBULENT MIXING IN CLOUDS

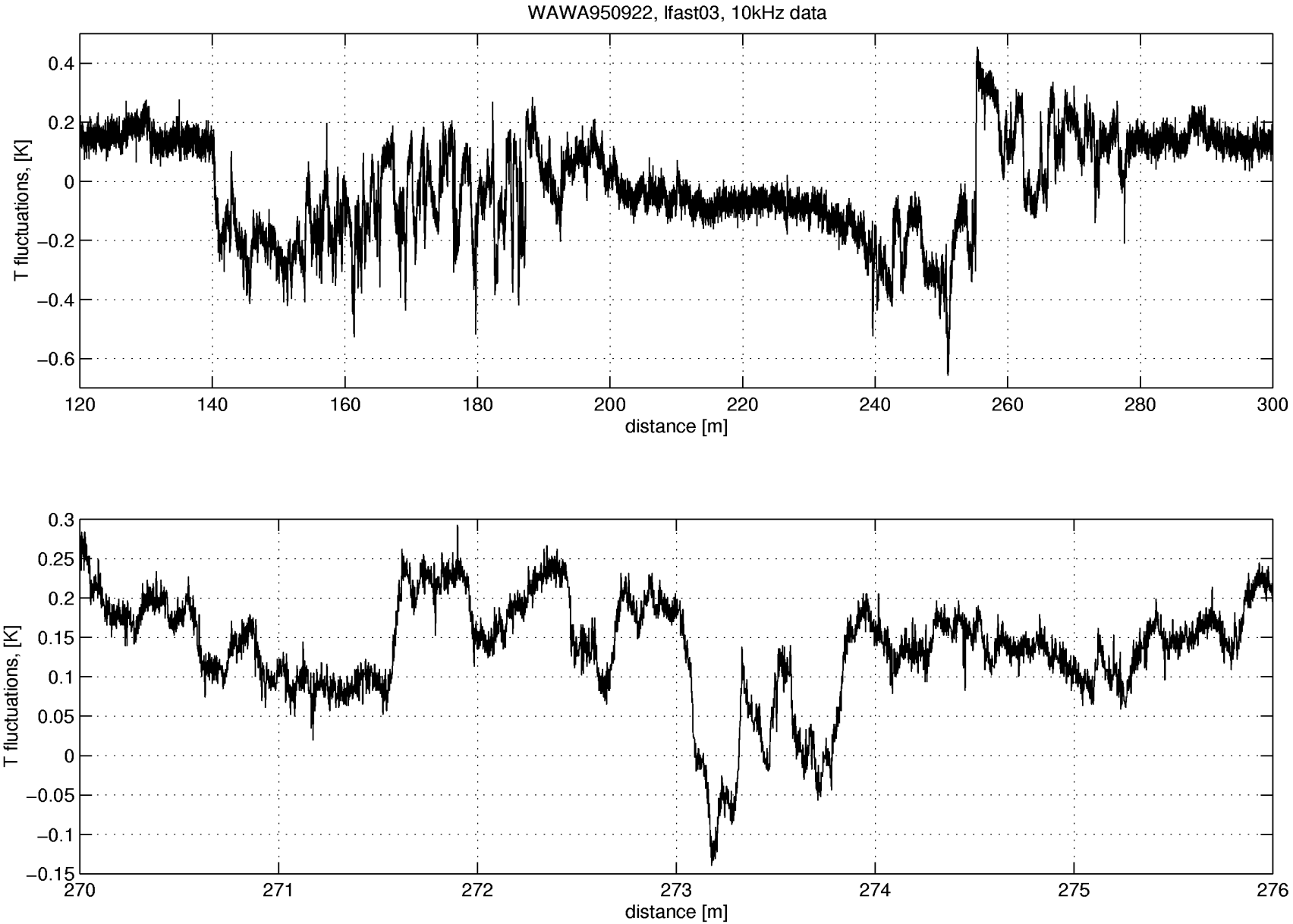

Haman and Malinowski 1996

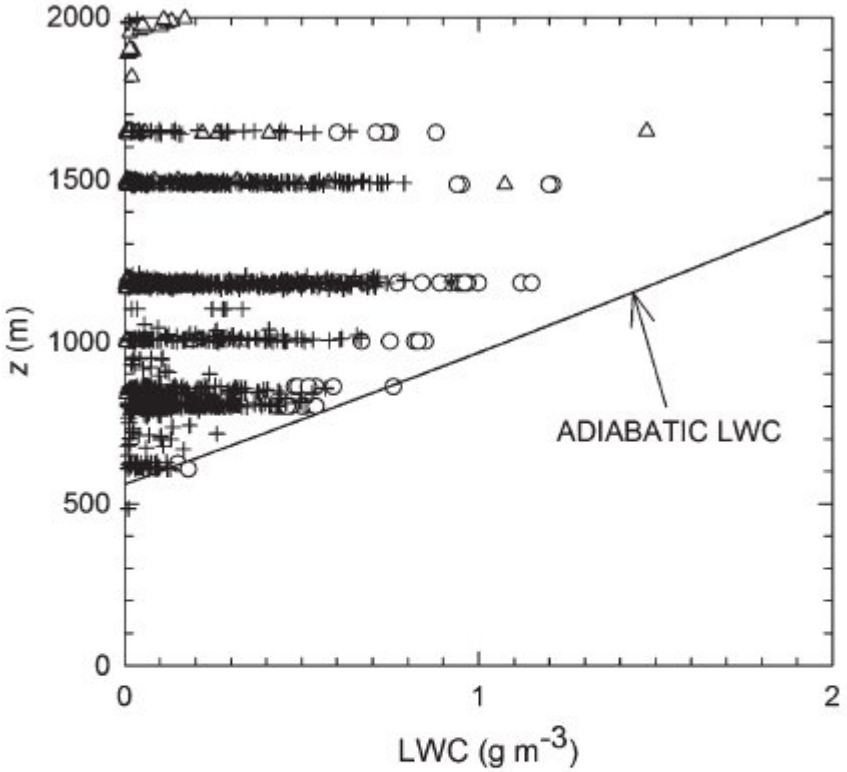

Fig. 1. Liquid water content LWC as a function of height z in RICO trade-wind Cu on C-130 flight RF12. Crosses are 1-hz PVM data, circles are 1000-hz PVM data, and triangles are 1-hz 2D-C data. The curve indicates the expected adiabatic LWC profile given cloud-base temperature and pressure.

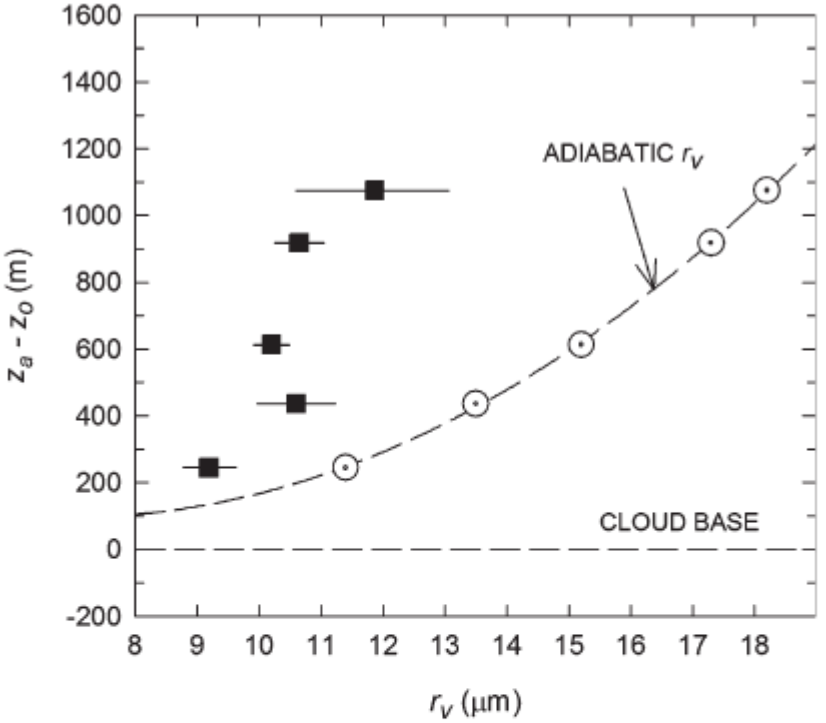

Fig. 3. Average measured values of mean volume radius r_v for the 7 conditionally-sampled Cu at each of 5 levels flown by the aircraft (solid squares); horizontal lines through the data indicate 2 standard deviations of data variability (similar horizontal lines in subsequent plots have the same meaning). Dashed line is the expected value of r_v given adiabatic ascent in the Cu.

Gerber et al., 2008

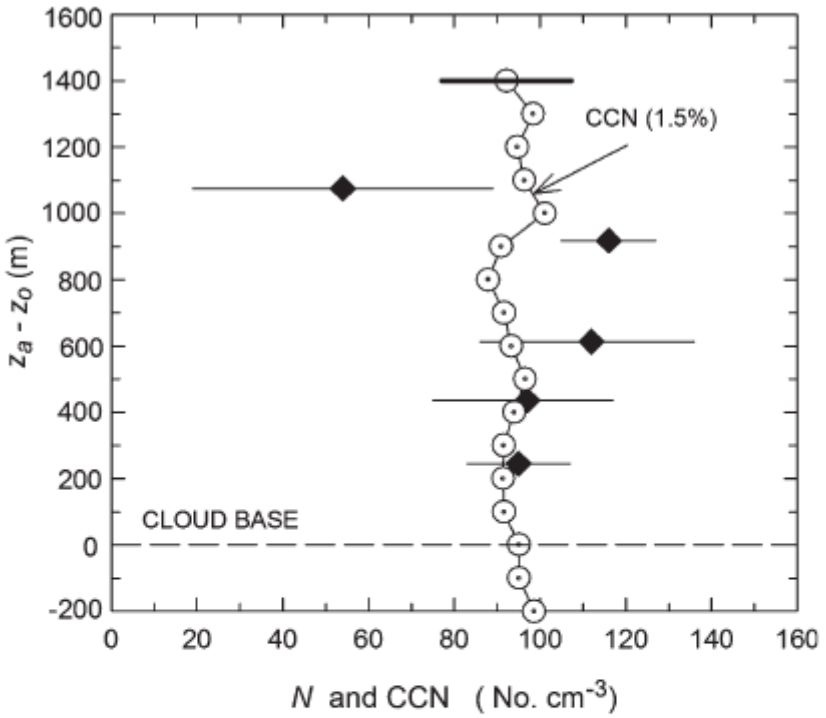

Fig. 4. Average number concentration N of cloud droplets (solid diamonds) for the 7 conditionally- sampled Cu at 5 levels above Cu base. Hollow circles indicate CCN (cloud condensation nuclei) for a critical supersaturation of 1.5% measured during vertical profiling of the aircraft outside of cloud. (The heavy horizontal line gives the average 2 std. dev. for the CCN data).

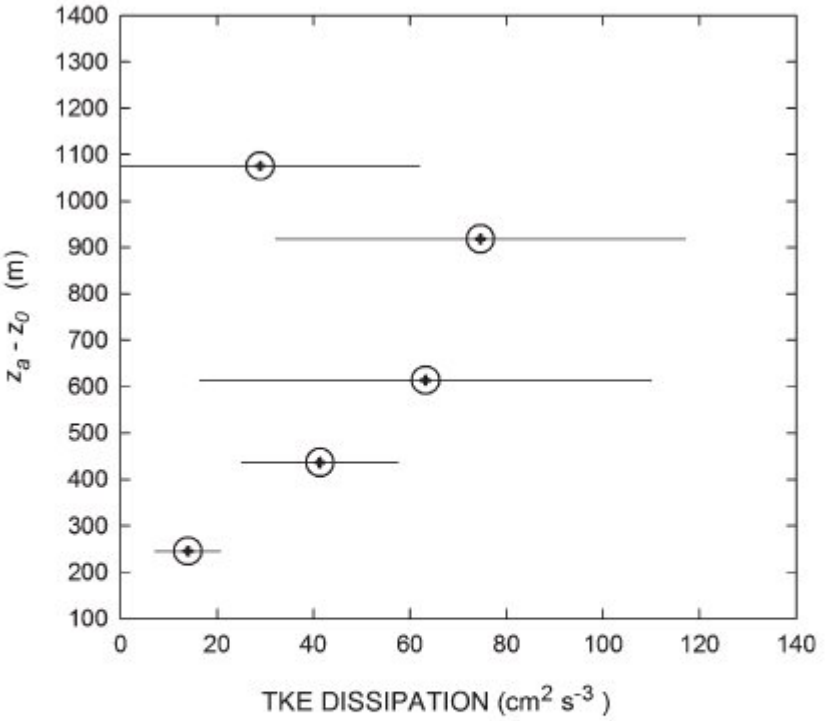

Fig. 5. Average TKE (turbulent kinetic energy) dissipation rate (ε) for the conditionally-sampled Cu as a function of height above cloud base.

Gerber et al., 2008

Table 2. General characteristics of the seven Cu at five different levels shown in Fig. 2, with mean values of cloud top z_t, cloud top minus aircraft level z_a, aircraft level minus z_o = LCL ~ 570 m, width of the turret W_d, length L_a of the aircraft pass through the turret, vertical velocity w, maximum vertical velocity w_{max} (w based on 4-m resolution data), bulk TKE dissipation rate ε, and fractional entrainment δ. s(xxx) indicates the mean of the sample standard deviation s for all cloud passes at the given level, and s[xxx] indicates s for the mean of the parameter xxx at the given level; the same convention is used in subsequent tables.

Level	$z_a - z_o$ (m)	z_t (m)	$z_t - z_a$ (m)	W (m)	s [W] (m)	L_a (m)	w (m/s)	s (w) (m/s)	w_{max} (m/s)	ε (cm^2/s^3)	s [ε] (cm^2/s^3)	δ (1/m)	s [δ] (1/m)
1	252	1009	187	544	162	331	1.18	.791	2.40	14.01	6.75	2.29e-3	1.28e-3
2	439	1205	196	484	261	266	1.25	1.13	3.01	41.34	16.26	1.26e-3	.54e-3
3	615	1398	213	453	168	402	1.92	1.58	4.28	63.24	46.76	.73e-3	.23e-3
4	918	1722	234	612	185	454	1.90	1.67	4.88	74.61	42.37	.91e-3	.13e-3
5	1074	1920	276	631	187	407	−.283	.869	1.29	29.00	32.90	6.12e-3	–

Table 3. Microphysics of the seven Cu at five different levels shown in Fig. 2, with mean values of LWC (liquid water content) and its sample standard deviation for three horizontal data resolutions, total droplet concentration N, and mean volume radius r_v. The latter two parameters correspond to 10-m resolution data. The subscript a indicates expected adiabatic values.

Level	LWC_a (g/m^3)	LWC (g/m^3)	s (10 cm) (g/m^3)	s (50 cm) (g/m^3)	s (1000 cm) (g/m^3)	N (No/cc)	s [N] (No/cc)	r_{va} (μm)	r_v (μm)	s (r_v) (μm)
1	.605	.284	.084	.078	.063	95	12	11.4	9.2	2.0
2	1.00	.427	.142	.136	.128	97	22	13.5	10.6	3.1
3	1.42	.520	.160	.153	.145	112	25	15.2	10.2	1.7
4	2.11	.536	.196	.184	.173	116	11	17.3	10.6	2.4
5	2.46	.331	.142	.135	.125	54	35	18.2	11.9	3.7

Gerber et al., 2008

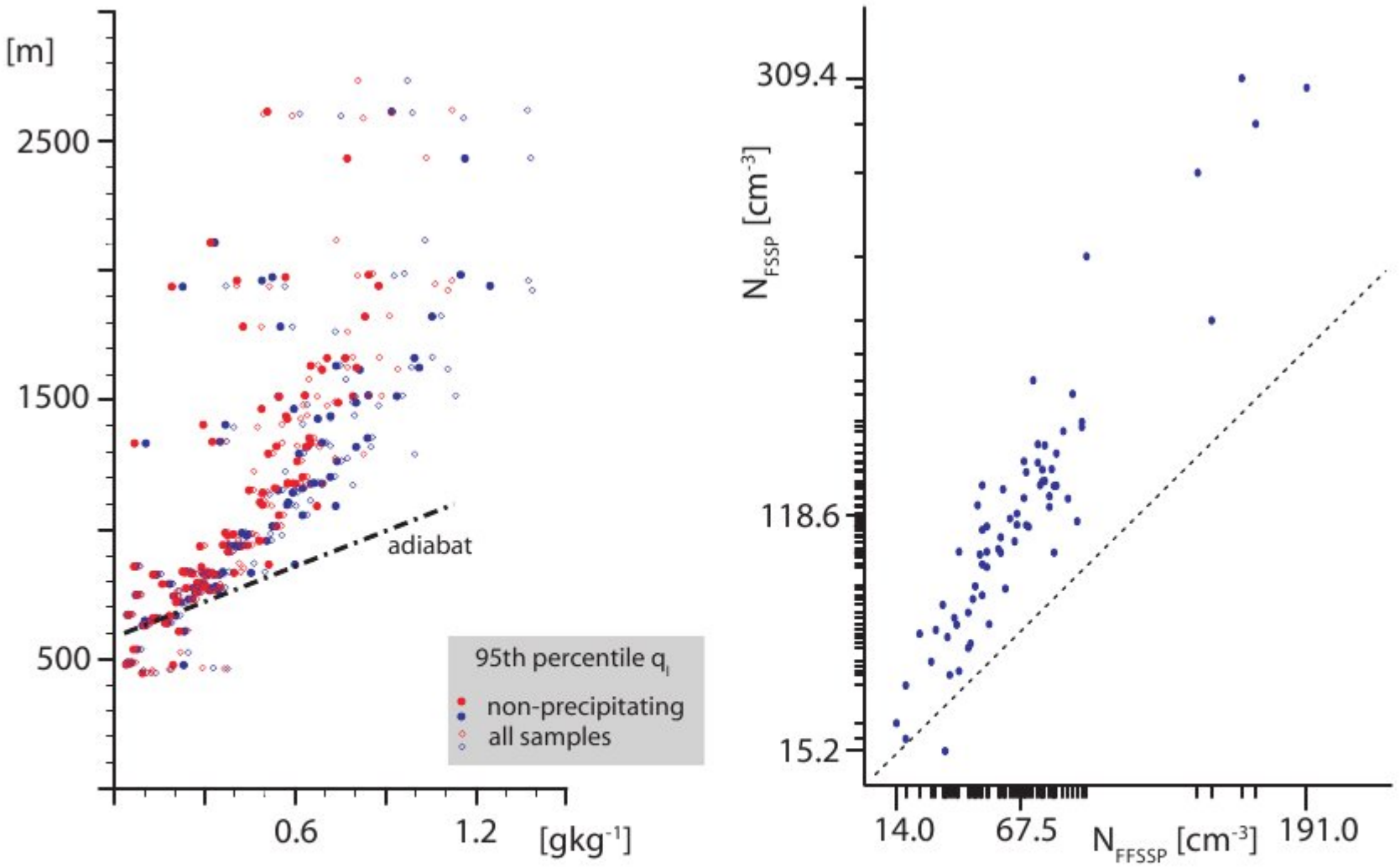

Figure 8: Cloud water and droplet concentration measurements from the C130. Left panel: 95th percentile of liquid water for non-raining 100 m clouds (closed circles) and all clouds (diamonds), red and blue denote measurements by two different King probes. Right panel: FSSP and Fast FSSP average drop concentrations for non-raining clouds wetter than the 95th percentile.

Gerber et al., 2008

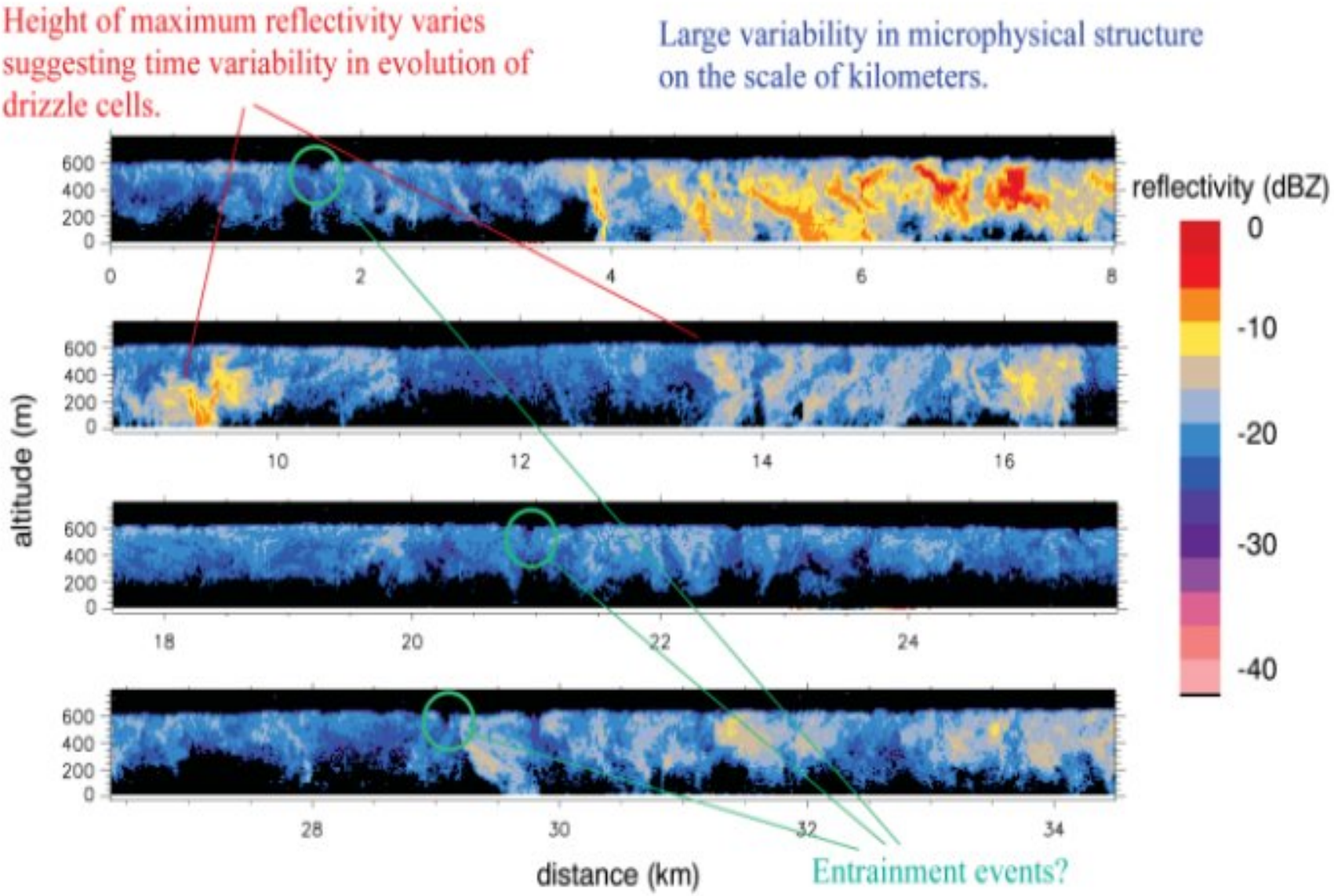

FIG. 5. Radar reflectivity for a segment of RF03. The axis scales are 1:1.

Stevens et al., 2003

Stevens et al., 2003

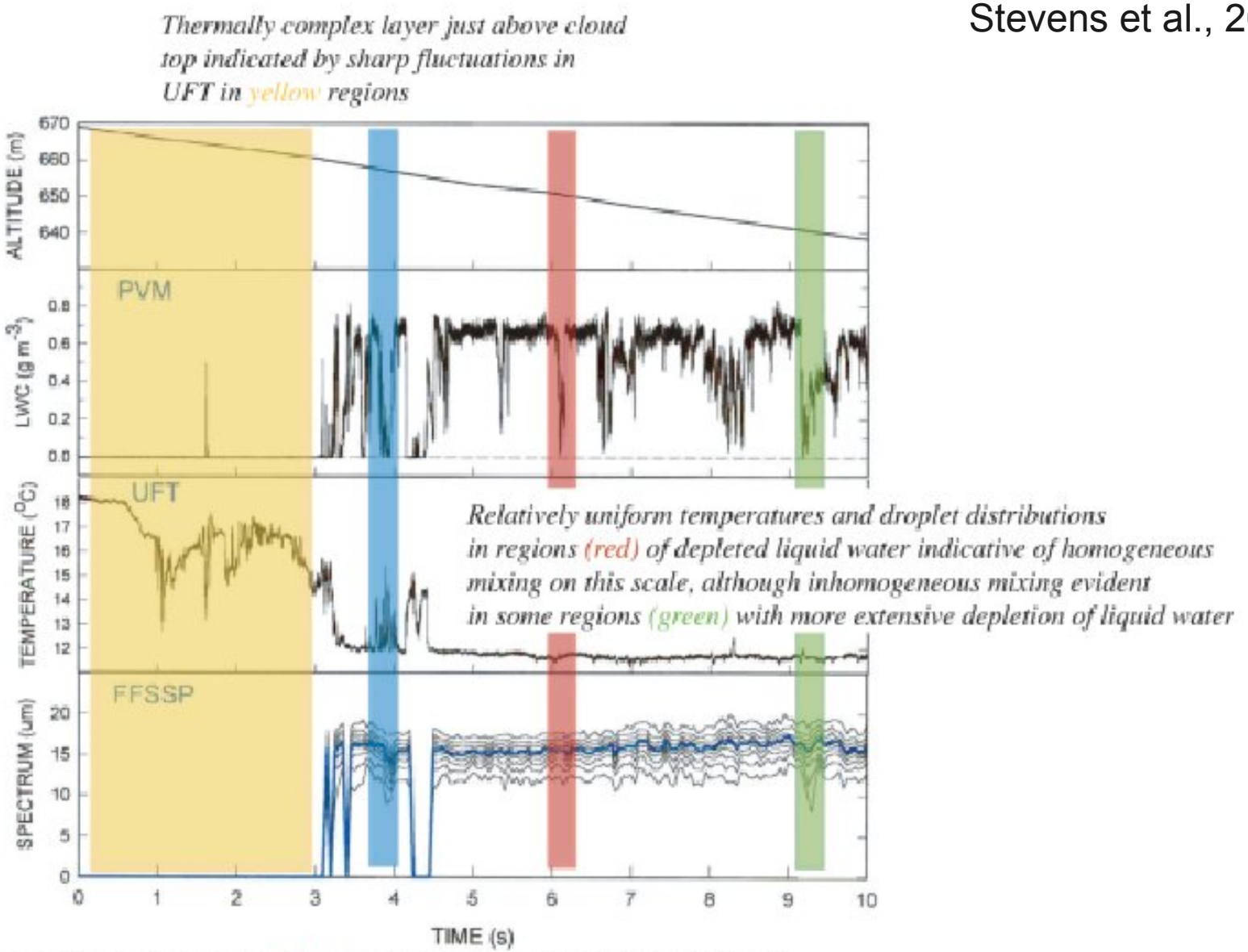

FIG. 7. Comparison of PVM, UFT, and FFSSP ultra-high-rate measurements during the flight of the NSF/NCAR C130 through the top of an unbroken layer of stratocumulus on 12 Jul (start of the 10-s interval is 12:05:38 UTC).

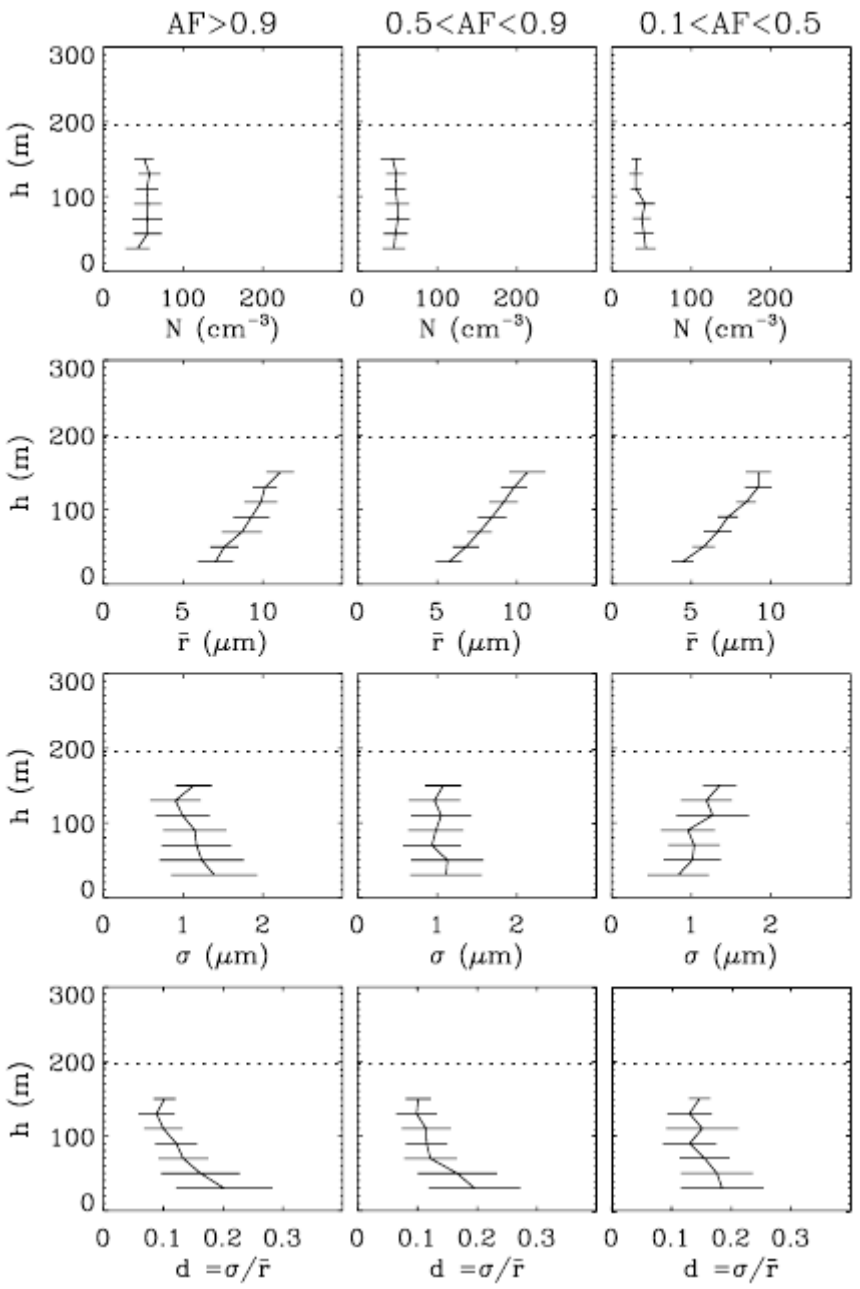

Figure 2. Results for the marine case of June 26.

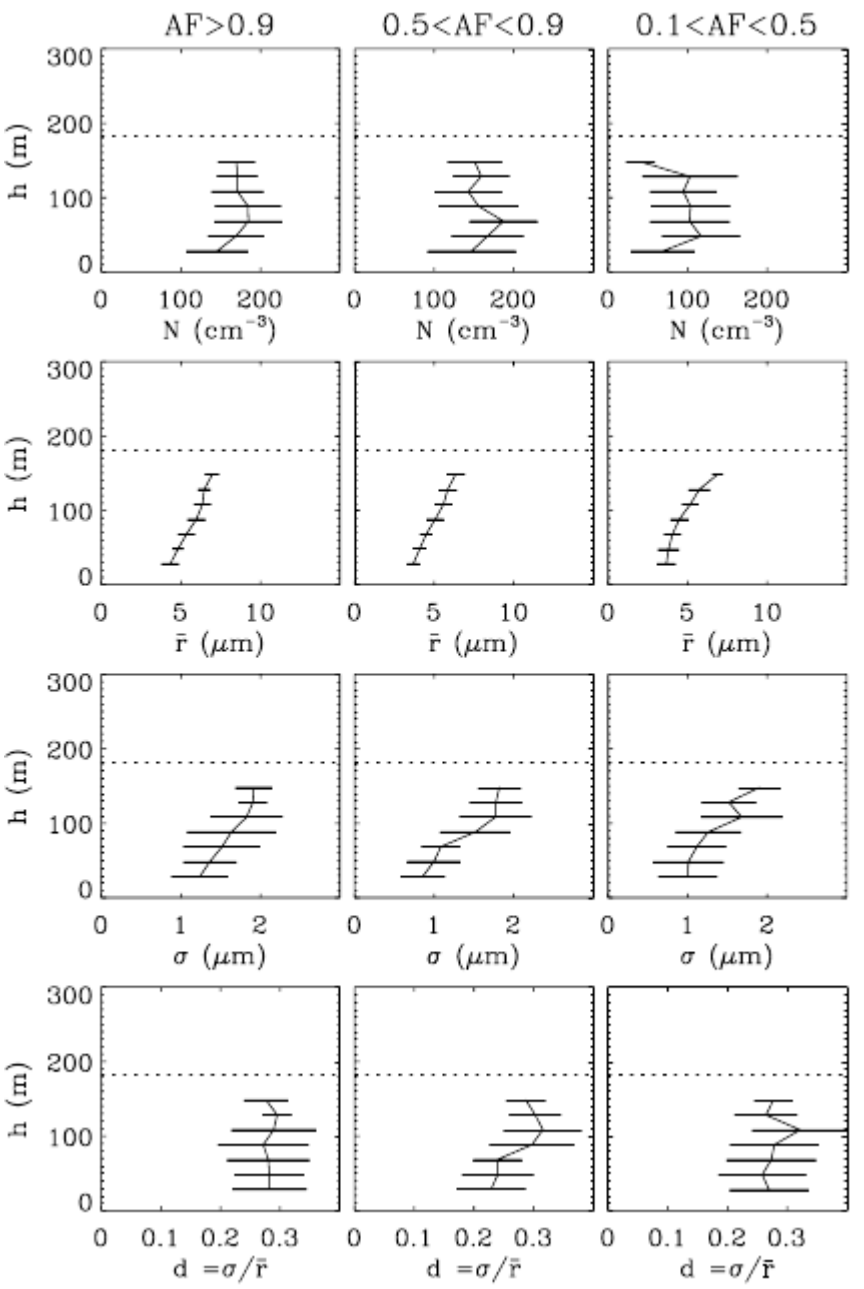

Figure 3. Results for the polluted case July 18.

The 1st, 2nd, 3rd, and 4th row shows the mean droplet concentration N, the mean radius r, the mean standard deviation s, and the mean relative dispersion d, respectively, at different heights above the cloud base. Left, middle, and right columns are for near-adiabatic (AF > 0.9), diluted (0.5 < AF < 0.9) and strongly diluted (0.1 < AF < 0.5) cloud samples, respectively. Horizontal lines represent one standard deviation around the mean value. The dashed line shows the mean height of the cloud top.

Pawlowska, Grabowski and Brenguier, 2006

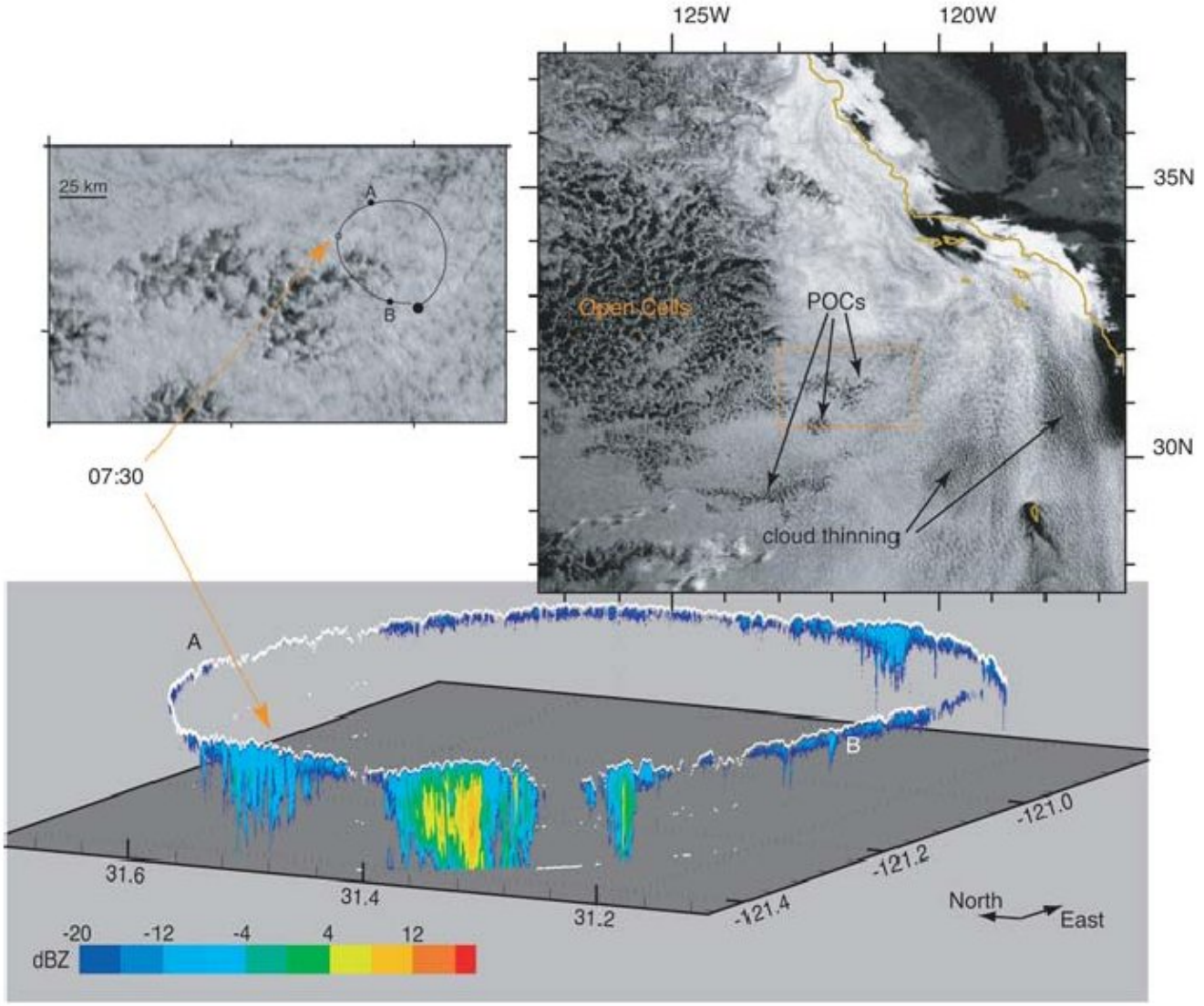

Stevens et al., 2005

FIG 3. (top right) Channel 1 (0.6 μm) reflectance over the northeast Pacific from *GOES-10* at 0730 LT (1430 UTC) for 11 Jul 2002. (top left) Zoomed image of reflectance field from boxed region in regional image; overlaid on this image is a flight segment from RF02 that spans the time of the overpass and from which radar and lidar data is presented in top left panel. The zoomed image highlights a tilde-shaped POC boxed in the image. (bottom) Time–height radar reflectivities filled, with cloud top height as estimated by downward-looking lidar shown by white line. Regions where lidar detects no cloud are shown by a lidar trace at the surface. The time for which the satellite image is valid is indicated on the flight tracks.

Cloud-scale and small-scale turbulence

Entrainment and mixing:
- Cumulus
- Stratocumulus
- Mechanisms for entrainment in clouds

Already partially discussed

Turbulence and cloud microphysics:
- motion of cloud droplets

Droplet size distribution
- Condensational growth and turbulence
- Collisions, coalescence and turbulence
  - Droplet relative velocity
  - Droplet clustering (preferential concentration)
  - Preferential sweeping
- The effect of entrainment on the droplet size distribution
  - Homogeneous and inhomogeneous mixing

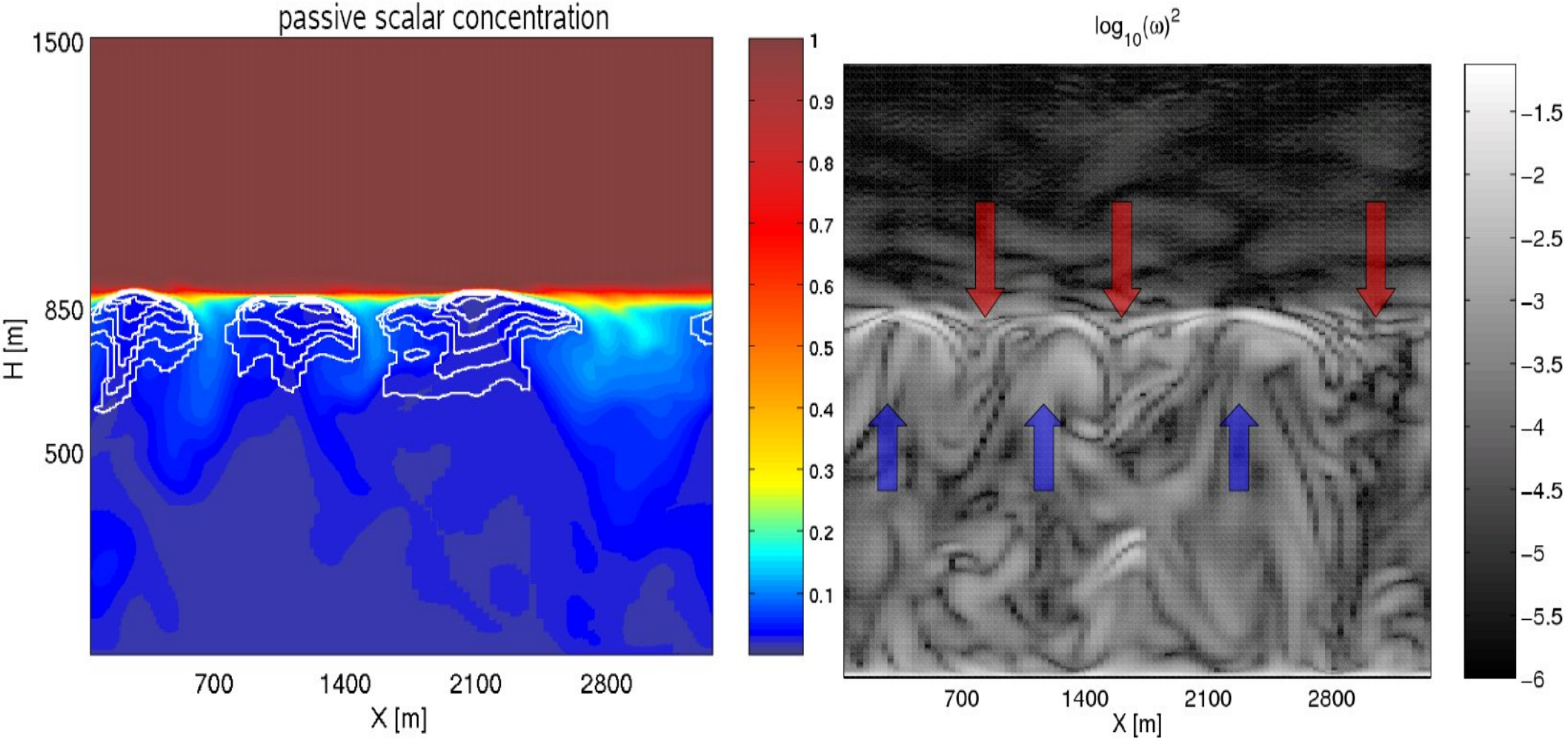

Passive scalar concentration χ (left, cloud water contours shown by white lines) and enstrophy (right), at 6 hours of simulations.

Kurowski, Malinowski, Grabowski 2009

Mixing diagram showing buoyancy (density temperature) of mixture of cloud and free-tropospheric air (upper lines) and cloud and EIL air (lower lines).

Negative buoyancy – below the blue line.

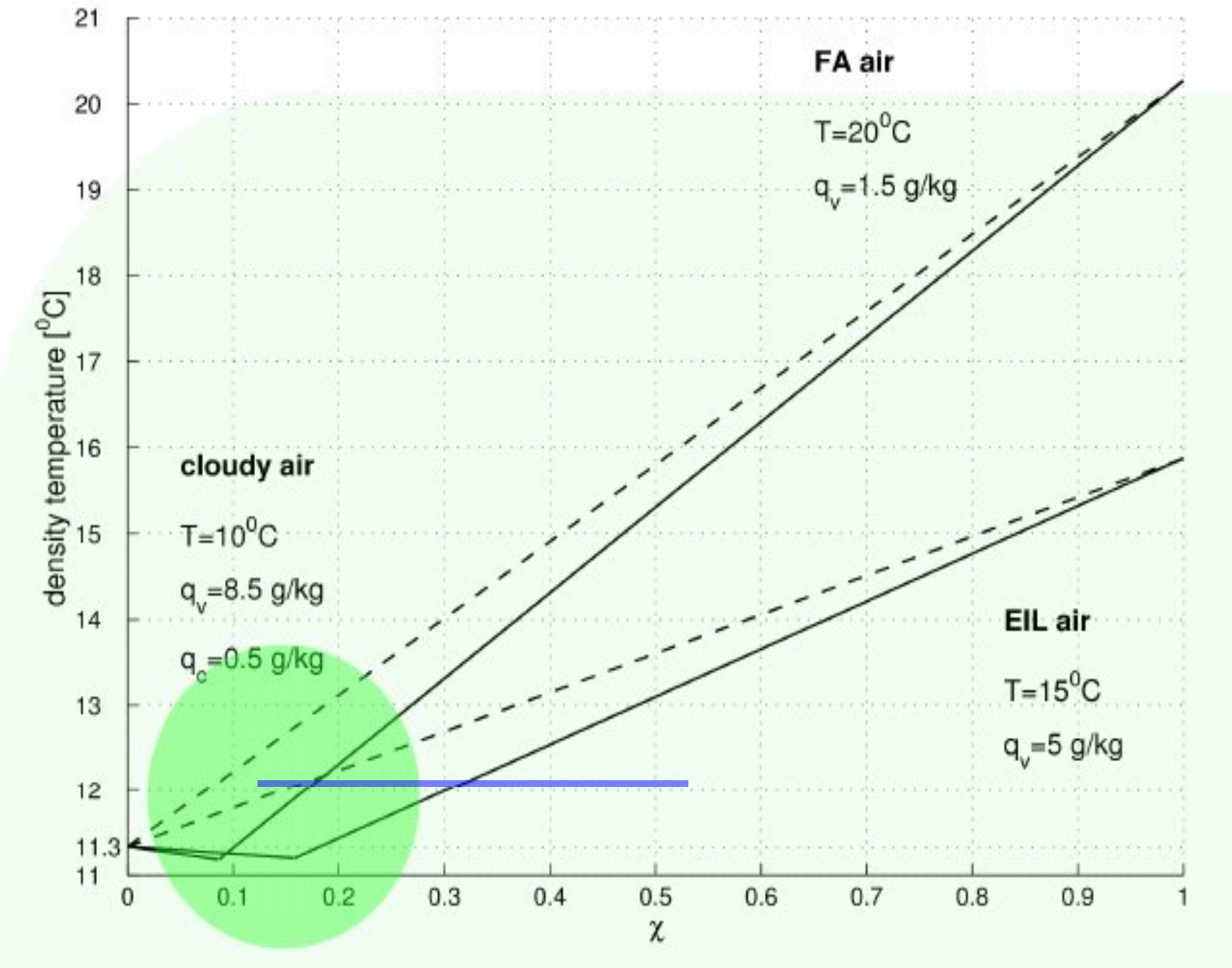

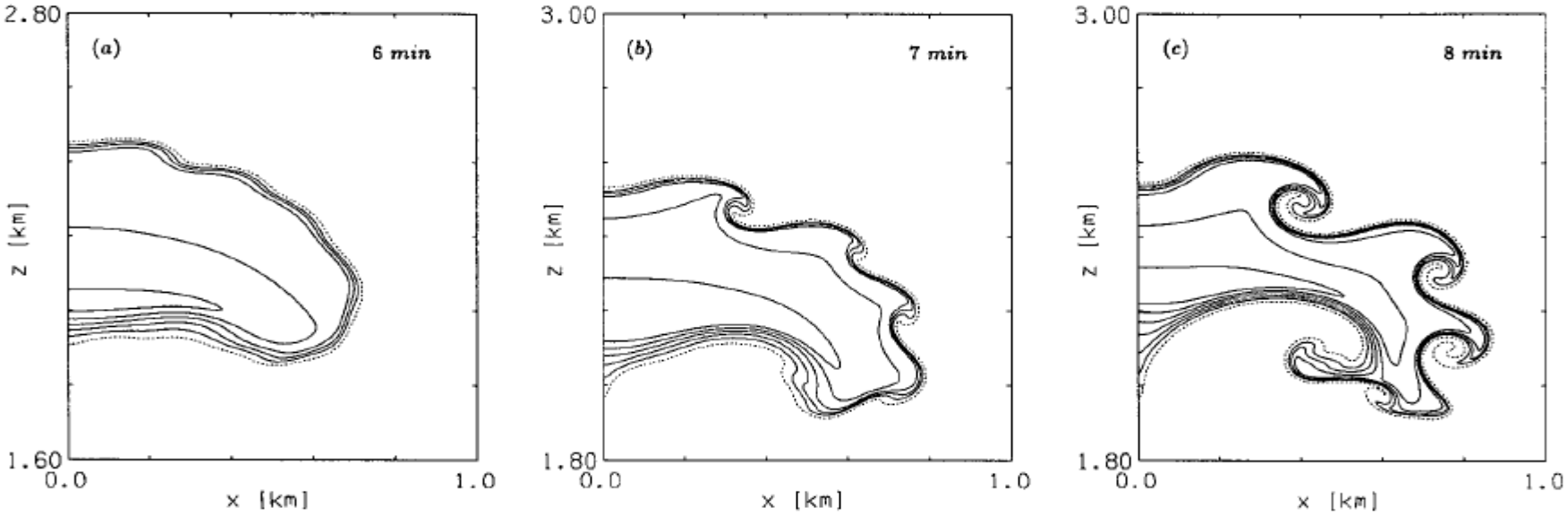

FIG. 19. Isolines of the q_c field at $t = 6$ (a), 7 (b), and 8 min (c) for the simulation of the large thermal with $K = 1$ m^2 s^{-1} and excitation as described in section 5. Contour interval is 0.3 g kg^{-1}.

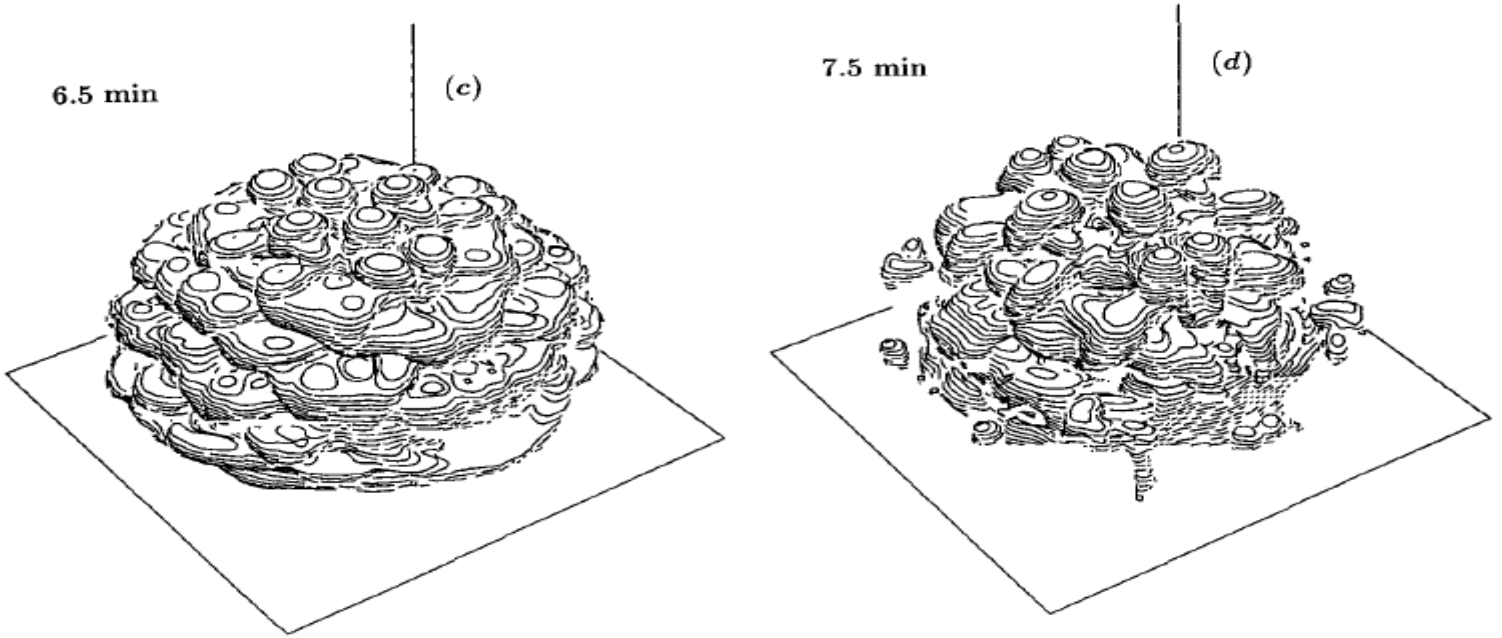

FIG. 4. As in Fig. 3 but for the perturbed 3D3M experiment. Note that data for the quarter of the thermal were used to plot the whole thermal with symmetries as assumed in the experimental setup.

Entrainment as a result of interfacial instabilities: Klaasen, Clark, Grabowski.....
Illustrations from Grabowski and Clark 1991, 1993

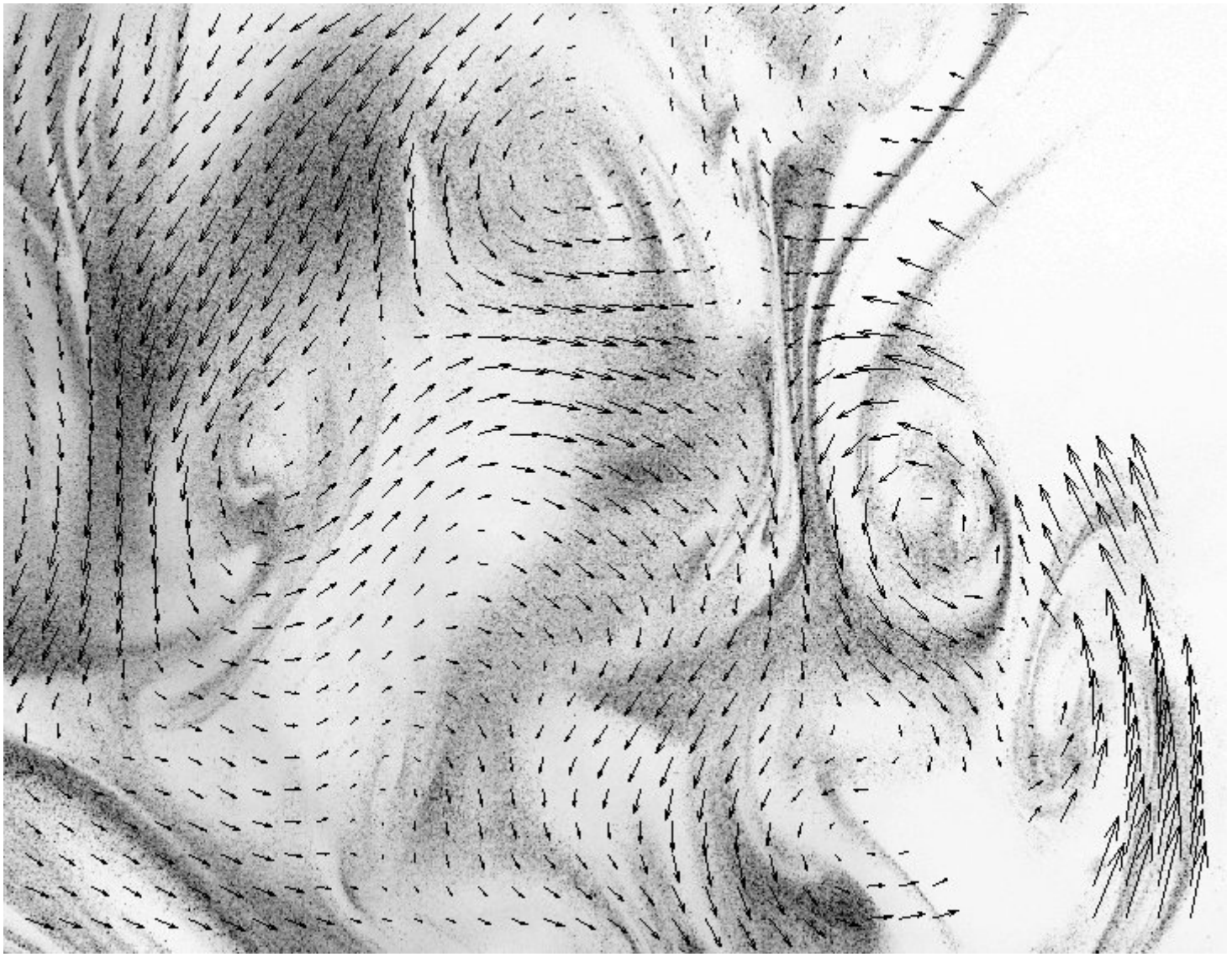

Effects due to turbulence:

preferential concentration,

varoius mechanism of enhanced collisions,

homogeneous vs. inhomogeneous mixing.

Cloud-scale and small-scale turbulence

Entrainment and mixing:
- Cumulus
- Stratocumulus
- Mechanisms for entrainment in clouds

Turbulence and cloud microphysics:
- motion of cloud droplets

Droplet size distribution
- Condensational growth and turbulence
- Collisions, coalescence and turbulence
  - Droplet relative velocity
  - Droplet clustering (preferential concentration)
  - Preferential sweeping
- The effect of entrainment on the droplet size distribution
  - Homogeneous and inhomogeneous mixing

Preferential concentration – enhanced local densities, more probable collisions?

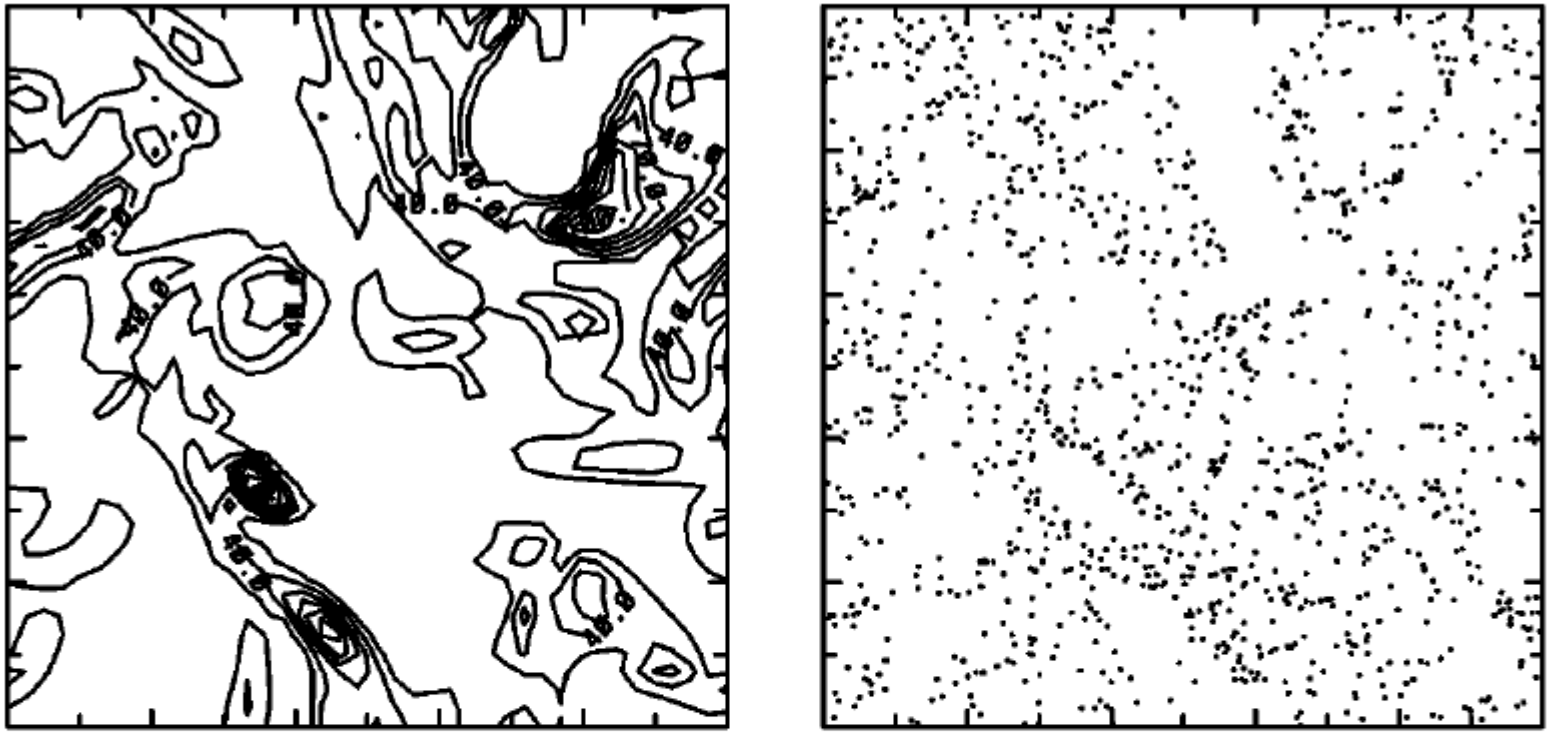

Figure 6 A slice through the computational domain of a direct numerical simulation of homogeneous, isotropic turbulence containing particles. The gravitational acceleration, particle Stokes number, kinetic energy dissipation rate, and Kolmogorov scales are matched to those typically encountered in an atmospheric cloud. Given these scales, the slice is 0.1 m on a side. The *left panel* shows vorticity contours, and the *right panel* shows droplet positions, illustrating the tendency of droplets to form clusters in regions of low vorticity. Figure adapted from Vaillancourt et al. (2002), courtesy of P. Vaillancourt, Meteorological Service of Canada.

(Shaw, 2003)

Stokes law, (after Shaw, 2003):

Fundamental to understanding the influence of turbulence on cloud processes is the motion of an individual cloud droplet. In many basic treatments of cloud processes, droplets are assumed to move with a steady-state fall velocity V_T, but this neglects the contribution of fluid accelerations, which under some flow conditions are of the same order or larger than the gravitational acceleration g. For small cloud droplets, the Reynolds number typically is sufficiently small so that the Stokes drag force is a reasonable approximation. In this limit, Newton's second law for a sphere with velocity $\mathbf{v}$ in a viscous fluid with uniform (but time varying) velocity $\mathbf{u}$ is:

$$\rho_d V_d \frac{d\mathbf{v}}{dt} = 6\pi\mu r\,(\mathbf{u}-\mathbf{v}) + \frac{1}{2}\rho_f V_d\,(\dot{\mathbf{u}}-\dot{\mathbf{v}}) + 6r^2\sqrt{\pi\rho_f\mu}\int_0^t \frac{\dot{\mathbf{u}}(t')-\dot{\mathbf{v}}(t')}{\sqrt{t-t'}}dt'$$
$$+ \rho_d V_d \mathbf{g} + \rho_f V_d\,(\dot{\mathbf{u}}-\mathbf{g})\,. \qquad (11)$$

Here, μ and ρ_f are the dynamic viscosity and density of the surrounding fluid (air), ρ_d is the density of the droplet (water), and $V_d = 4/3\pi r^3$ is the droplet volume. The terms on the right are, in order, the Stokes drag force, the "added mass" force due to acceleration of the surrounding fluid, the Basset "history" force due to diffusion of vorticity from an accelerating particle, the gravitational force, and finally, two terms resulting from the stress field of the fluid flow acting on the particle (including a shear stress term and a pressure gradient or buoyancy term).

Lagrangian accelerations are dominant at the smallest spatial scales of the flow, corresponding to the dissipation or Kolmogorov scale λ_k . Because it is assumed that properties of the dissipation scale eddies depend only on v and it follows that these eddies will have a timescale $\tau_k = (v/\varepsilon)^{1/2}$, where ε is the TKE dissipation rate.

Therefore the Stokes number for droplets in a turbulent flow is:

$$S_d = \frac{\tau_d}{\tau_k} = \frac{2\rho_d \epsilon^{1/2} r^2}{9\rho_f \nu^{3/2}}.$$

For typical cloud conditions ($\varepsilon \sim 10^{-2}$ m^2 s^{-3} , $v \sim 10^{-5}$ m^2 s^{-3}) and $r \sim 10^{-5}$ m, the Stokes number is close to the order $S_d \sim 10^{-1}$.

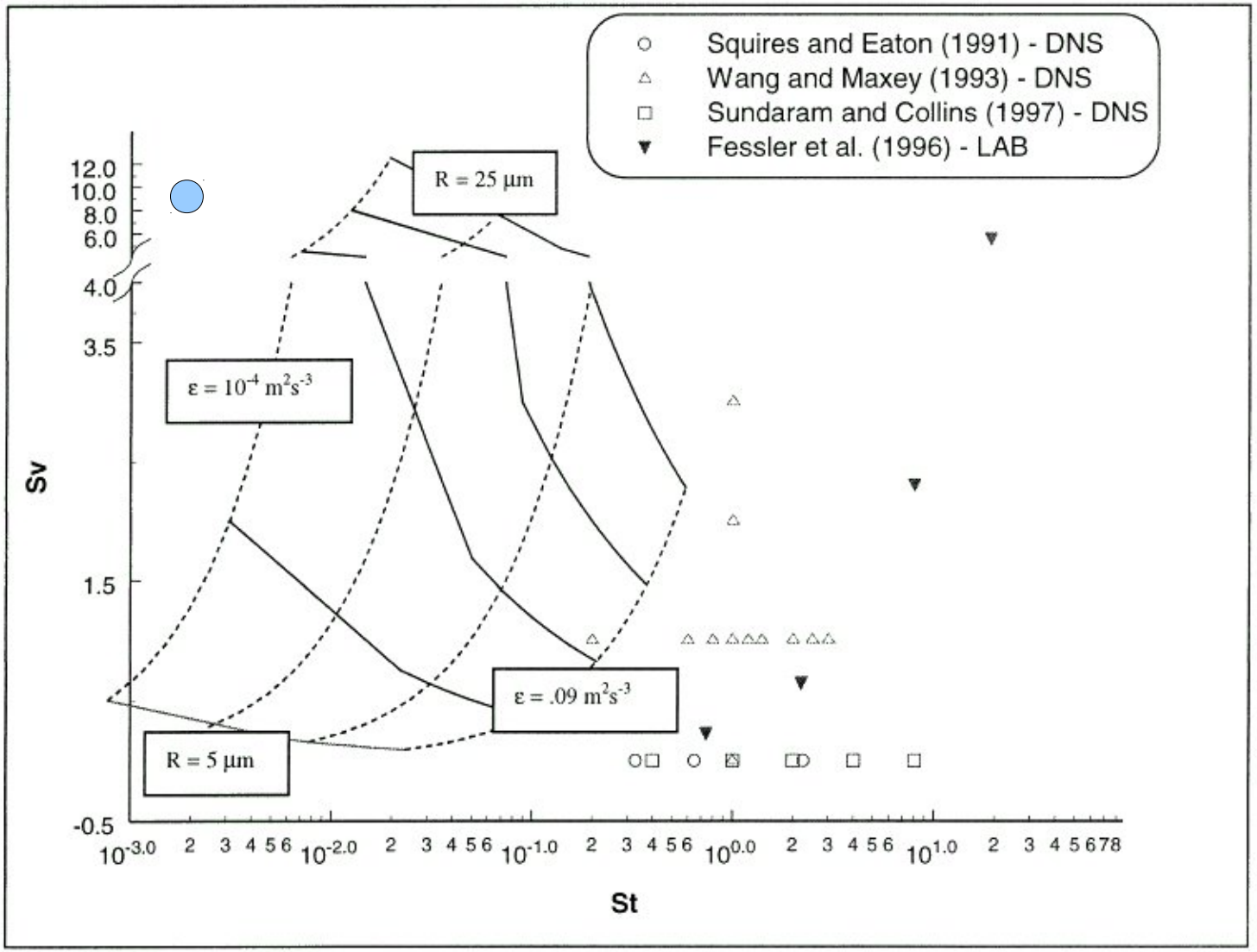

Vaillancourt and Yau, 2000

Stokes number is the ratio between the particle's response time (τ_P) and a characteristic timescale of the flow (τ_F), $St = \tau_P/\tau_F$

Velocity ratio: terminal velocity of the particle nondimensionalized by the Kolmogorov velocity

$Sv = V_T / v_\eta$

FIG. 1. Stokes number (S_t)–velocity ratio (S_v) diagram showing location of direct numerical simulations (DNS) and laboratory experiments (LAB) for particles in 3D turbulence. The S_t–S_v region for cloud droplets of 5–25-μm radius is shown for an appropriate range of eddy dissipation rates (10^{-4}–0.09 m^2 s^{-3}). The dashed lines are for constant eddy dissipation rates (10^{-4}, 10^{-3}, 10^{-2}, and 0.09 m^2 s^{-3}) and radii varying from 5 to 25 μm, while the solid lines are for constant radii (5, 10, 15, 20, and 25 μm).

EXAMPLE:
droplets in
prescribed vortex
flow

Bajer et al., 2000

$$m\frac{d\mathbf{V}}{dt} = -6\pi R\mu(\mathbf{V}-\mathbf{u}) + m\mathbf{g}, \qquad (1)$$

where μ is the viscosity of the air, $\mathbf{g}$ is gravitational acceleration and $\mathbf{u}$ is a the air flow field in the cloud which for the sake of this problem we assume to be prescribed, i.e. unaffected by the droplets. Although droplets are passively carried by the air they are not passive tracers, as the trajectories they trace out are different from the paths of the fluid elements.

Let (r, θ, z) be polar co-ordinates with the Oz direction along the vortex axis inclined at an angle ϕ from the vertical. In this frame of reference the gravity force takes the form

$$\mathbf{g} = g\sin\phi\cos\theta\hat{\mathbf{e}}_r - g\sin\phi\sin\theta\hat{\mathbf{e}}_\theta - g\cos\phi\hat{\mathbf{e}}_z. \qquad (2)$$

The velocity field $\mathbf{u}$ is a sum of the flow due to the uniform irrotational straining flow, and the flow due to an axisymetric vortex having azimuthal velocity $u(r)$,

$$\mathbf{u} = -\tfrac{1}{2}\alpha r\hat{\mathbf{e}}_r + \alpha z\hat{\mathbf{e}}_z + u(r)\hat{\mathbf{e}}_\theta. \qquad (3)$$

The equation (1) takes the form

$$\tau_d \left(\frac{dV_r}{dt} - \frac{V_\theta^2}{r} \right) = - \left(V_r + \tfrac{1}{2}\alpha r \right) + V_g \sin\phi \cos\theta, \quad (4)$$

$$\tau_d \left(\frac{dV_\theta}{dt} + \frac{V_\theta V_r}{r} \right) = - \left(V_\theta - u(r) \right) - V_g \sin\phi \sin\theta, \quad (5)$$

$$\tau_d \frac{dV_z}{dt} = - \left(V_z - \alpha z \right) - V_g \cos\phi, \quad (6)$$

where $\tau_d = m/(6\pi R\mu)$ is the characteristic time of the droplet response to the changes in fluid velocity and $V_g = g\tau_d$ is the terminal velocity of the gravitational settling.

In the following we will consider a model vortex with total circulation Γ and gaussian distribution of vorticity. The azimuthal velociy $u(r)$ is given by

$$u(r) = \frac{\Gamma}{2\pi r}\left(1 - \mathrm{e}^{-(r/2\delta)^2}\right), \quad \delta = N\sqrt{\nu/\alpha}. \quad (7)$$

Here the dimensionless number N is the ratio of the vortex radius δ and the radius of the familiar Burgers vortex, an exact steady solution of the Navier-Stokes equation likely to be a good model of the small-scale coherent structures in turbulence.

In the Stokes regime (1) droplets of radius R adapt their speed to that of ambient flow on the time-scale

$$\tau_d = (2\rho_w R^2)/(9\mu), \tag{8}$$

where ρ_w is the density of water and μ is the viscosity of air and the corresponding length scale is equal

$$S = \sqrt{\Gamma \tau_d / 2\pi}. \tag{9}$$

The motion along the vortex axis separates and in dimensionless units equations (4-5) governing the motion in the vertical plane take form

$$\ddot{r} - r\dot{\theta}^2 = -\tfrac{1}{2} L_1 r - \dot{r} - L_2 \sin\theta, \tag{10}$$

$$2\dot{r}\dot{\theta} + r\ddot{\theta} = r^{-1} - r\dot{\theta} - L_2 \cos\theta, \tag{11}$$

where

$$L_1 = \alpha \tau_d, \quad L_2 = g\tau_d^2 (2\pi/\Gamma\tau_d)^{1/2} \tag{12}$$

are two non-dimensional numbers characterising the droplet.

Equations (10-11) have one stable fixed point when $L_1 < L_2^2$ and one limit cycle otherwise. Small droplets tend to the limit cycle and keep circulating around the vortex axis. Large droplets move towards the fixed point (figure 1).

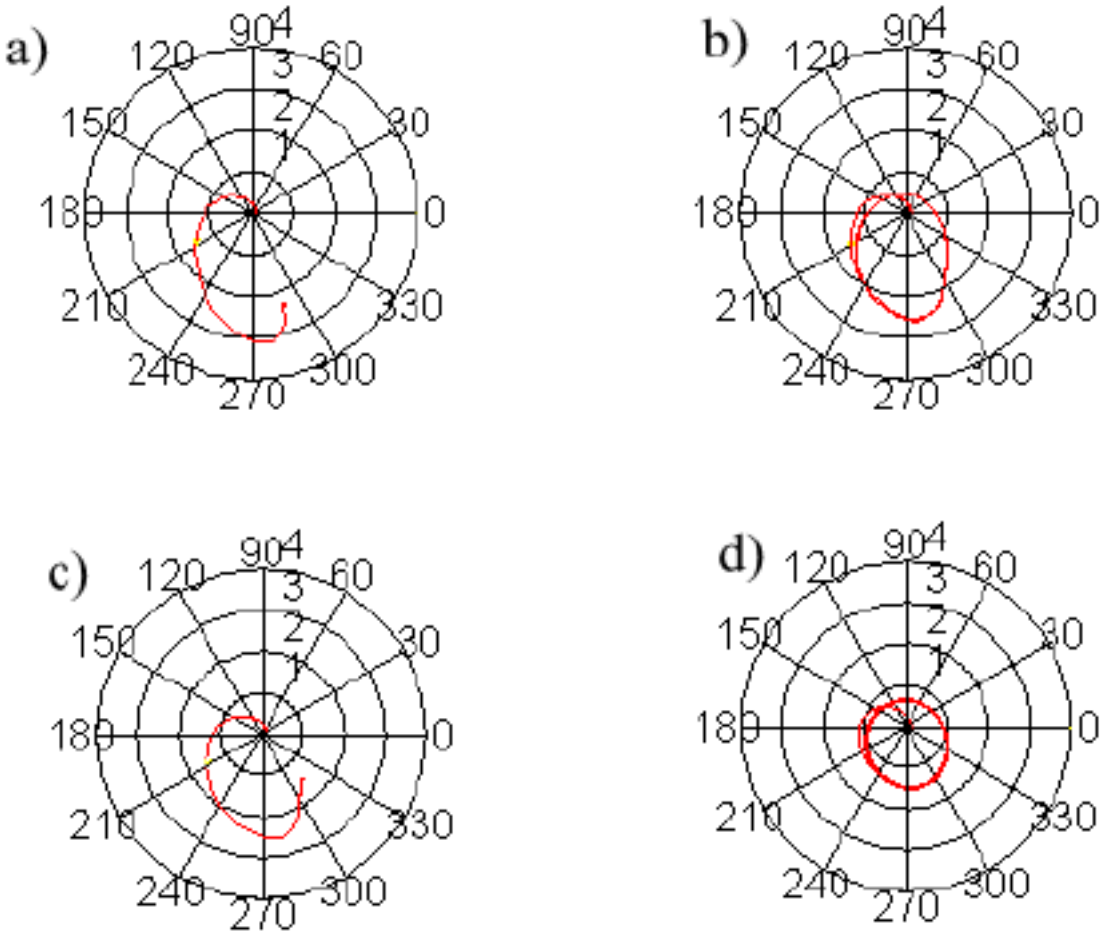

Figure 1: The trajectories of droplets with L_1 / L_2^2 equal a) 0.8; b) 1.004; c) 1; d) 2.

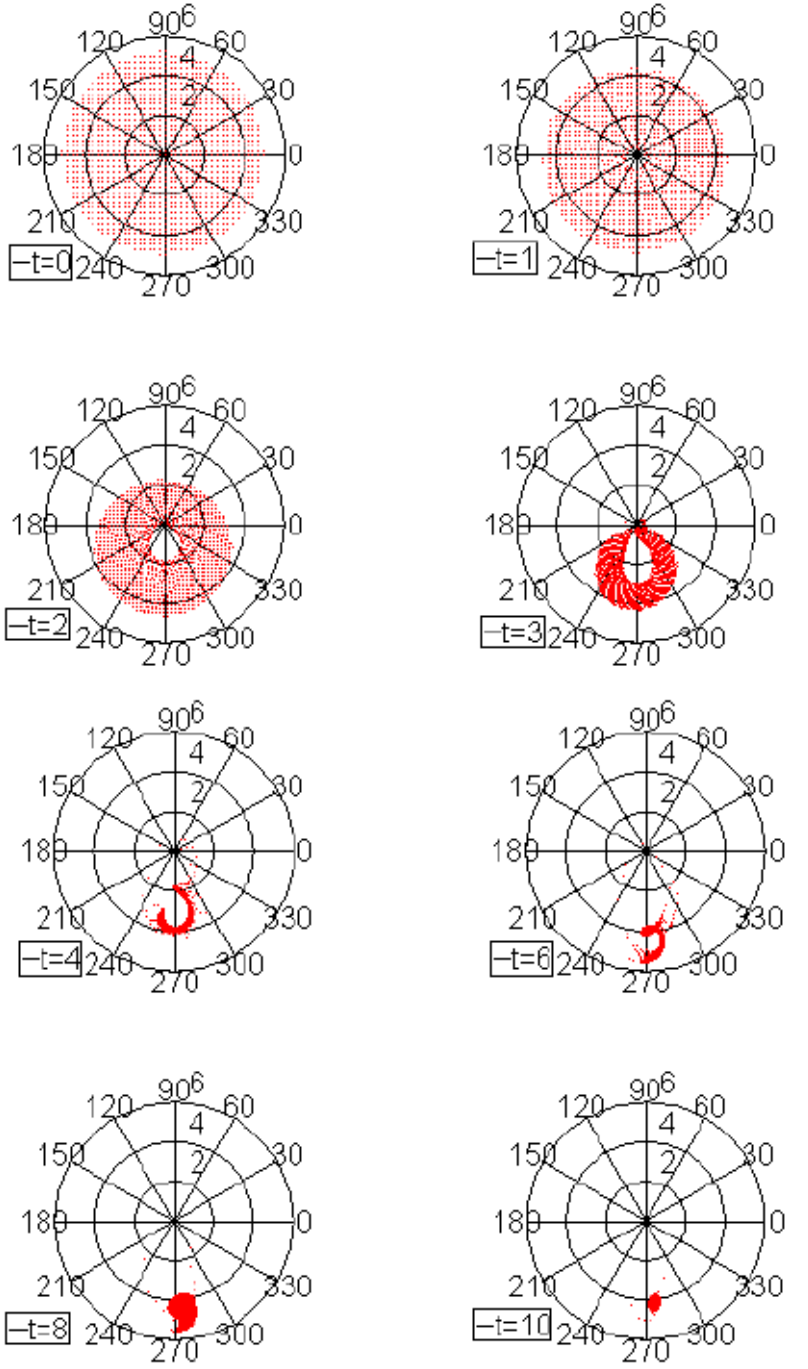

Figure 2: Temporal evolution of the distribution of identical droplets near a horizontal vortex with axial stretching.

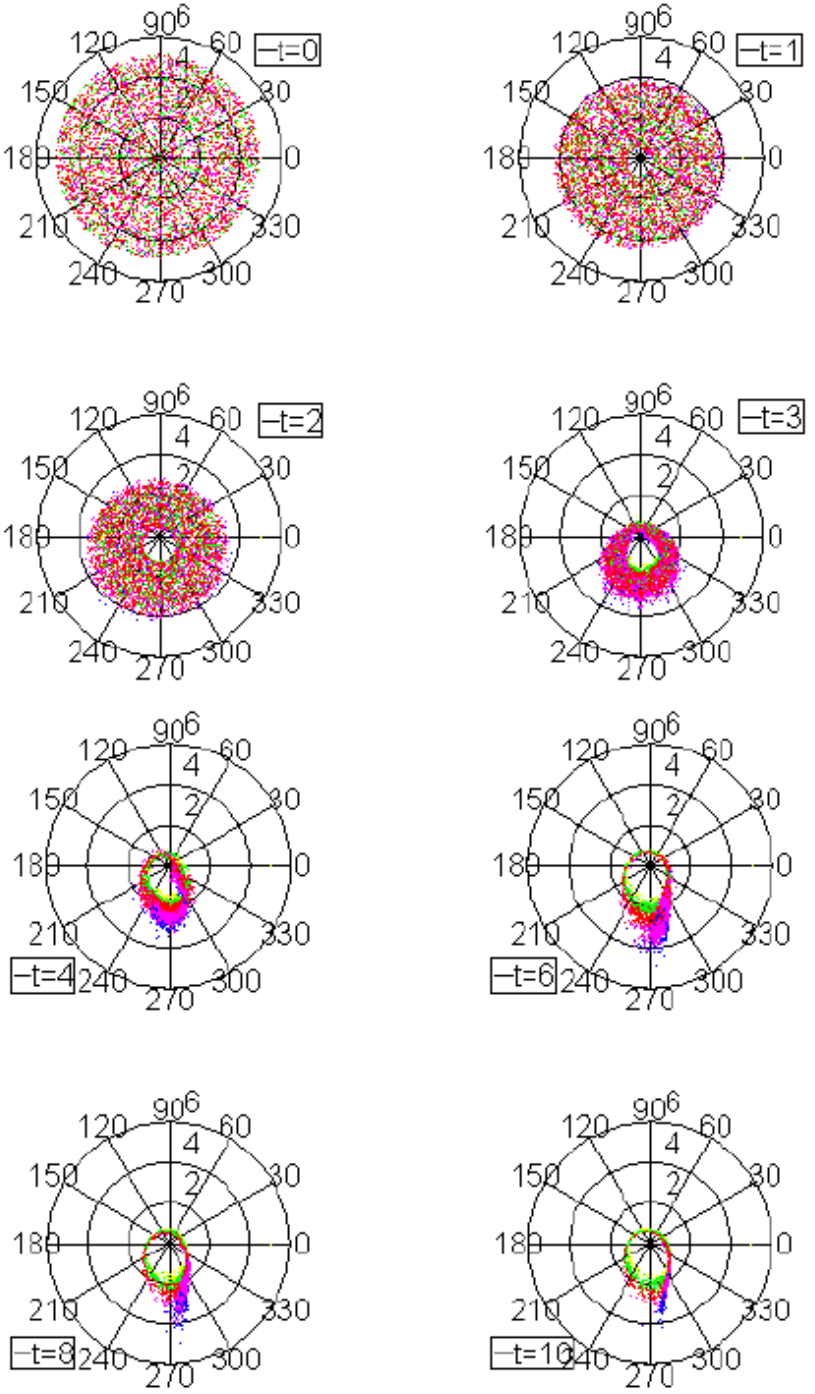

Figure 4: Temporal evolution of the distribution of droplets with gaussian spectrum near a horizontal vortex with axial stretching.

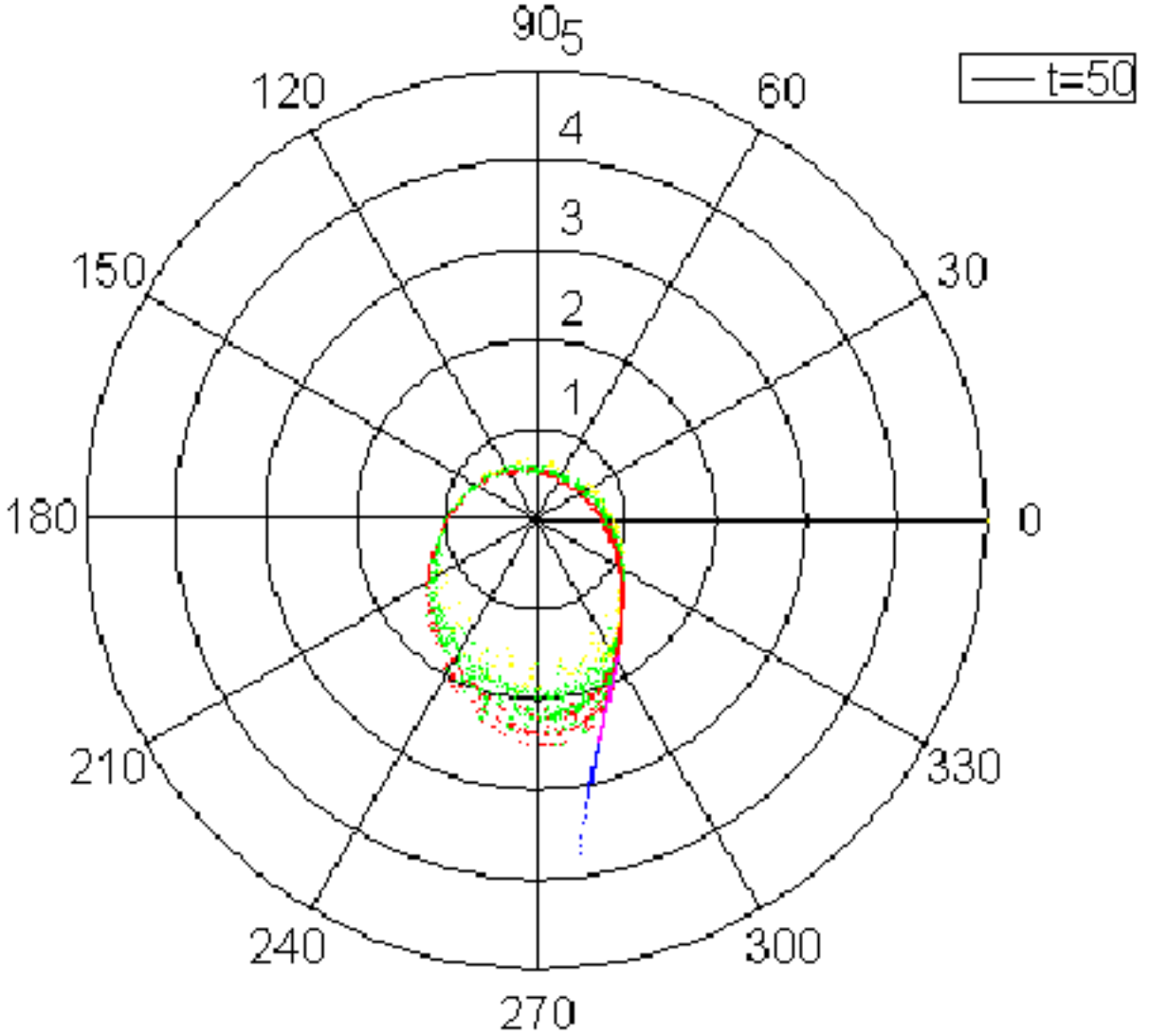

Figure 5: Distribution of droplets with gaussian spectrum after 2.5 turnover times of the vortex. Initial distribution was spatially uniform.

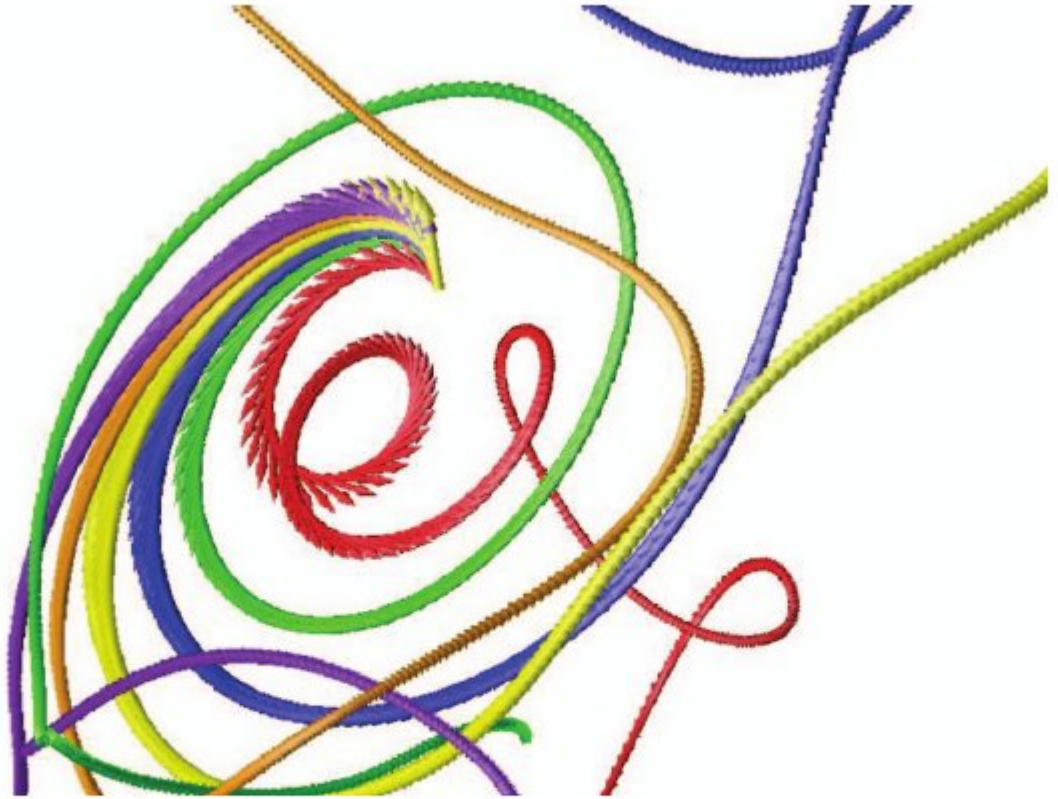

FIGURE 1. – *Particles with different inertia released at the same position and inside a small scale vortical structure of the fluid. The neutrally buoyant particles (red) remain strongly trapped, while particles with higher and higher inertia, respectively greeen, blue, yellow etc, are less and less sensitive to small scale vorticity.*

F.Toschi

Cloud-scale and small-scale turbulence

Entrainment and mixing:
- Cumulus
- Stratocumulus
- Mechanisms for entrainment in clouds

Turbulence and cloud microphysics:
- motion of cloud droplets

Droplet size distribution
- Condensational growth and turbulence
- Collisions, coalescence and turbulence
  - Droplet relative velocity
  - Droplet clustering (preferential concentration)
  - Preferential sweeping
- The effect of entrainment on the droplet size distribution
  - Homogeneous and inhomogeneous mixing

Length scales associated with condensational growth of droplets.

The condensational growth of droplets is characterised by vapour pressure and temperature gradients in the ambient air. In the classical theory of droplet growth by water vapour diffusion, ambient conditions are defined by prescribed fields far from an isolated droplet (infinity). Imposing them at a radius similar to the mean distance between droplets does not result in significant modifications .

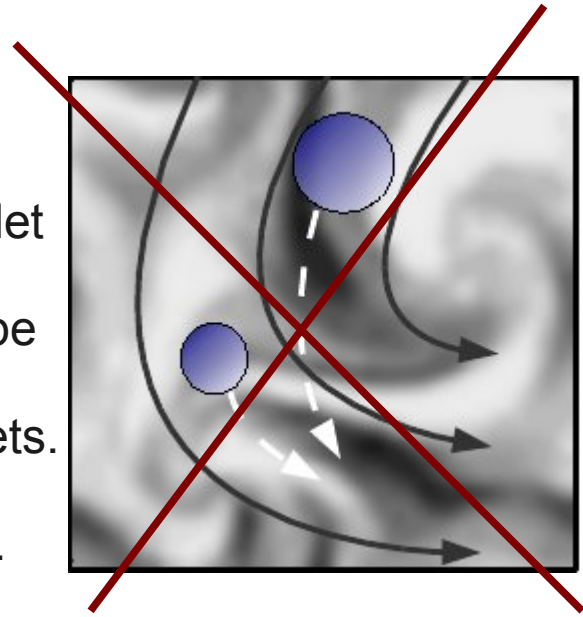

However, when the growth of an ensemble of droplets in turbulent air is considered, the temperature and the moisture fields away from the droplet may vary considerably.
Following Vaillancourt et al. (2001) we define the ambient conditions to be the moisture and temperature fields in the vicinity of a given droplet averaged over the volume defined by the mean distance between droplets. This simplification is frequently applied in numerical models of droplet condensation in turbulence (e.g. Celani et al., 2005, 2007; Lanotte et al. 2009).

Most studies of the growth of an ensemble of droplets in cloud physics neglect the direct interaction between droplets. Justification is based on the argument that the mean distance between cloud droplets (~ 2mm for a typical concentration of 100 cm^{-3}) is at least an order of magnitude larger than the distance (~ 10a or less) affected by the variation of moisture and temperature. Thus, the volume of air occupied by a single cloud droplet is much larger than the volume affected by variations in the moisture and temperature due to cloud droplet growth.

After Devenish et al., 2010

Time scales associated with condensational growth of droplets

There are a number of **time scale**s associated with the condensational growth of cloud droplets.
The first is associated with the diffusional growth of an isolated droplet and in typical conditions **is less than 1×10^{-3} s**.

Another **time scale** occurs when the boundary conditions for water-vapour concentration and temperature at the surface of the droplet are not assumed constant. During condensation water vapour diffuses onto the surface of the droplet, latent heat is released, and consequently **the surface temperature (the psychometric temperature) of the droplet changes**. The **relaxation time** associated with this process lies typically between **5×10^{-4}s and 1×10^{-2}s for droplet radii between 5 μm and 25 μm**) and is therefore the slowest time scale associated with the condensational growth of a droplet.
Vaillancourt et al. (2001) showed that, for a=20μm and ε=100 cm^2 s^{-3} , the ratio of this time scale to fastest time scale associated with changes to the ambient conditions due to turbulence (either τ_η or τ_v) is much less than one and the assumption of a steady-state distribution of water-vapour concentration and temperature is valid.

Numerical simulations byf Celani et al. (2005, 2007), Lanotte et al. (2009) , Sidin et al., (2009) suggest that cloud droplet spectra can be broadened during condensation, which is different from simulations of Vaillancourt et al. (2002) and from the measurements in real clouds (as we can interpret them).

Collisions, coalescence and turbulence

The collision and coalescence of droplets in a turbulent flow are governed by
(i) geometric collisions due to droplet-turbulence interactions;
(ii) collision efficiency due to droplet-droplet interactions and
(iii) coalescence efficiency due to droplet surface properties.

In practice, it is difficult to distinguish between collision and coalescence and the experimentally measurable quantity is collection efficiency defined as the ratio of the actual cross-section for droplet coalescence to the geometric cross-section.

Geometric collisions
DNS results (e.g. Franklin et al. 2007; Ayala et al. 2008a) show that **turbulence can increase the collision kernel relative to the case of stagnant air by two effects:**

droplet relative velocity

droplet clustering.

Turbulence may also affect the droplet relative velocity through preferential sweeping whereby droplets bias their downward trajectories towards regions of higher turbulence thus increasing their terminal velocities relative to still air.

In multidisperse suspensions, $|w_{12}|$ is always larger than its monodisperse counterpart. This can be understood by considering a limiting case of monodisperse suspension, in the absence of gravity. For low St, velocities of equally sized droplets are strongly correlated, both with the fluid and each other.
As St increases, the correlation of the droplets with the flow and each other decreases and $|w_{12}|$ increases. However, for St>>1, droplets respond slowly to changes in the fluid velocity and $|w_{12}|$ decreases.

For multidisperse droplets, the velocities of the droplets decorrelate more rapidly than the equivalent monodisperse cases since the droplets with different inertia respond differently to changes in the flow.

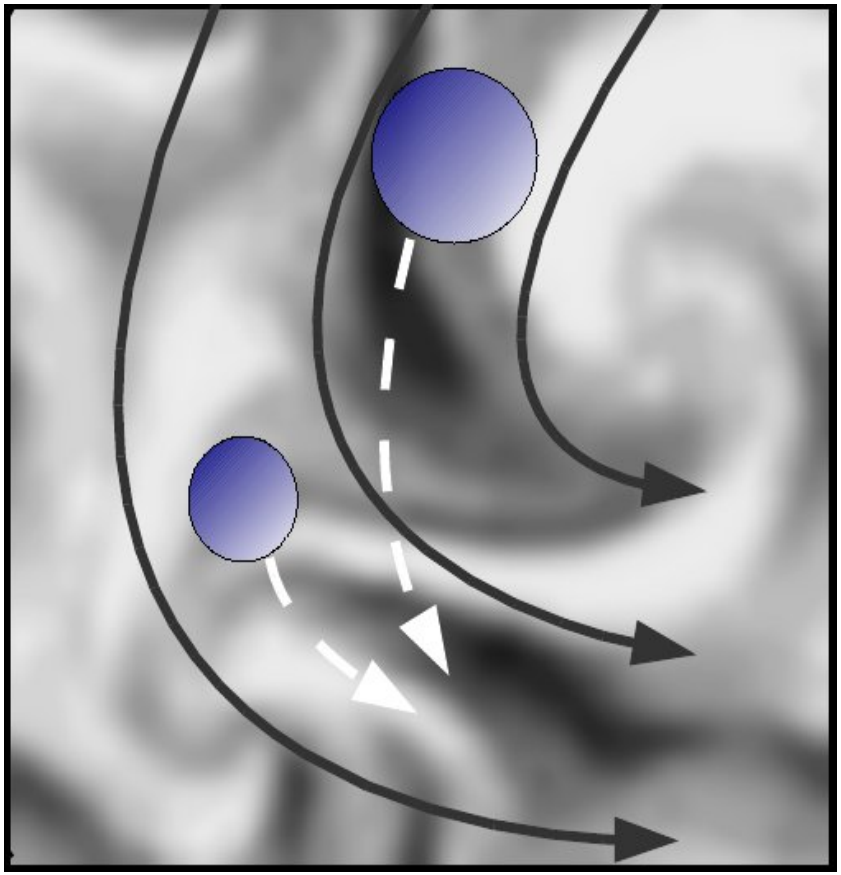

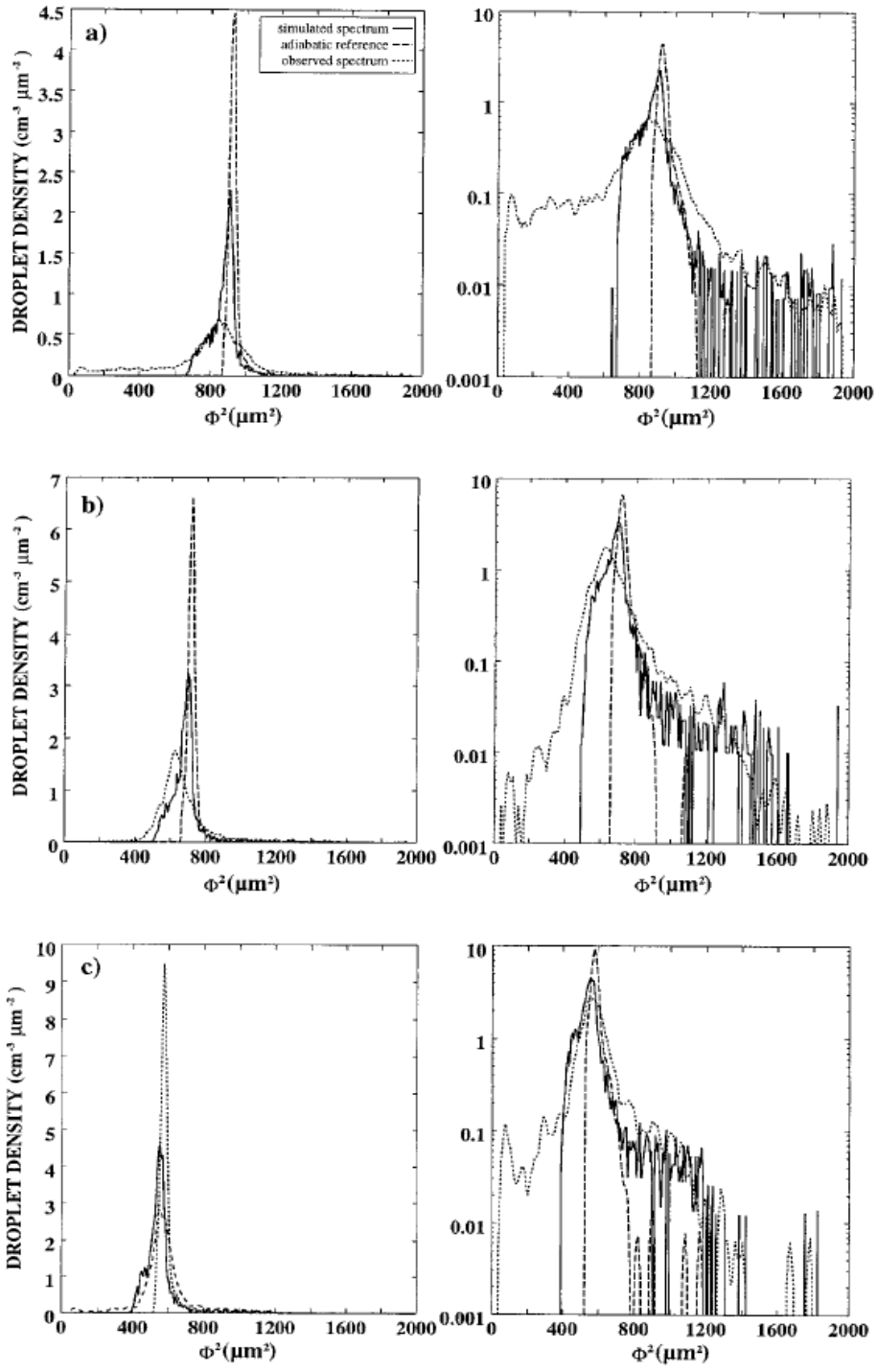

FIG. 4. Three examples of the comparison between an observed spectrum (dotted line) and the adiabatic reference (dashed line), after instrumental broadening by the Fast-FSSP simulator (solid line). The total droplet number concentrations are, respectively, 225 (a), 329 (b), and 455 cm^{-3} (c).

With the improved size and spatial resolutions of the Fast-FSSP measurements it has been possible to identify very narrow spectra in most of the cloud traverses performed at the upper levels of cumulus clouds during the SCMS experiment. These spectra are much narrower than previously measured with the standard probe. The regions of narrow spectra show characteristics close to the adiabatic reference, such as LWC values slightly lower than the adiabatic value at that level and values of droplet concentration close to the maximum value within the cloud traverse. The spectra observed in these regions are narrow but still broader than the adiabatic reference.

The high concentration densities of droplets with diameter smaller than the mode can be attributed to partial evaporation of some droplets resulting from the mixing with dry air. The occurrence of this process is attested by the slightly subadiabatic values of LWC.

Chaumat and Brenguier, 2001

Preferential concentration – enhanced local densities, more probable collisions?

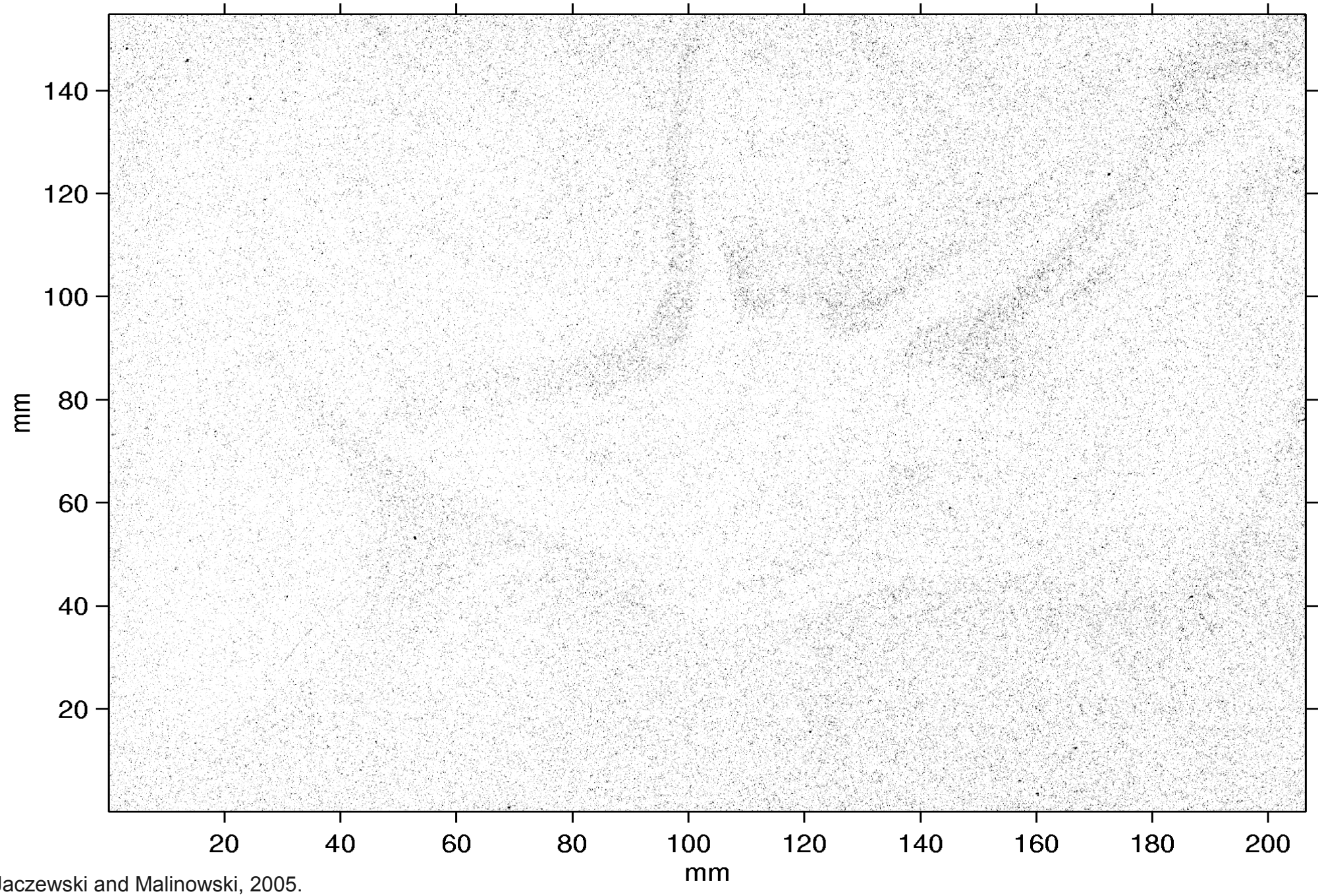

Jaczewski and Malinowski, 2005.

Observations of droplet clustering in real clouds remain ambiguous which has led some authors to question its importance in real clouds.

Moreover, DNS of sedimenting droplets has shown that turbulent enhancement of collision rates occurs primarily through changes to the droplet relative velocity and the collision efficiency.

Nevertheless, some argue that the vortex tubes that are associated with small-scale turbulence at high Reynolds numbers persist for long and droplets with a considerable range of St are able to spin out of the vortex.

The importance of intermittency in potentially increasing droplet clustering has also been raised by Falkovich et al. (2002)who based on theoretical arguments claim that clustering can increase collisions by a factor of 10.

Without a clear theoretical basis for the R_λ -dependence of clustering, which will remain valid in the large-R_λ limit, it is likely that these arguments will continue.

Small-scale turbulence/rain formation in clouds – a subgrid scale process

a) inadequate measurement capabilities
(resolution problem, different sampling volumes of various sensors)
b) subgrid-scale processes in cloud resolving and LES simulations.

Closing the gap in resolved scales

a) DNS and particles in turbulence;
b) laboratory experiments with particle tracking and collisions.
c) in situ efforts.

Issues

a) (almost) no combined measurements of microphysics,
turbulence and dynamics in small-scales;
b) problems with the statistical interpretation of data from measurements;
c) unclear subgrid-scale parameterizations in cloud simulations.


UFT-F
PVM
FFSSP

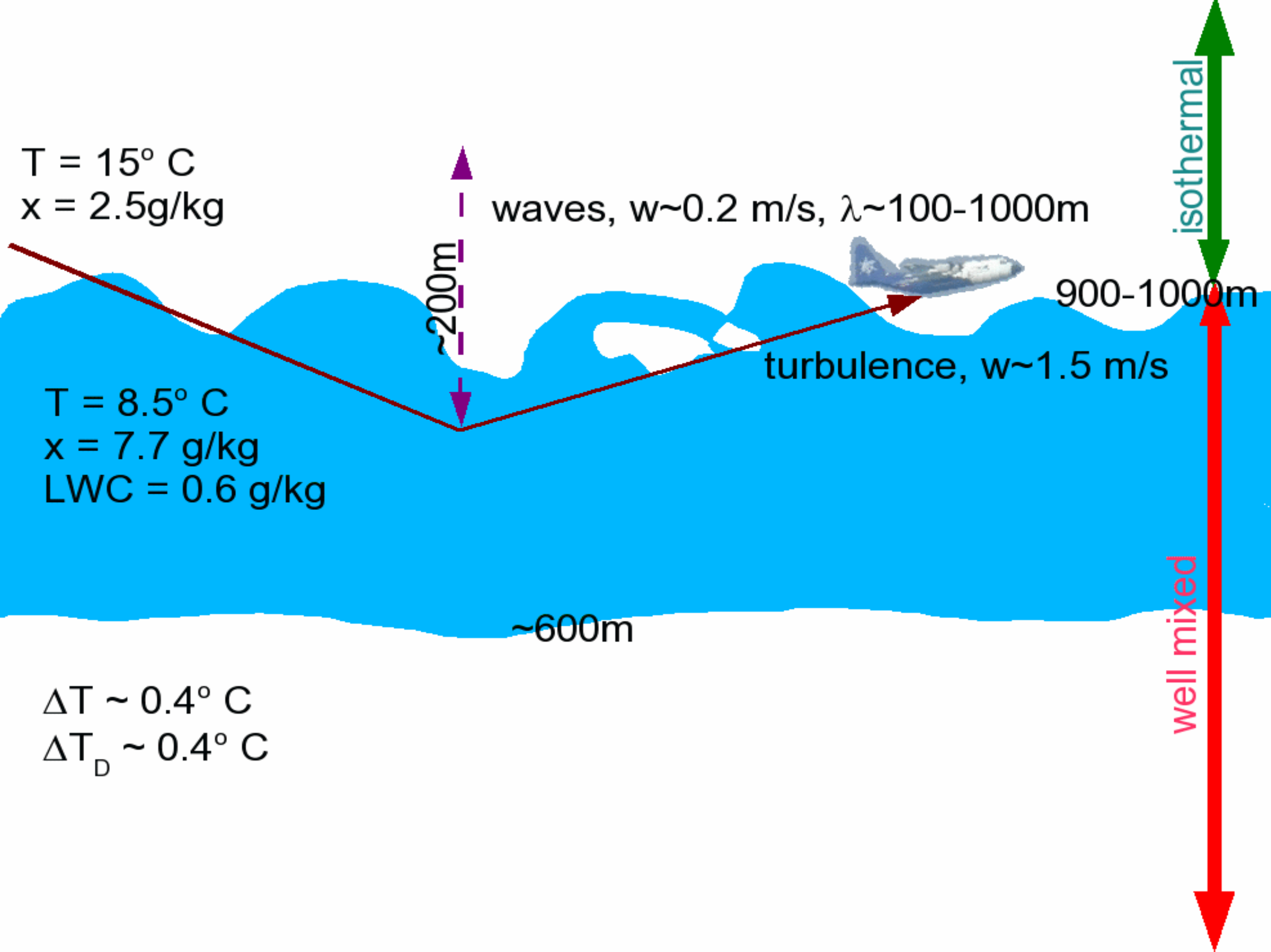
T = 15° C
x = 2.5g/kg
waves, w~0.2 m/s, λ~100-1000m
~200m
isothermal
900-1000m
turbulence, w~1.5 m/s
T = 8.5° C
x = 7.7 g/kg
LWC = 0.6 g/kg
~600m
well mixed
ΔT ~ 0.4° C
ΔT_D ~ 0.4° C

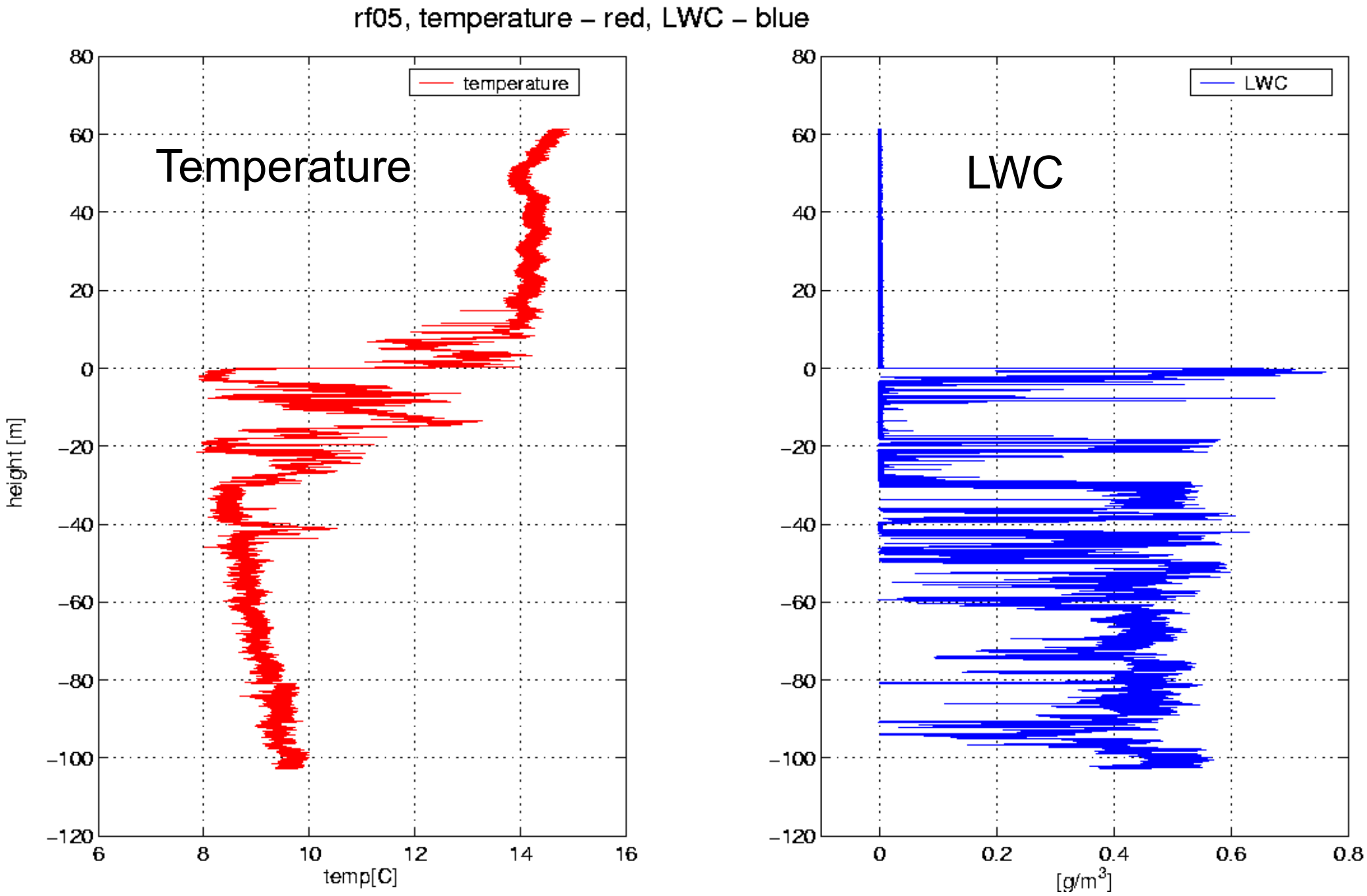
rf05, temperature – red, LWC – blue
temperature
Temperature
LWC
height [m]
temp[C]
[g/m3]
80
60
40
20
0
−20
−40
−60
−80
−100
−120
6
8
10
12
14
16
0
0.2
0.4
0.6
0.8

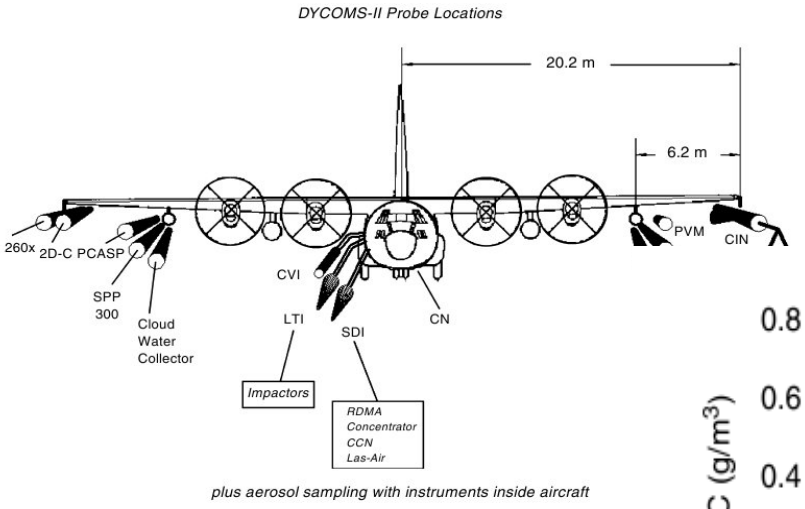

Examples of the cloud edge in 1000 Hz temperature (thin line) and LWC (thick line) records. Sharp jumps in LWC and temperature at distances of the order of 10 cm (data resolution) are currently observed. Notice a shift between the temperature and LWC records resulting from the 6 m separation between the instruments and the low pitch angle of the aircraft with respect to the cloud clear air interface.

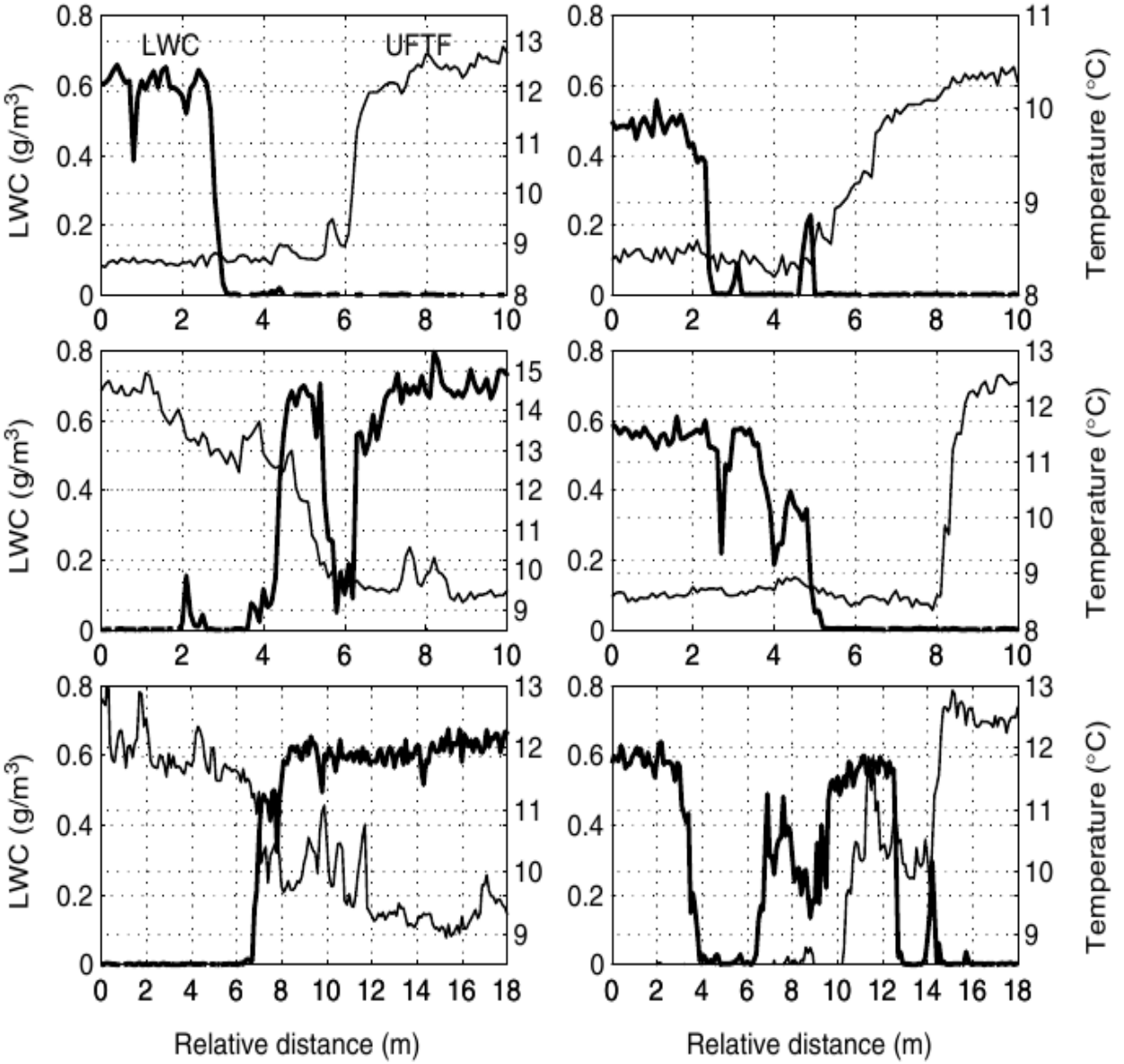

Haman et al., 2007

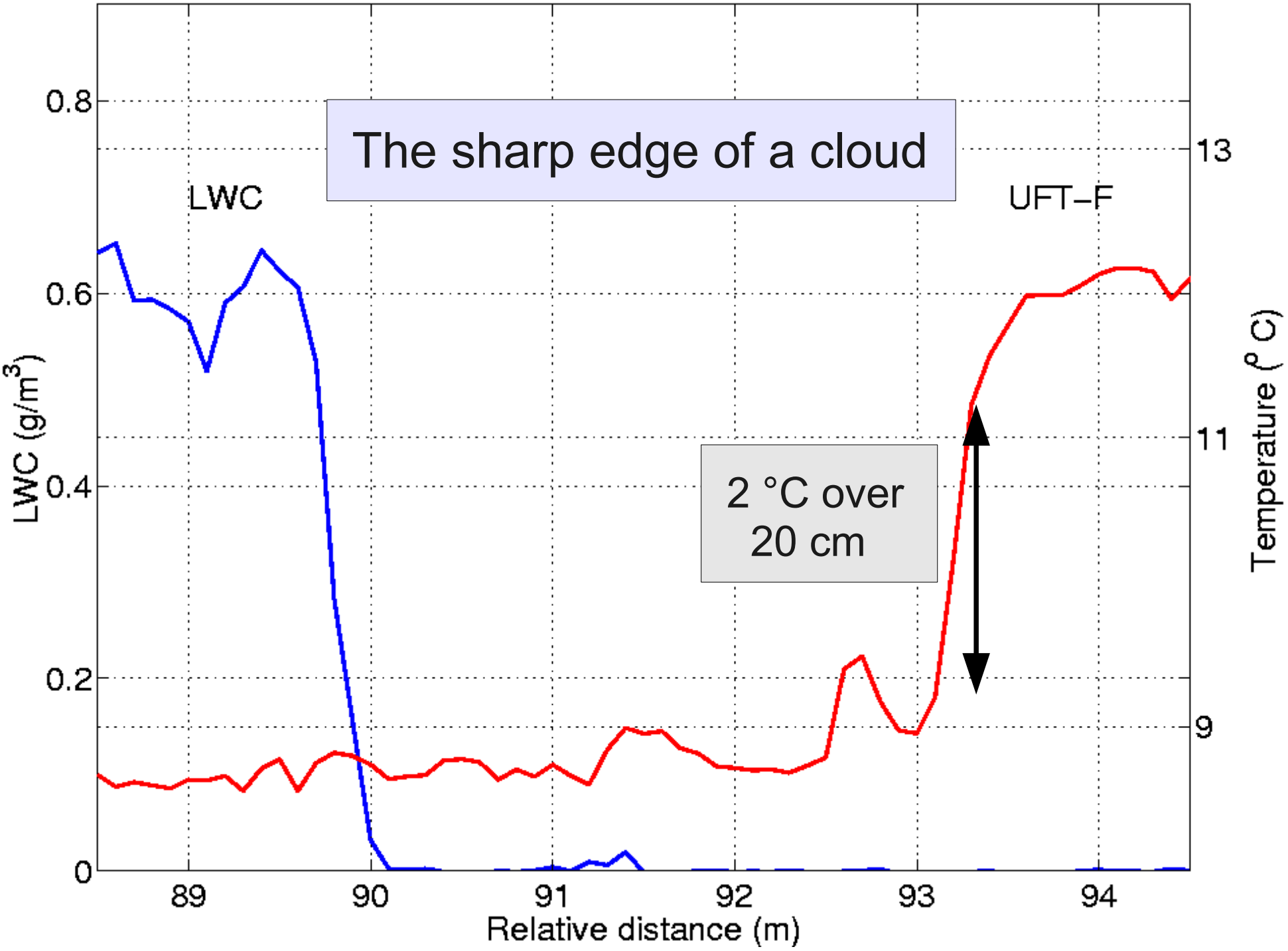
The sharp edge of a cloud
LWC
UFT–F
2 °C over
20 cm
LWC (g/m3)
Temperature (° C)
Relative distance (m)
0
0.2
0.4
0.6
0.8
9
11
13
89
90
91
92
93
94

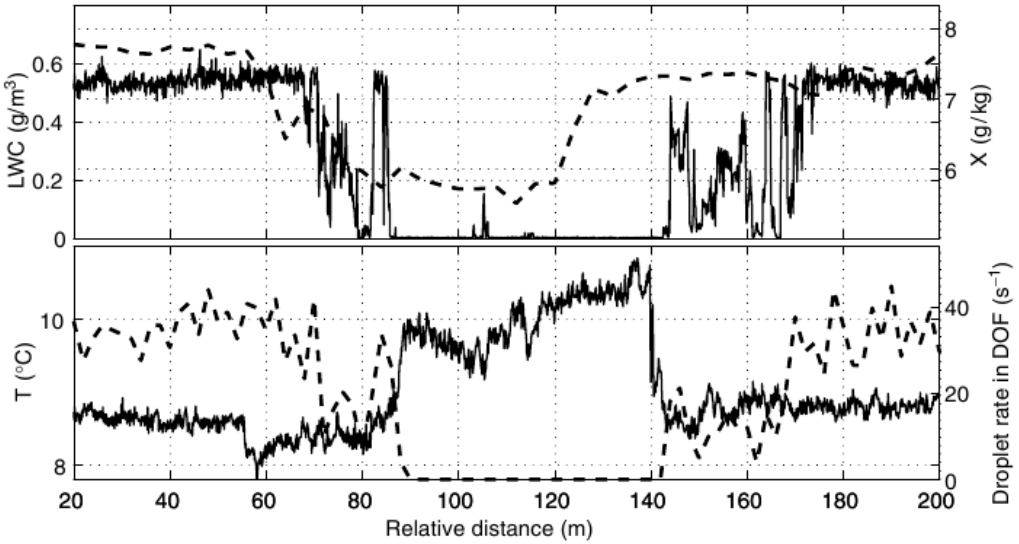

Penetration through a mixing event at Sc top

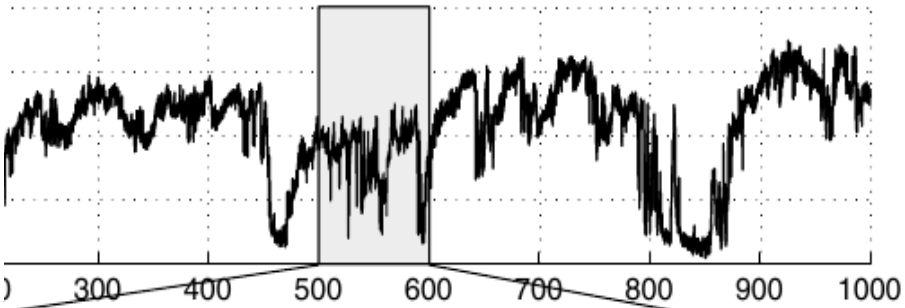

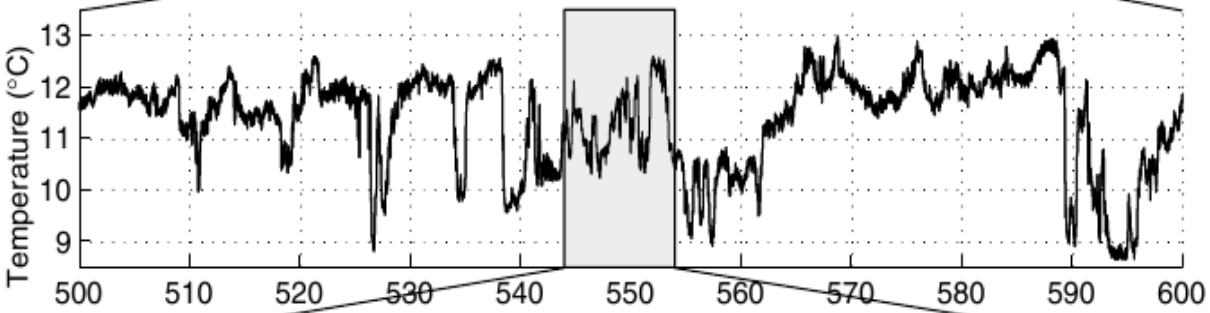

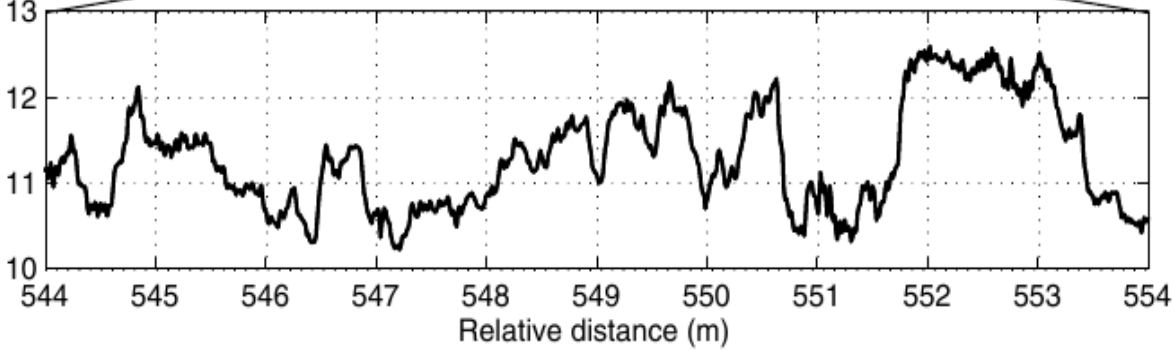

From the top to the bottom: successive ‘blow ups’ of 10 kHz temperature records showing self-similar structures – filaments of significantly different temperatures separated by narrow interfaces. The bottom panel presents the evidence for filaments of thickness of the order of 10 cm as well as for the steep gradients of temperature. Notice that UFT-F in its present configuration and signal conditioning (low-pass filtering) is still too slow to resolve adequately all interesting small-scale features of the temperature field.

Numerical simulations of small scales of cloud mixing with the environment.

$$B \equiv g\left[\frac{T - T_0}{T_0} + \varepsilon(q_v - q_{v_0}) - q_c\right],$$

$$D/Dt \equiv \partial/\partial t + \mathbf{v} \cdot \boldsymbol{\nabla}$$

$$\frac{D\mathbf{v}}{Dt} = -\boldsymbol{\nabla}\pi + \mathbf{k}B + \nu\nabla^2\mathbf{v},$$

$$\boldsymbol{\nabla} \cdot \mathbf{v} = 0,$$

$$\frac{DT}{Dt} = \frac{L}{c_p}C_d + \mu_T\nabla^2 T,$$

$$\frac{Dq_v}{Dt} = -C_d + \mu_v\nabla^2 q_v,$$

$$\frac{Dq_c}{Dt} = C_d.$$

$$\frac{D^*f}{D^*t} = -\frac{\partial}{\partial r}\left(f\frac{dr}{dt}\right) + \eta,$$

$$D^*/D^*t \equiv \partial/\partial t + (\mathbf{v} - \mathbf{k}v_t) \cdot \boldsymbol{\nabla}$$

$$C_d = \int f\frac{dm}{dt}\,dr,$$

Non-standard symbols:

π – normalized pressure fluctuation
C_d – condensation rate
q_v, q_c – specific humidity, liquid water content

B – normalized buoyancy

Andrejczuk et al., 2004,
Abdrejczuk et al., 2006

LWC after 11s

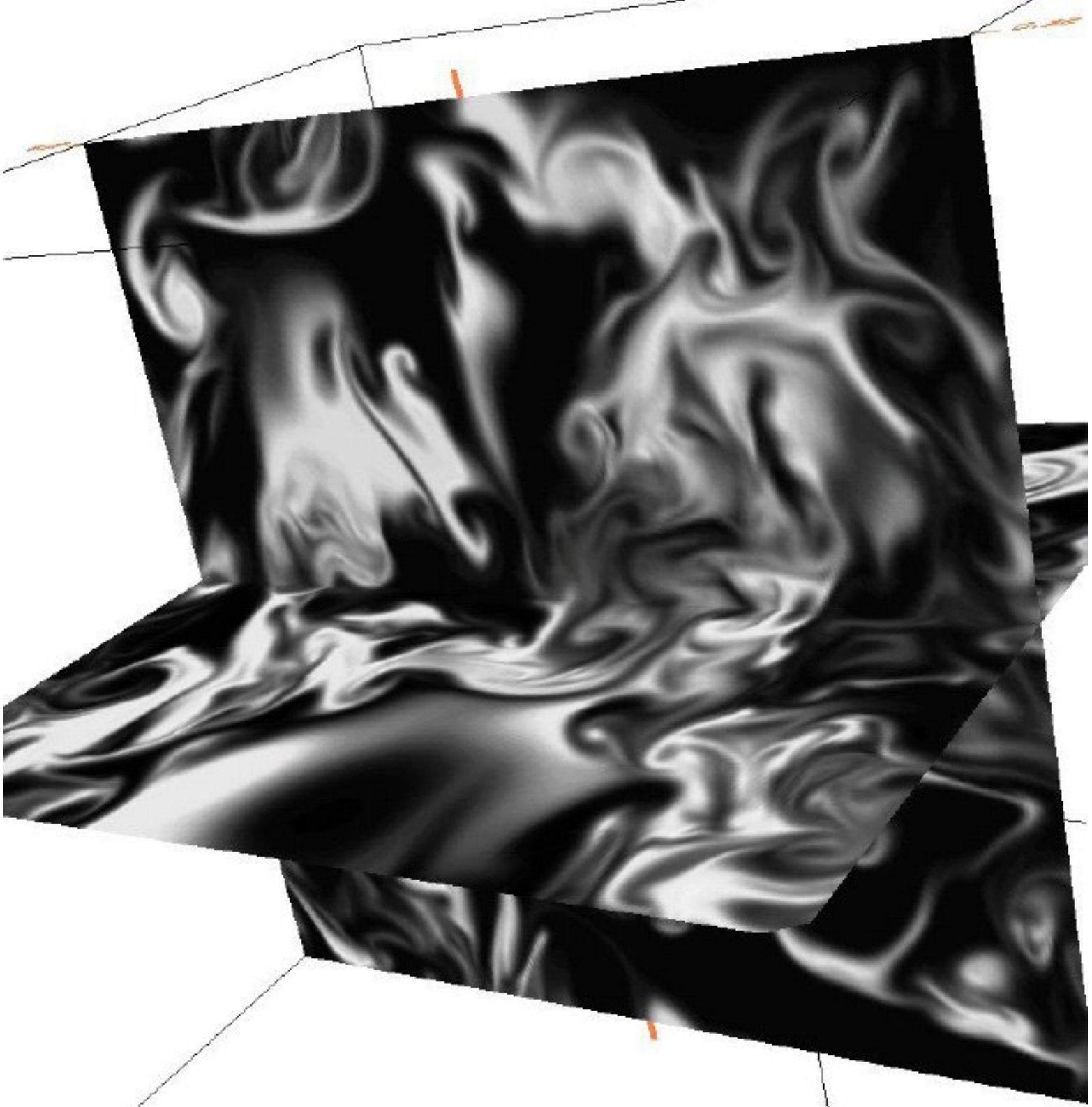

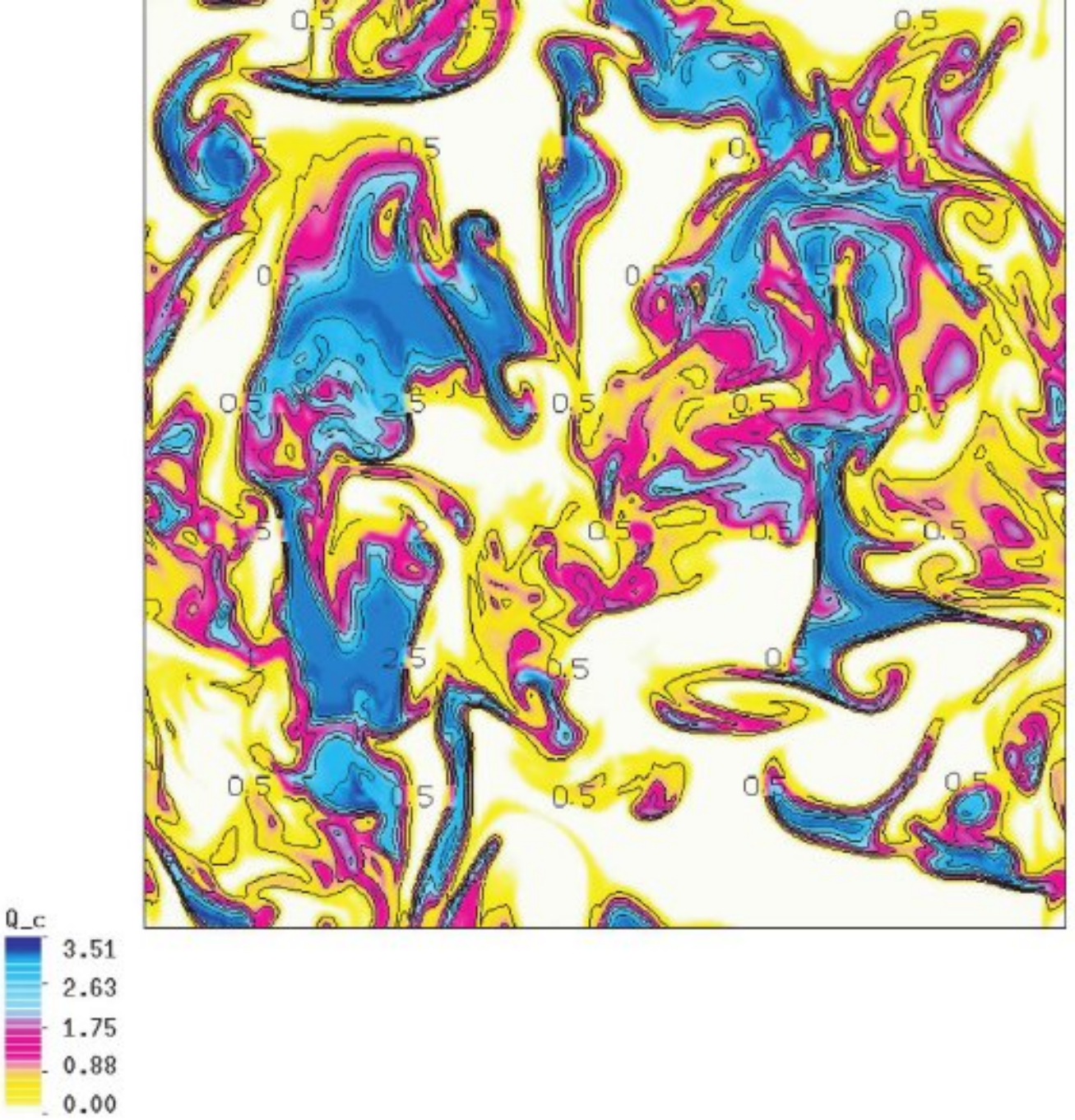

Malinowski et al., 2008

Figure 7. LWC (Q_c) in a vertical cross section through the computational domain after 10.8 s of the simulation. The area of the cross section is 64 cm × 64 cm, and white regions represent clear air filaments.

Mixing diagram of cloudy and environmental air.

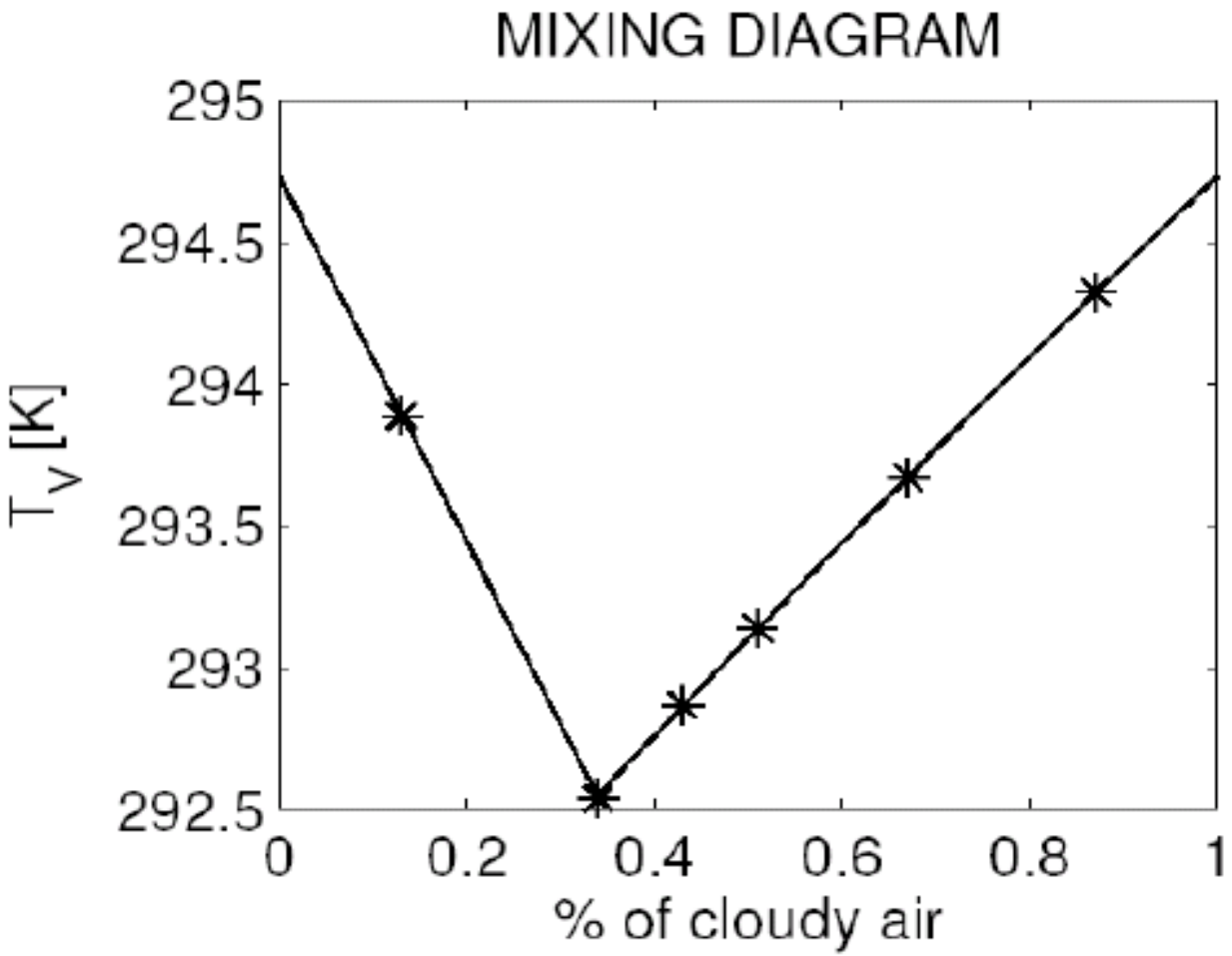

$T_v = T(1 + \varepsilon q_v + q_c)$ – „density temperature”

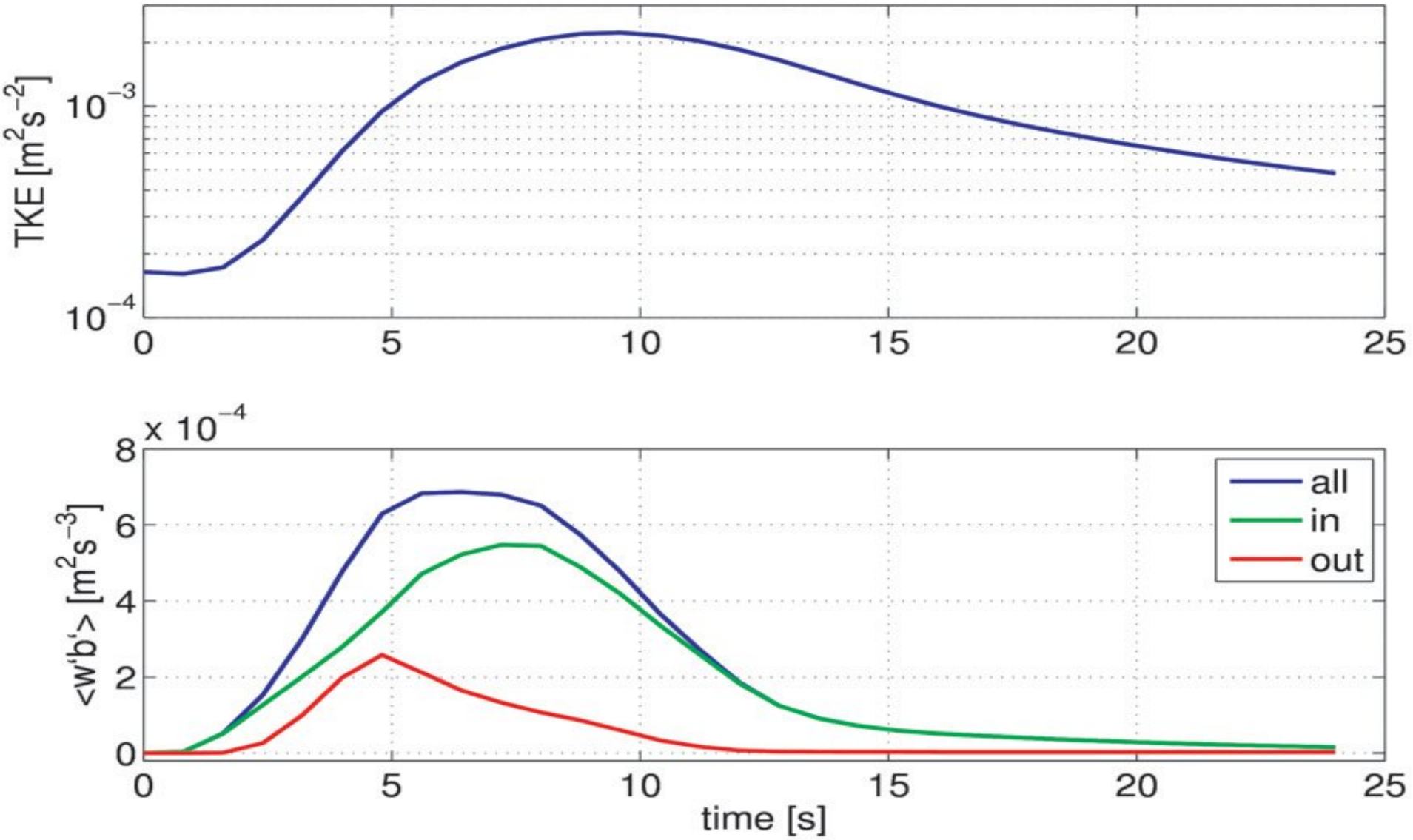

Evolution of the volume-averaged TKE (upper panel) and its buoyant production (lower panel, blue line); contributions to the buoyant production by buoyancy fluctuations within and outside the limits resulting from isobaric and adiabatic mixing are shown in green and red lines, respectively.

Malinowski et al., 2008

$$T_\rho = T\,(1 + \varepsilon q - l)\,,$$

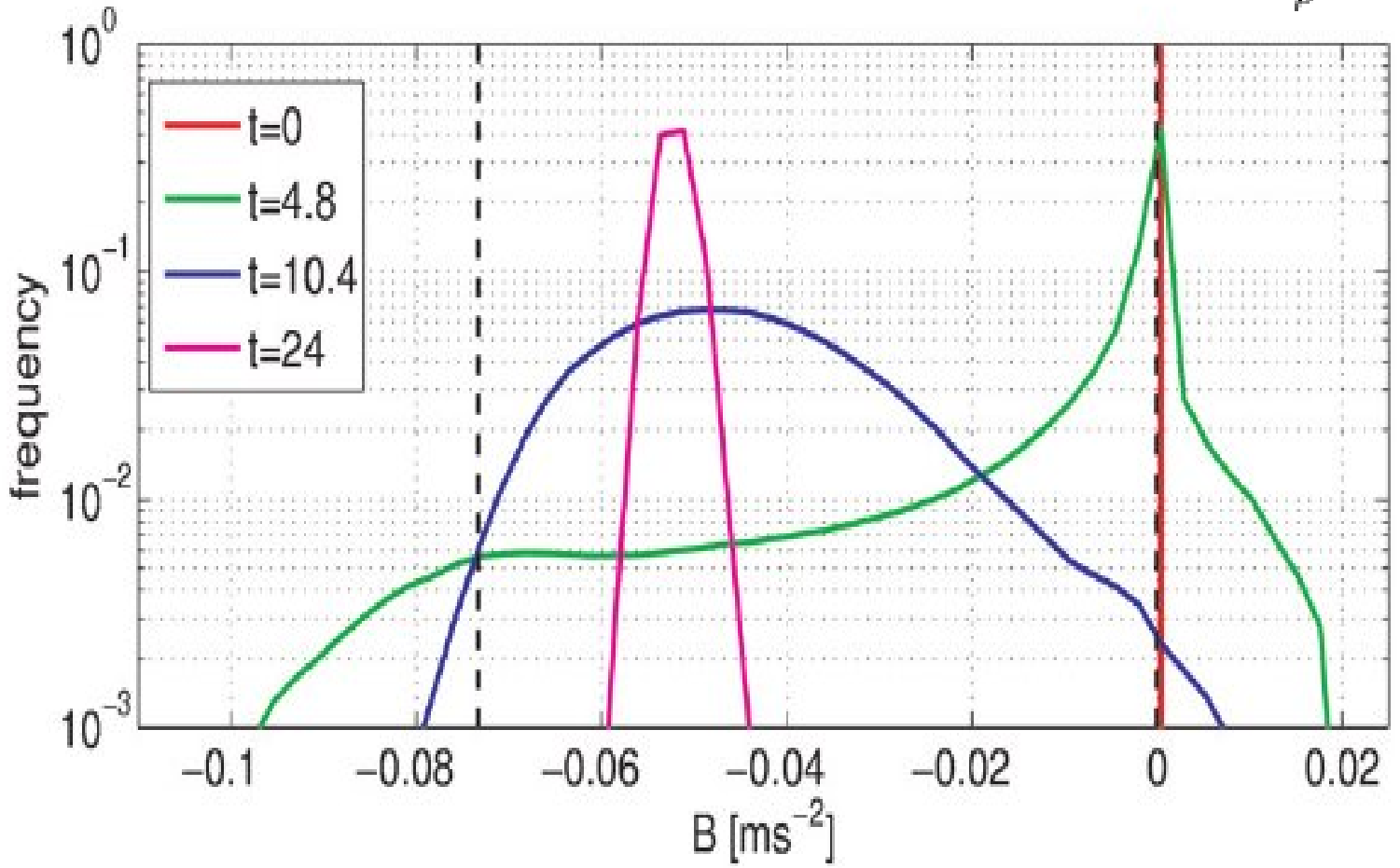

Figure 3. Histograms of buoyancy within the model domain at the beginning of calculations and at times of 4.8, 10.4 s and at the end of calculations (24 s). Dashed black lines show the range of buoyancy fluctuations due to isobaric and adiabatic mixing.

Malinowski et al., 2008

$$\tau_{mix} \equiv \frac{L}{U(L)} \sim \left(\frac{L^2}{\epsilon}\right)^{1/3} \qquad \tau_{evap} \equiv r\left(\frac{dr}{dt}\right)^{-1} = \frac{r^2}{A(1-RH)}$$

Homohenenous vs. Inhomogeneous mixing (Baker and Latham 1979;

In the homogeneous mixing scenario, the number of droplets does not change and the mean droplet size decreases. In the extreme inhomogeneous mixing scenario, droplets from a fraction of the cloudy volume evaporate completely to bring the mixture to saturation, and the droplets from the rest of the cloudy volume are dispersed over the combined volumes without changing their size.

If the droplet evaporation time scale is much larger than the time scale of turbulent homogenization, the mixing is expected to be close to homogeneous. In the opposite limit (i.e., the droplet evaporation time scale much smaller than the time scale of turbulent homogenization), the mixing is supposed to be close to the extremely inhomogeneous.

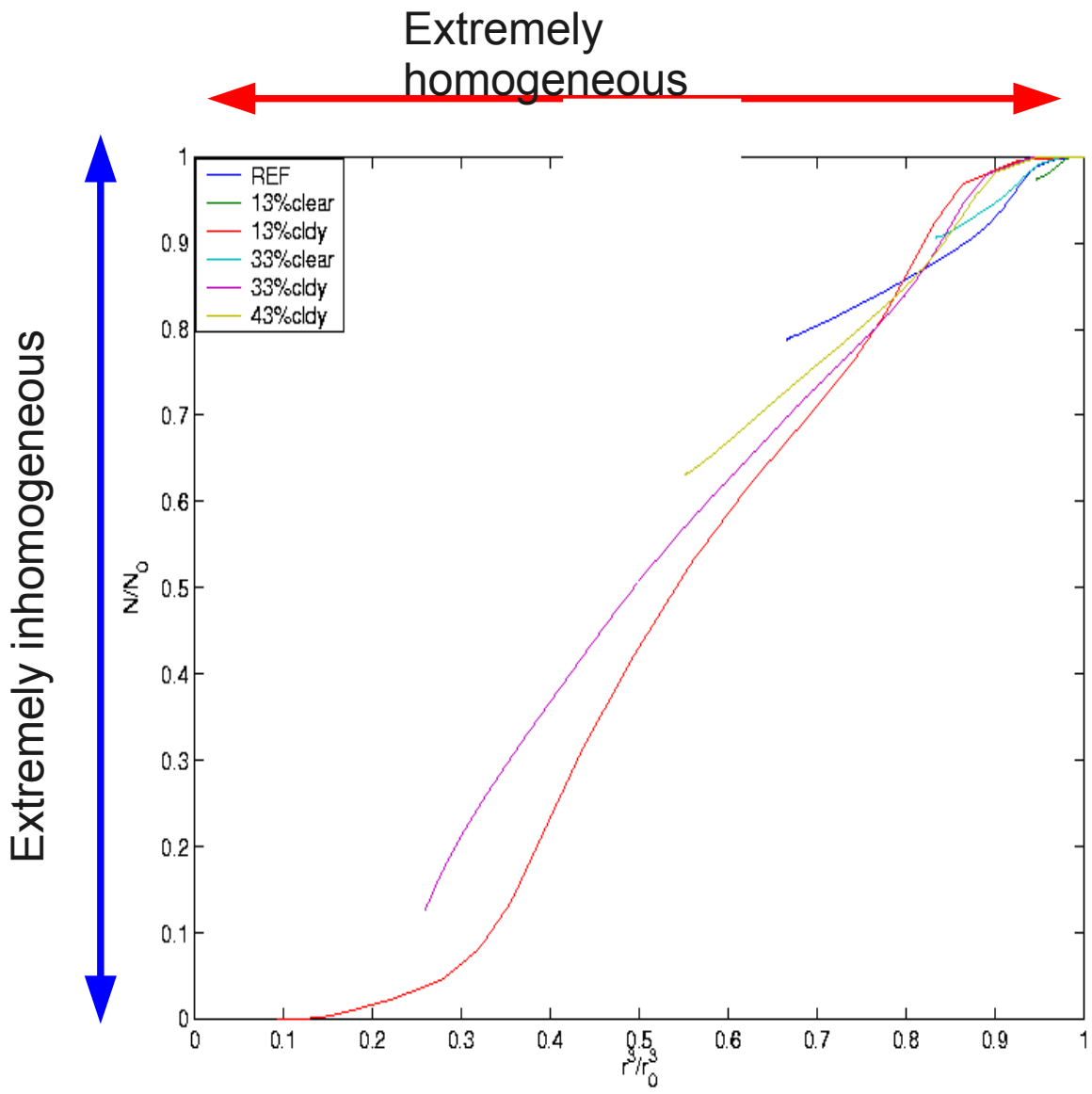

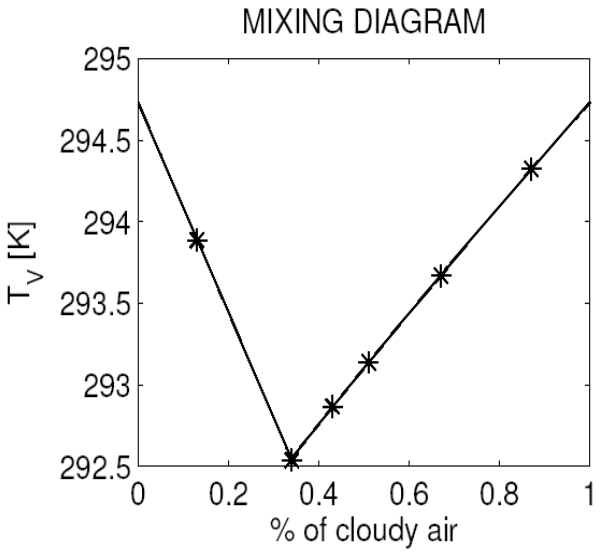

HIGH TKE

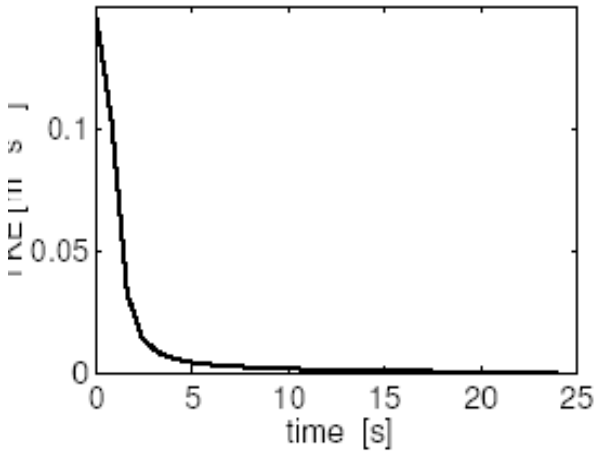

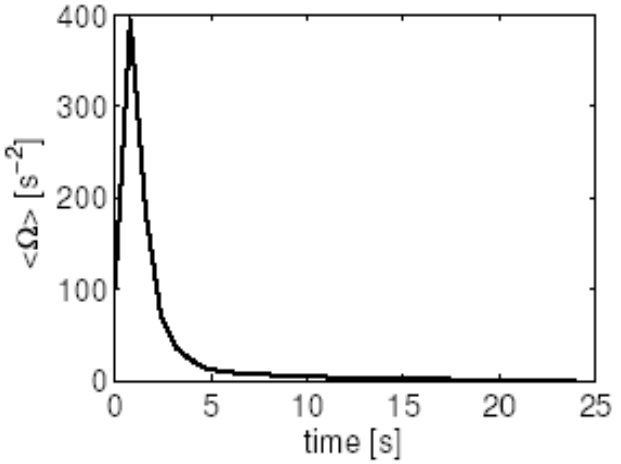

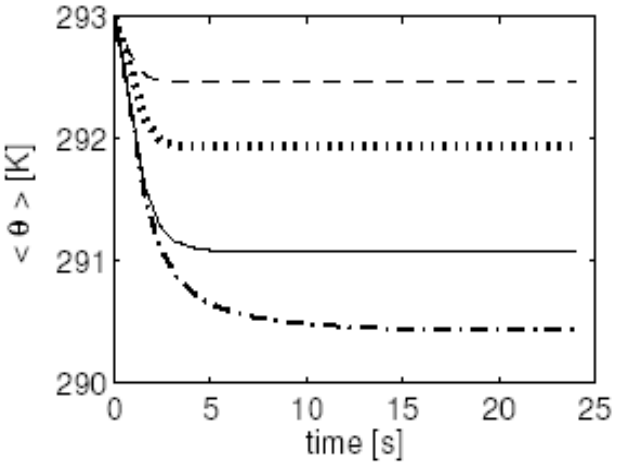

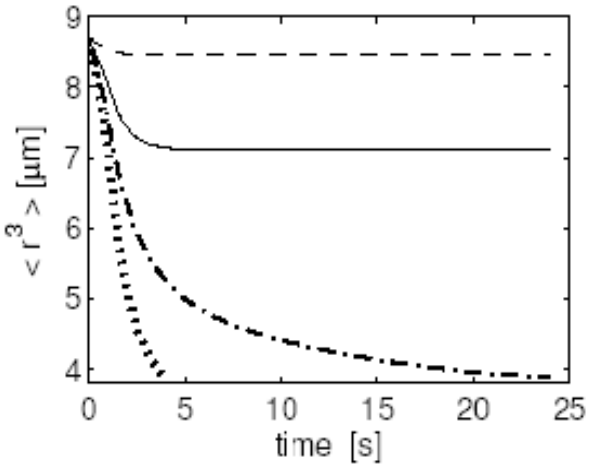

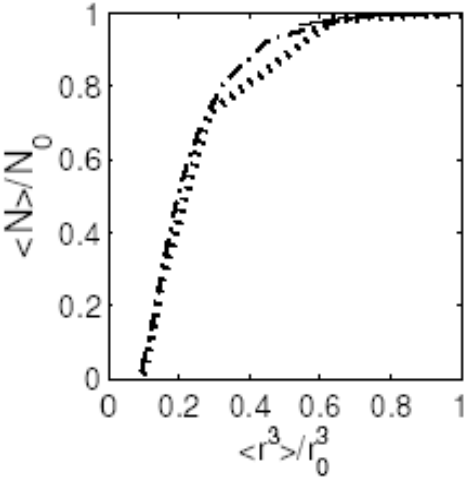

Evolution of mixing for various initial proportions of cloudy and clear air in the mixing event, detailed microphysics, high initial TKE.

Andrejczuk et al., 2006

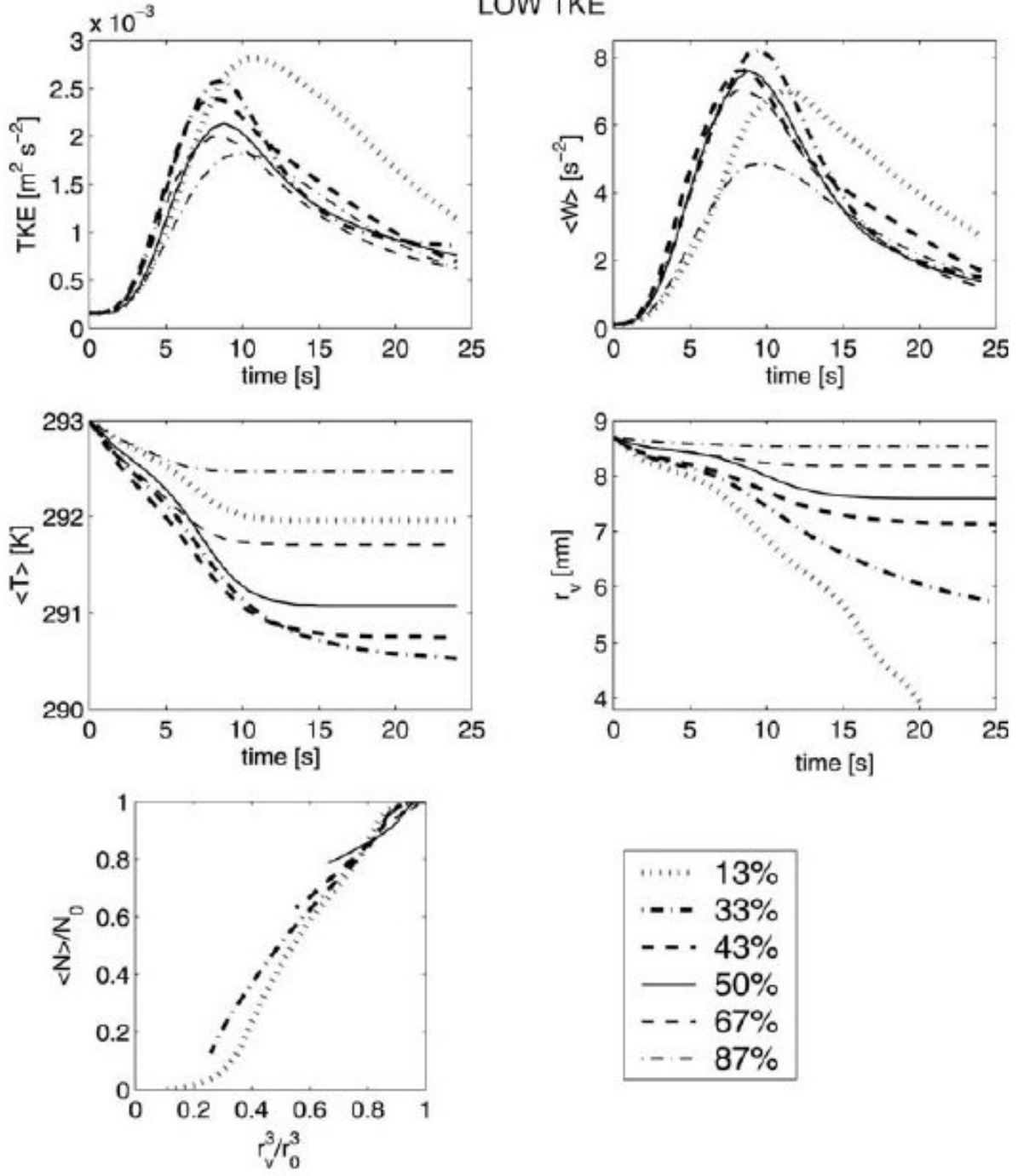

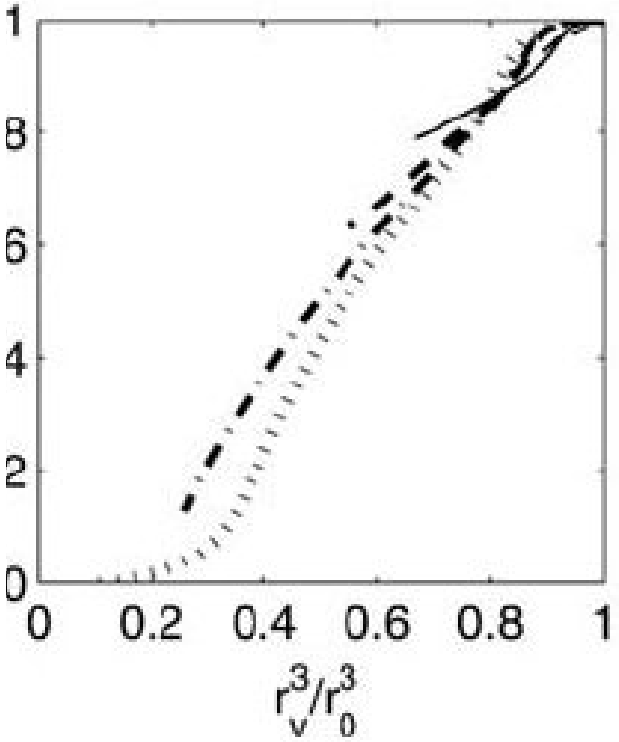

FIG. 6. Results from the set of numerical simulations with low-TKE input and detailed microphysics applying the reference setup: set S2a. The evolution of the (top left) TKE and (top right) mean enstrophy. The evolution of the (middle left) mean temperature and (middle right) mean volume radius. (bottom left) The evolution of the microphysical properties using the $r - N$ diagram.

Andrejczuk et al., 2009

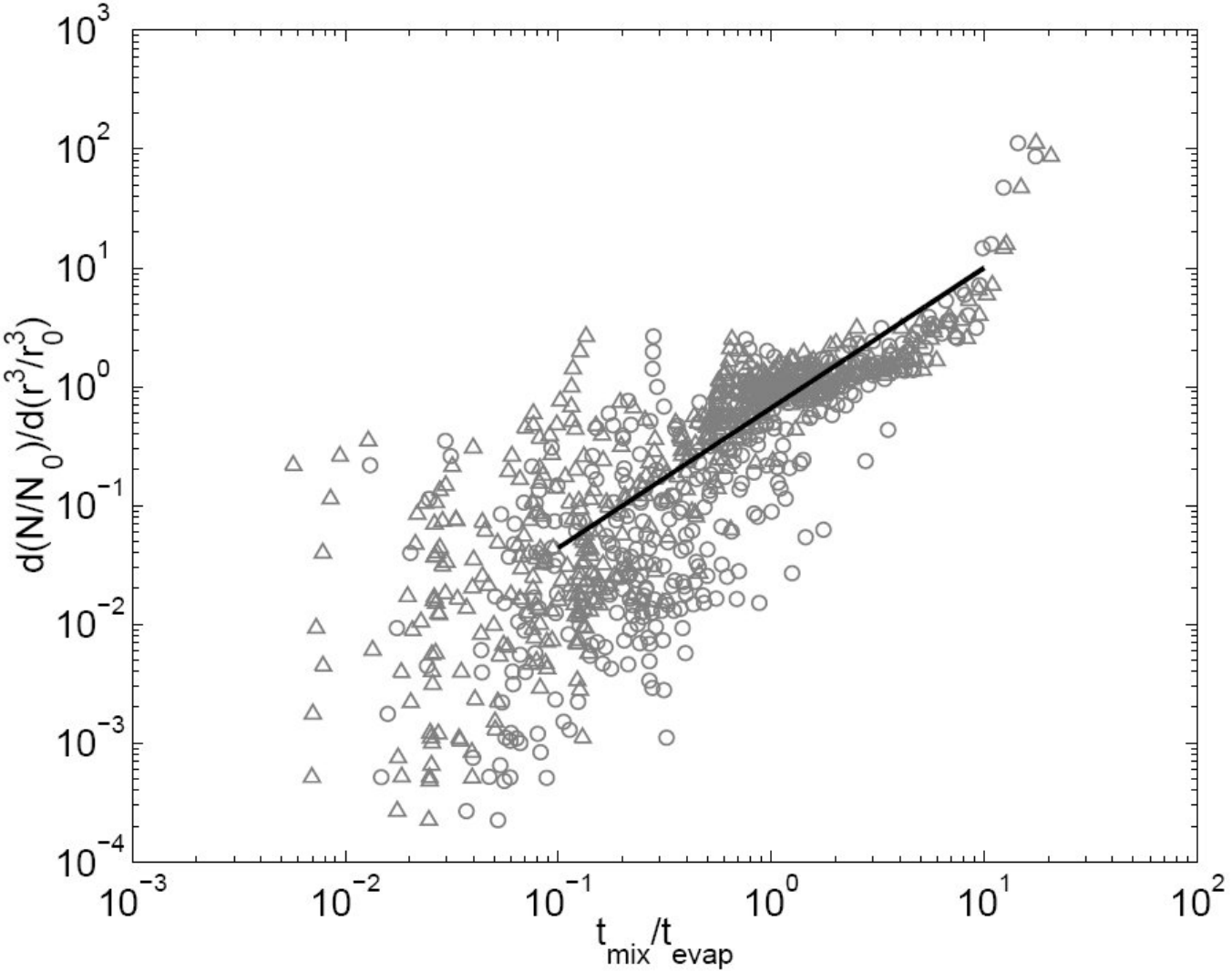

$$\tau_{mix} \equiv \frac{L}{U(L)} \sim \left(\frac{L^2}{\epsilon}\right)^{1/3}$$

$$\tau_{evap} \equiv r\left(\frac{dr}{dt}\right)^{-1} = \frac{r^2}{A(1-RH)}$$

Scatterplot of the slope of the mixing line on the r − N diagram versus the ratio between the turbulent mixing and the droplet evaporation time scales. Each datapoint represents analysis of instantaneous DNS data as explained in text, with triangles (circles) depicting datapoints with the mixing time scale calculated using TKE (enstrophy). The solid line is the proposed relationship to be used in subgrid-scale modeling.

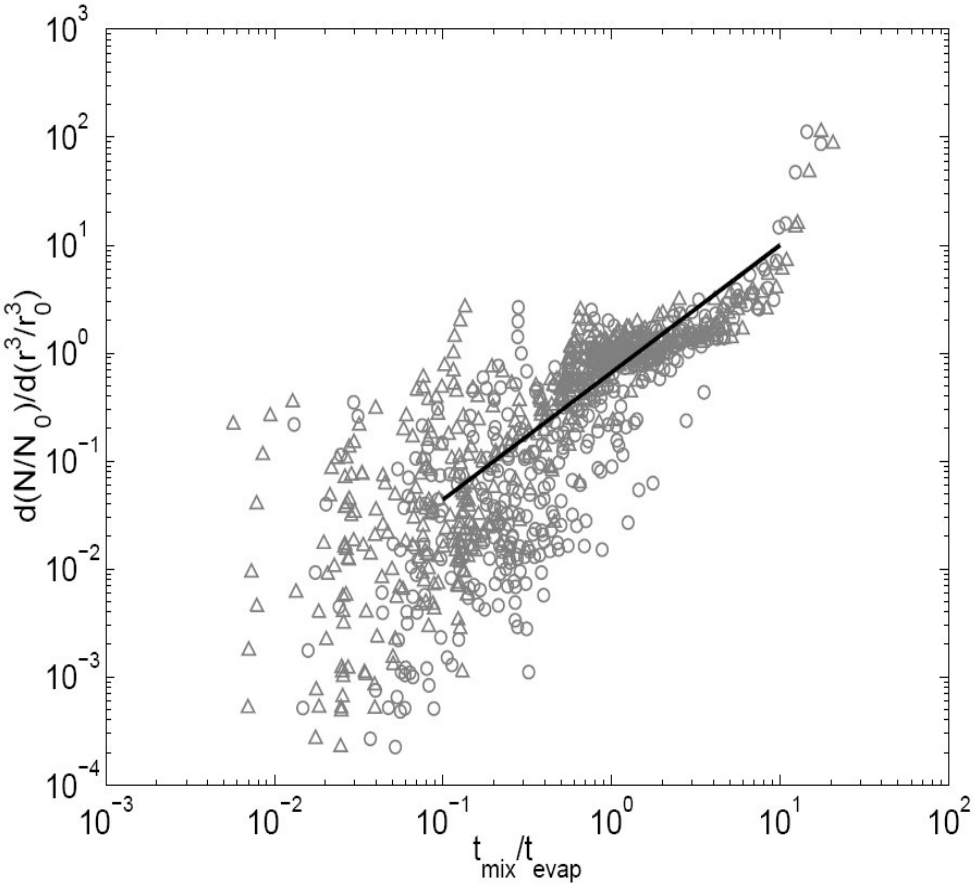

For practical purposes, all slopes smaller than 0.01, or perhaps even 0.1, lead to similar results, that is, large changes in the droplet radius and negligible changes in the number of droplets. In other words, when the slope is smaller than 0.1, the mixing differs insignificantly from the theoretical limit of the homogeneous mixing. Similarly, the slope larger than a 100 (and perhaps even 10) implies negligible changes in the mean volume radius of cloud droplets compared to the theoretical limit of the extremely inhomogeneous mixing. An important result is that in the critical range of the slopes, say, between 0.1 and 10, the relationship is relatively tight and thus one can suggest a simple parameterization.

For the Damkoehler number around 5, Jeffery (2007) predicts the mixing regime change from the inhomogeneous to the homogeneous. This agrees with the break in scaling behavior seen in Figure at $\tau_{mix}/\tau_{evap} \simeq 5$.

Smaller slopes, indicating increasing levels of homogeneity at lower ratios correspond to homogeneous evaporation regime in Jeffery's terminology.

The set-up of the experiments is designed to mimic basic aspects of small-scale turbulent mixing of a cloudy air with unsaturated environment.

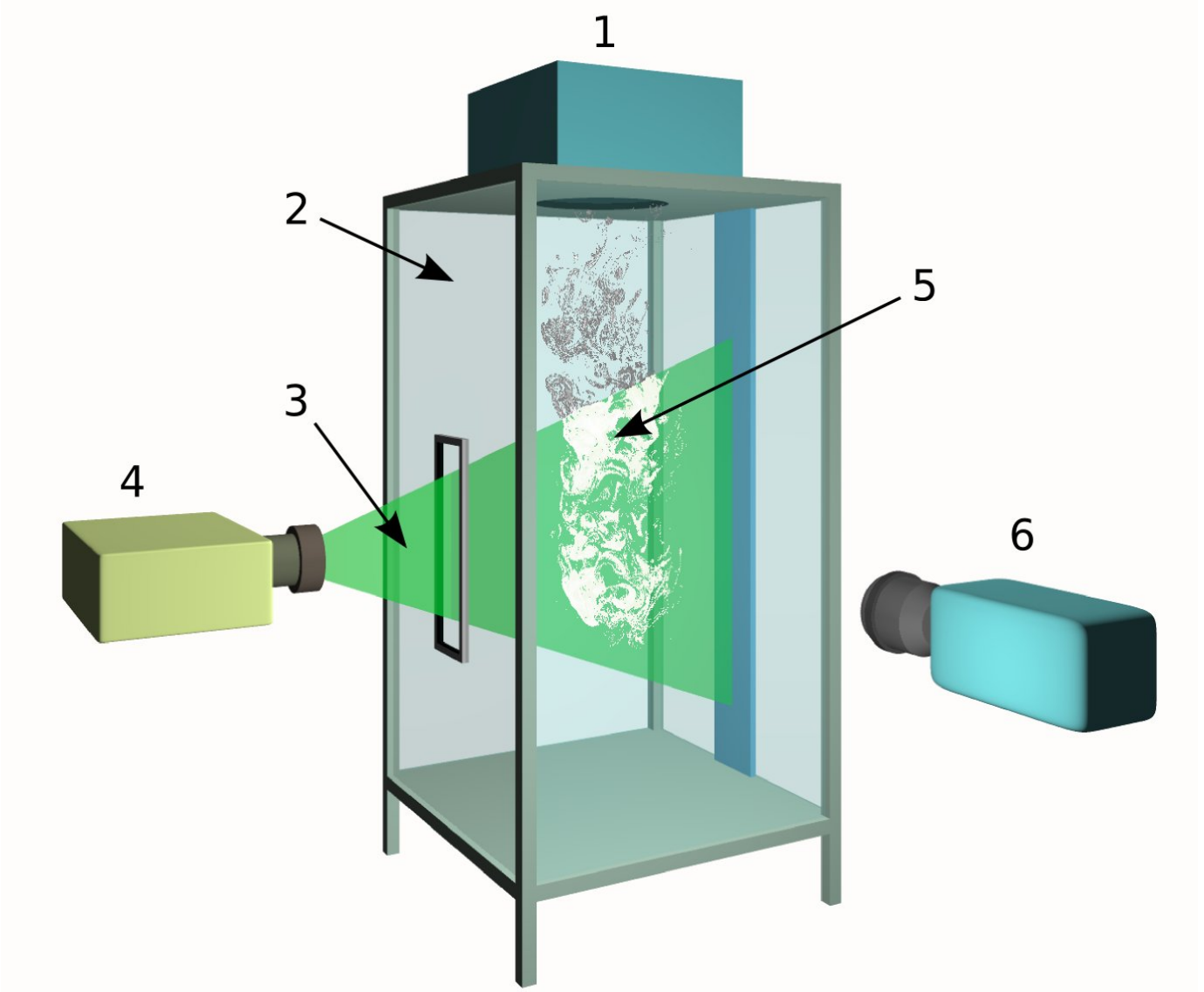

Schematic view of the experimental setup.
1 – box with the droplet generator; 2-cloud chamber; 3 – light sheet; 4 – pulsed laser, 5 – cloudy plume, 6 - camera.

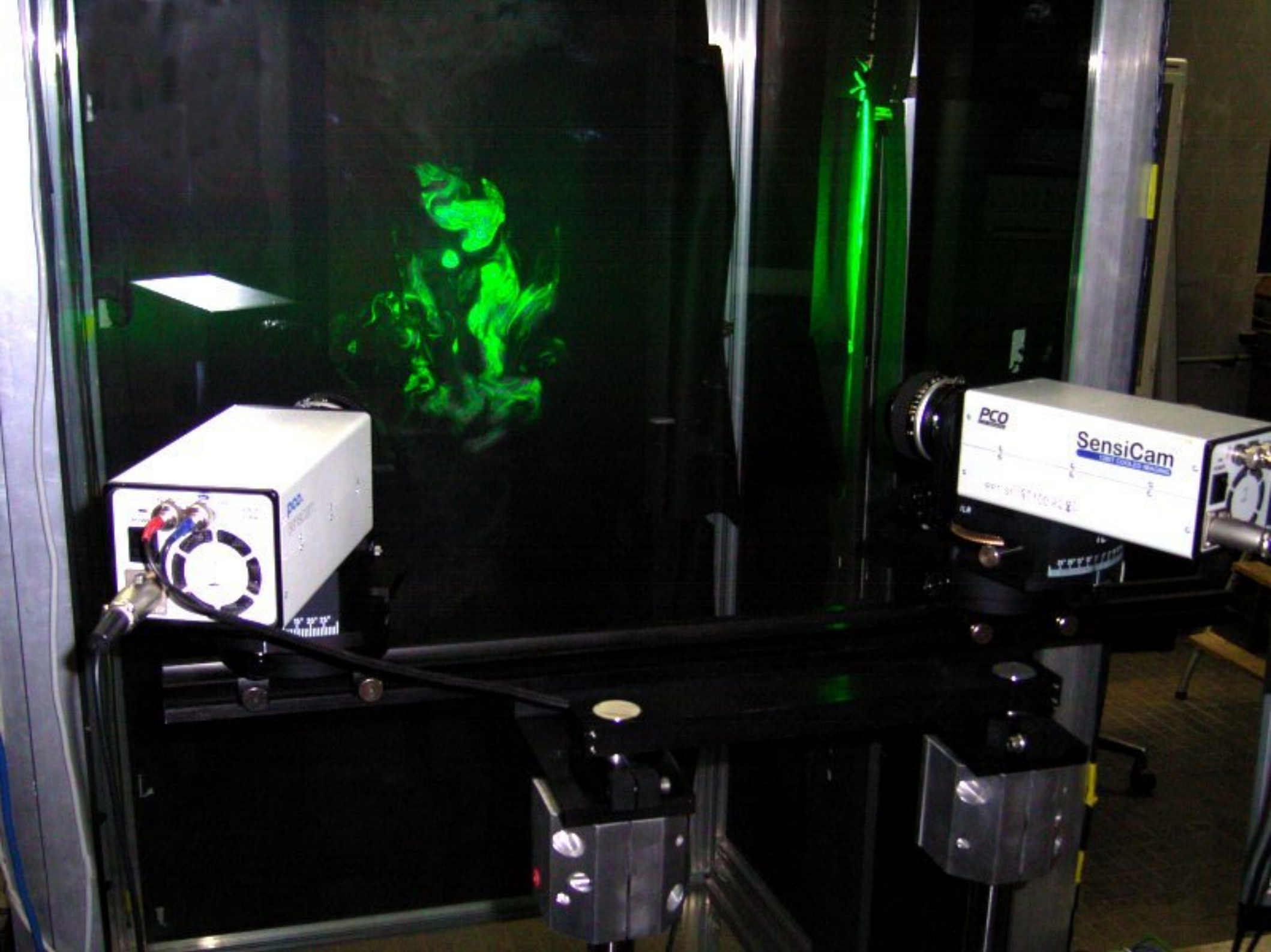
PCO
SensiCam

PIV – Particle Imaging Velocimetry

Principle:

two consecutive frames compared; displacement of patterns allows to determine two components of the velocity

Special algorithm:

- iterative (with the increasing resolution) correlation of patterns;
- mean motion removal;
- iterative deformation of patterns;
- median filtering.

Result:

benchmark scenes show the average accuracy of the displacement detection =0.3 pixel size.

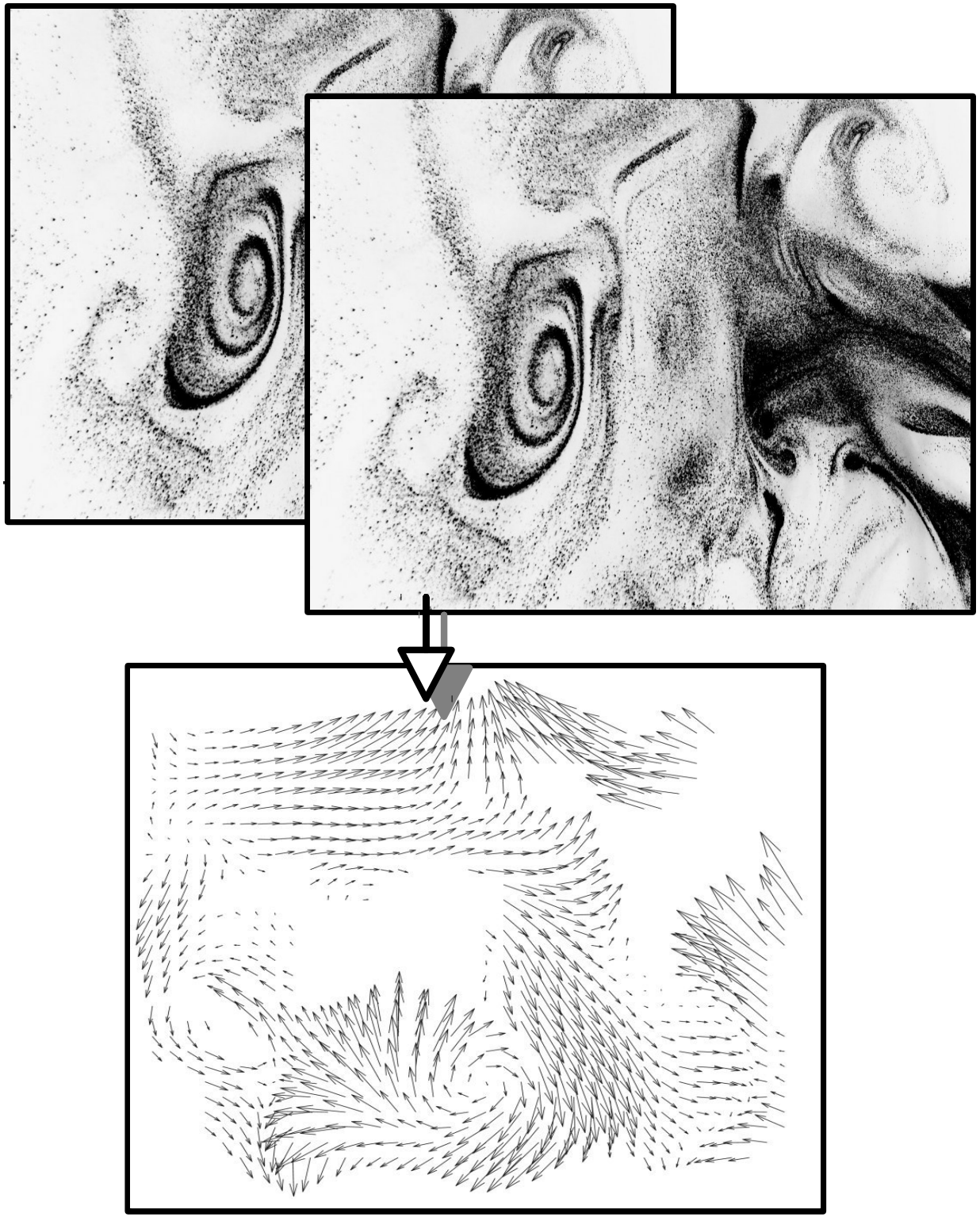

Thermodynamic conditions in the chamber.

LWC in the plume ~24 g/kg .

Plume temperature ~ 25^{o}C, the same as temperature of the unsaturated chamber air.

Relative humidity of the clear air inside the chamber varies in the range 20%~65% for different experiments.

Temperatures and humidities monitored on several levels.

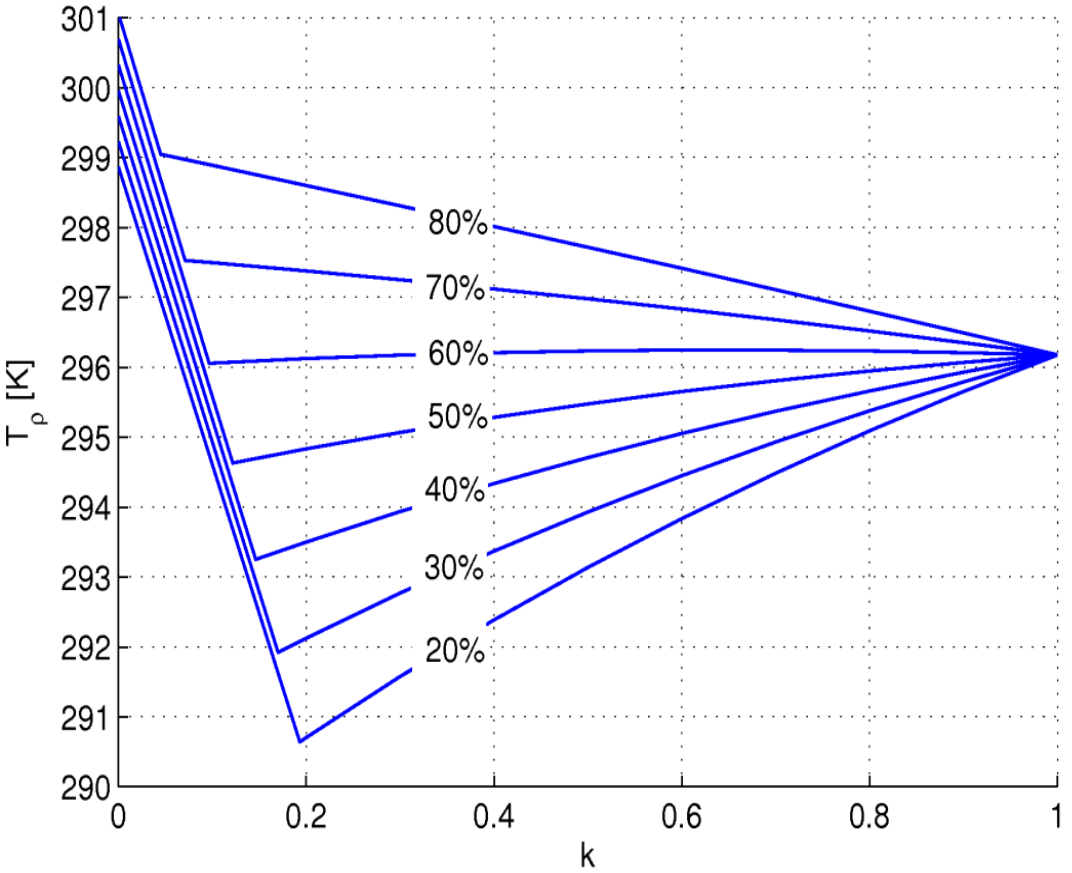

Mixing diagram:
k – fraction of cloudy air in the mixture,
T_ρ – density temperature.

Plume is NEGATIVELY BUOYANT.

Additional negative buoyancy due to evaporative cooling at the edges of cloudy filaments, dominant at ambient humidities less than 60%.

Anisotropy of turbulent velocities
(Malinowski et al., 2008)

Experimental -
average for 20 different runs:

	Std dev. (cm s^{-1})	Skewness	Kurtosis
u_1	**5.4**	−0.01	3.2
u_3	**8.0**	−0.2	3.1

$$(u_1)^2 / (u_3)^2 = \mathbf{0.46 \pm 0.07}$$

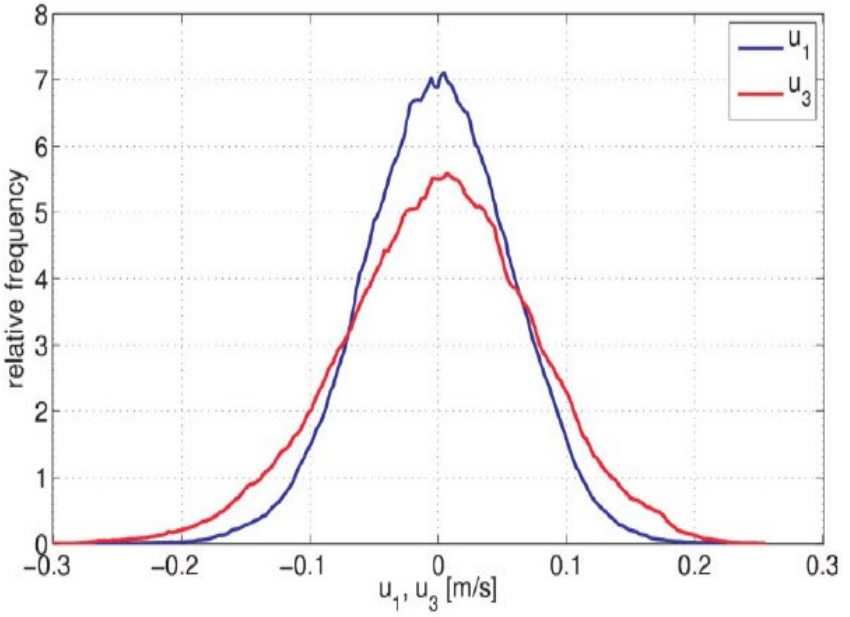

Numerical (LWC 3.2 g/kg):

	Std dev. (cm s^{-1})	Skewness	Kurtosis
u_1	**3,19**	0.01	3.3
u_2	**3,23**	−0.03	3.2
u_3	**4,69**	0.13	2.9

$$(u_{hor})^2 / (u_3)^2 = \mathbf{0.52 \pm 0.07}$$

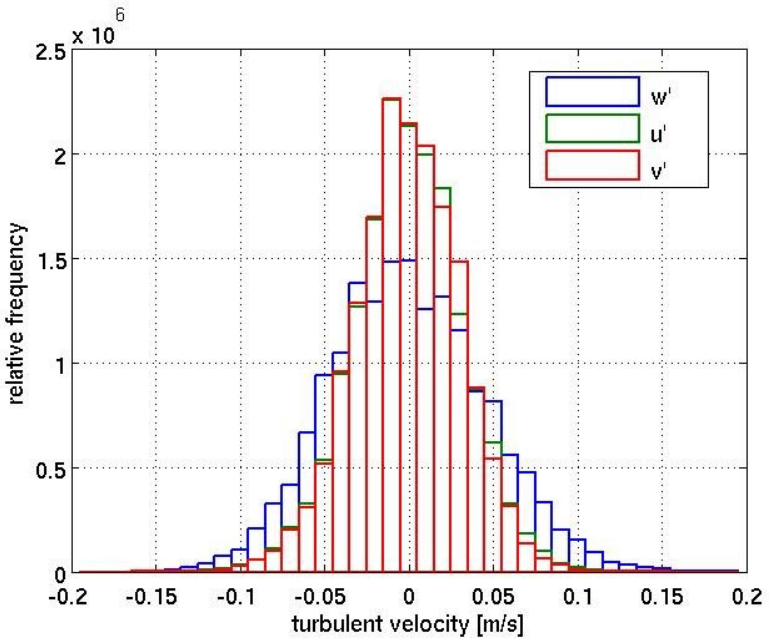

Airborne measurements of small-scale turbulent mixing in clouds

POST – Physics of Stratocumulus Top, California, 2008

aerosol (CCN)

microphysics

temperature,
humidity,
liquid water,
turbulence,

droplet counting

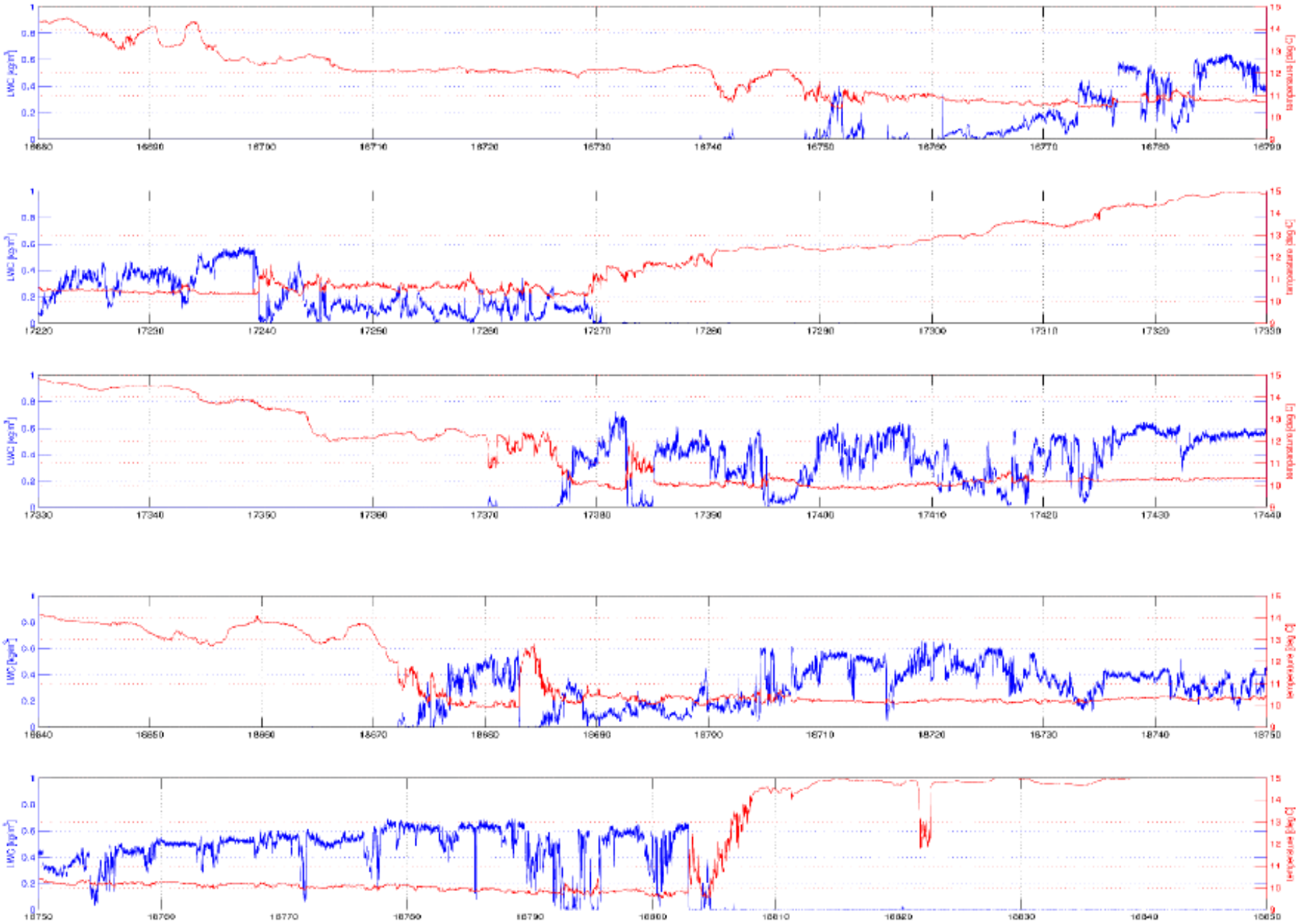

Fig.5 *100S/s (~50cm spatial resolution) records of temperature and LWC on few porpoises from the investigated leg of TO13 research flight. Notice remarkable temperature fluctuations above cloud (four uppermost sections), regions of depleted LWC close to the cloud top (sections 1,2,4), sharp temperature jump above sharp cloud top (lowest section).*

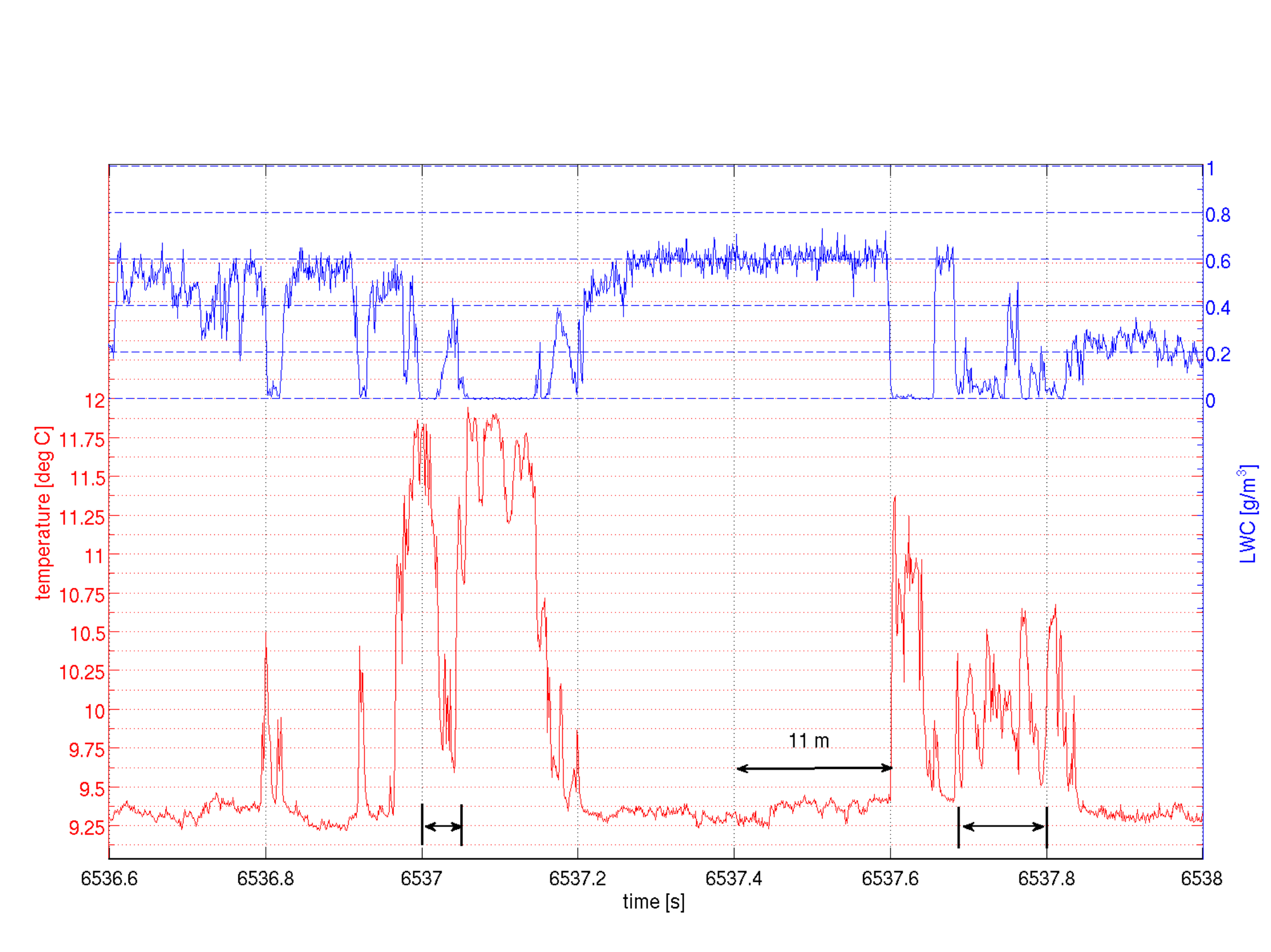
temperature [deg C]
12
11.75
11.5
11.25
11
10.75
10.5
10.25
10
9.75
9.5
9.25
LWC [g/m^3]
1
0.8
0.6
0.4
0.2
0
11 m
6536.6
6536.8
6537
6537.2
6537.4
6537.6
6537.8
6538
time [s]

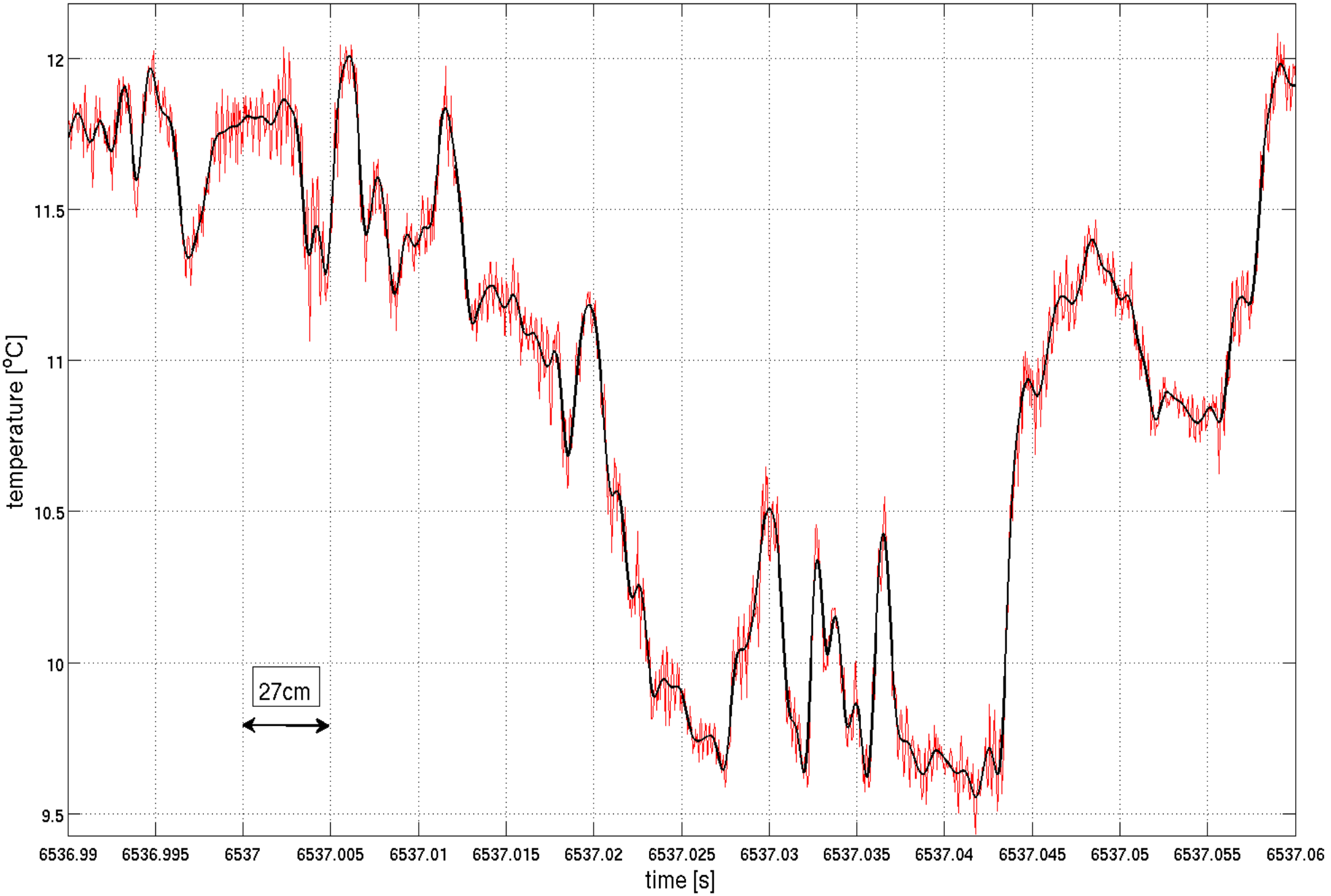
12
11.5
11
10.5
10
9.5
temperature [°C]
27cm
6536.99
6536.995
6537
6537.005
6537.01
6537.015
6537.02
6537.025
6537.03
6537.035
6537.04
6537.045
6537.05
6537.055
6537.06
time [s]

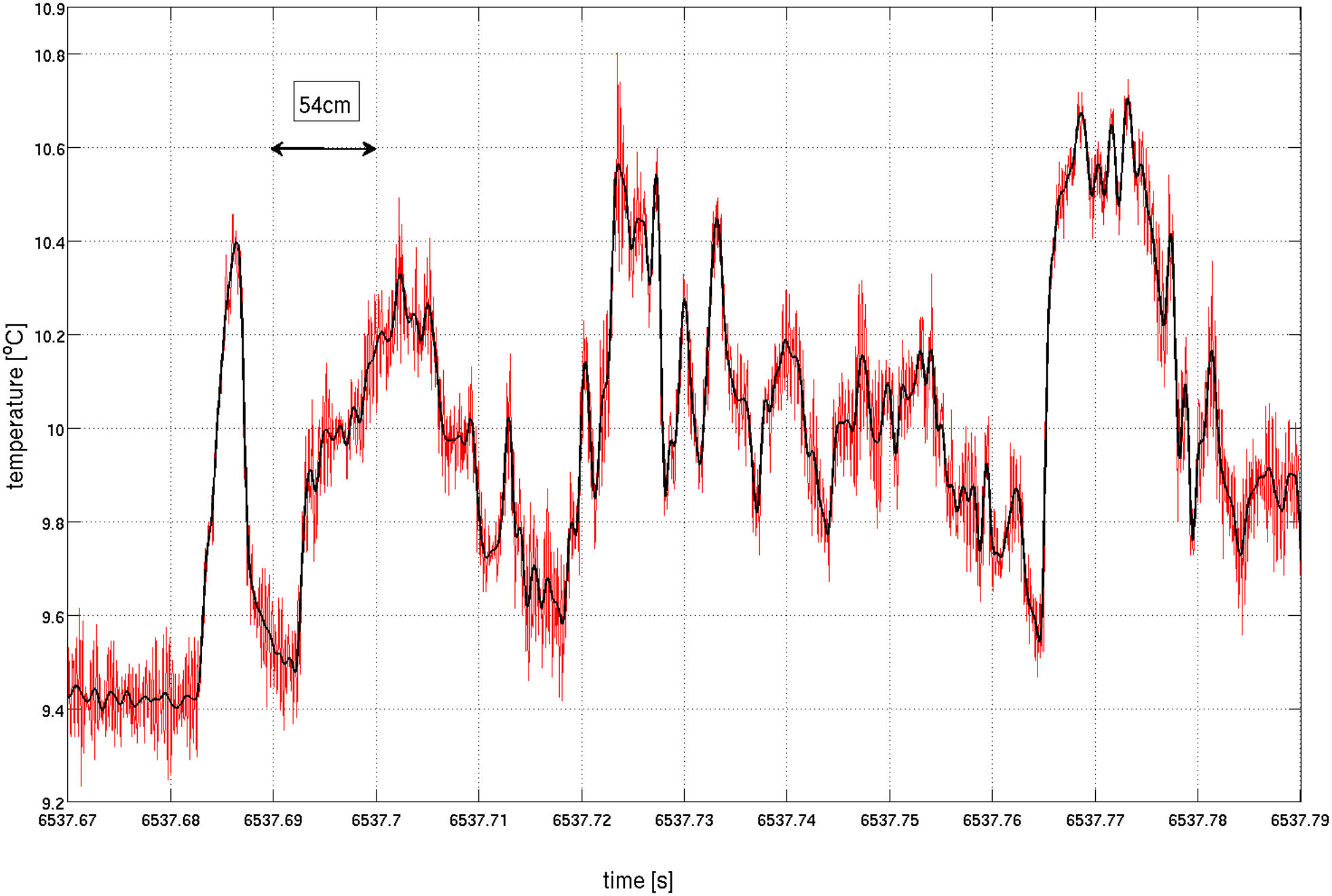
54cm
temperature [°C]
time [s]
10.9
10.8
10.6
10.4
10.2
10
9.8
9.6
9.4
9.2
6537.67
6537.68
6537.69
6537.7
6537.71
6537.72
6537.73
6537.74
6537.75
6537.76
6537.77
6537.78
6537.79

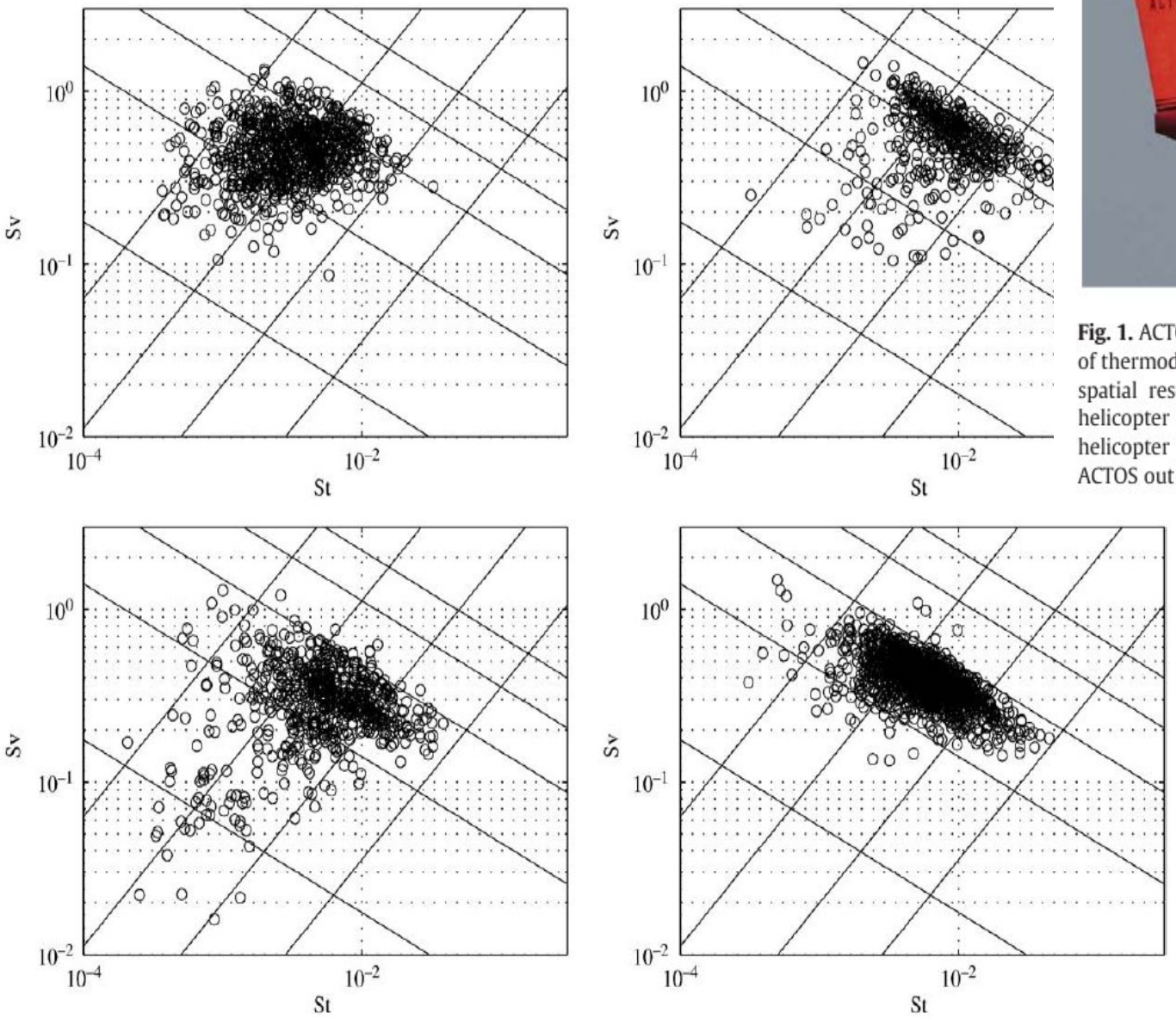

Fig. 1. ACTOS comprises instrumentation for comprehensive measurements of thermodynamic, microphysical, and turbulent variables in clouds, at high spatial resolution. The ACTOS measurement payload is attached to the helicopter by means of a 140 m long tether cable. The true airspeed of the helicopter is about 15 m/s, sufficient to enable stable flight conditions of ACTOS out of the helicopter's downwash.

Siebert et al., 2010

Fig. 9. The distribution of cloud microphysical and turbulence properties in a dimensionless Stokes–settling parameter space. The upper left plot is for a stratocumulus cloud and the remaining three are for small cumulus clouds. Each point represents data in a 1-second (approximately 15 m) average. Diagonal lines with positive slope are contours of constant turbulent energy dissipation rate, ε, at values of 10^{-4}, 10^{-3}, 10^{-2}, and 10^{-1} (lower right to upper left corners). Diagonal lines with negative slope are contours of constant droplet diameter at values of 5, 10, 15, 20 and 25 μm (lower left to upper right corners).

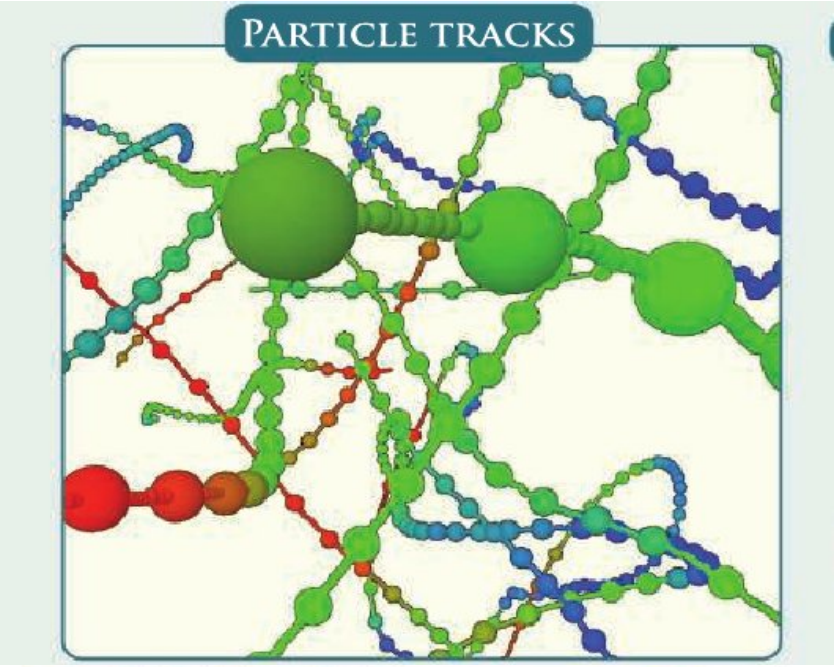

Particle tracking

Bodenschatz et al.

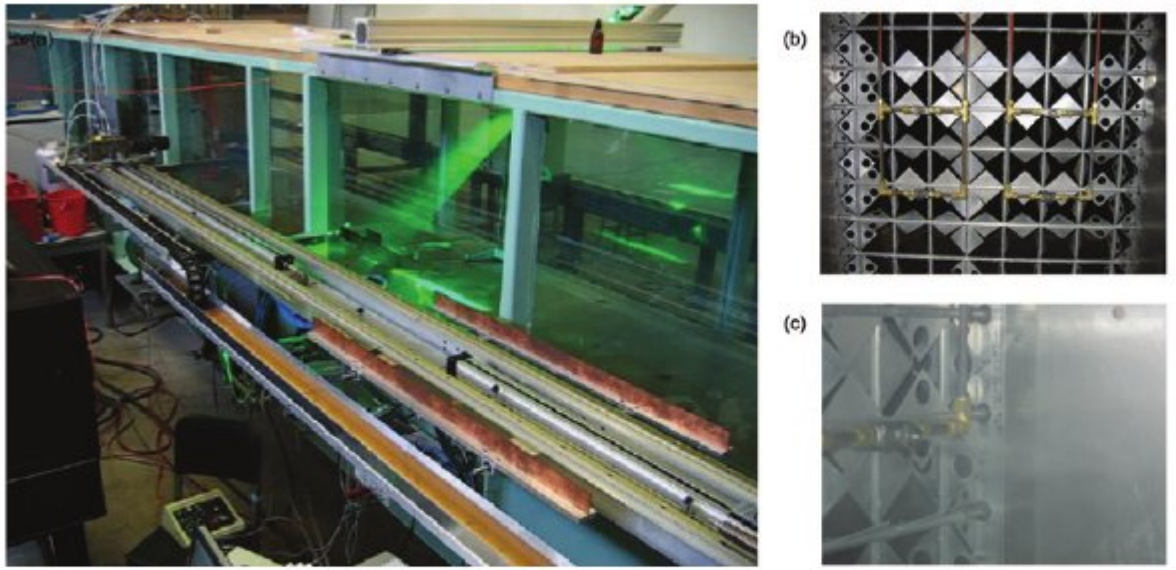

Wahrhaft et al.

Figure 8. The wind tunnel in the DeFrees laboratory at Cornell used to study inertial particles in high Reynolds number turbulence; (a) the plexiglass-open circuit-tunnel (1 m × 0.9 m × 20 m) showing the camera (far left, at the beginning of its trajectory), the sled and the laser sheet. (b) The active grid (used to generate high Reynolds number turbulence) and (c) the spray system. They are located at the far left of (a).

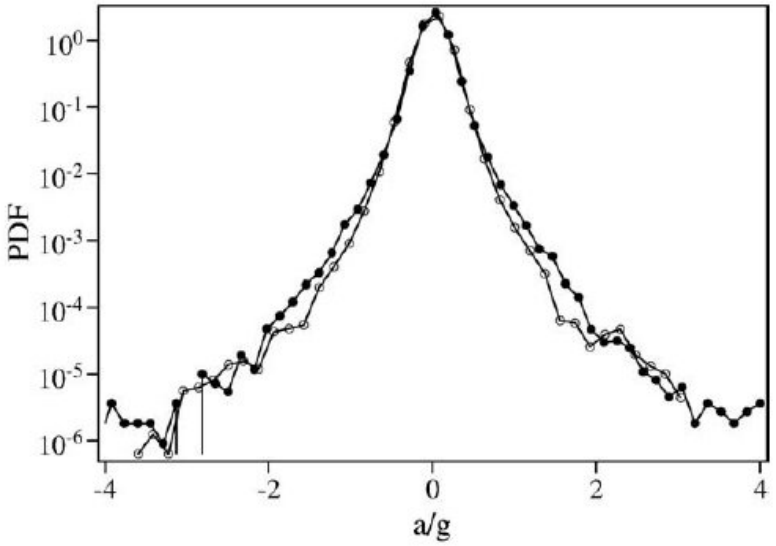

Fig. 12. Probability density function of the Lagrangian acceleration of droplets in a turbulent wind-tunnel flow. The accelerations have been normalized by the gravitational acceleration and scaled to reflect atmospheric conditions (see text). The two PDFs are for flows with Taylor microscale Reynolds numbers $R_\lambda = 100$ (open circle) and 240 (filled circle) and Stokes number $St = 0.072$. Notice that the tails clearly show droplets undergoing accelerations greater than those due to gravity.
Modified from Gerashchenko et al. (2008).

Siebert et al., 2010

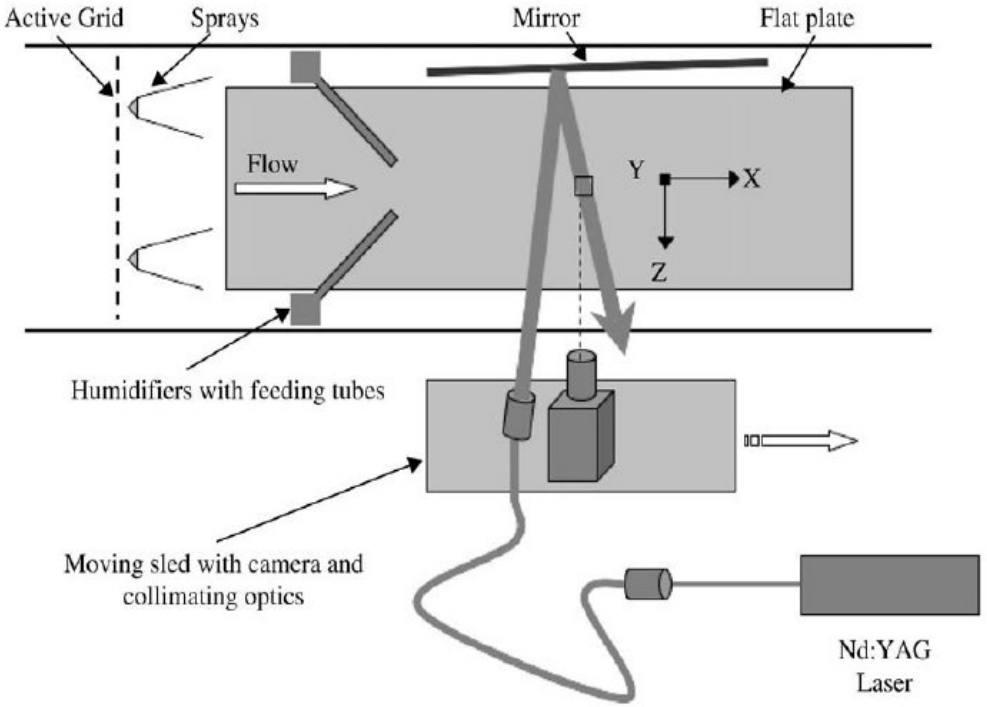

Fig. 10. Schematic of the forward scatter experiment (top view). The two separate methods of introducing the droplets are shown together. When the sprays are operating, the humidifiers and feeding tubes are removed from the tunnel. The y coordinate is measured vertically from the plate.
From Gerashchenko et al. (2008). Copyright Cambridge University Press.

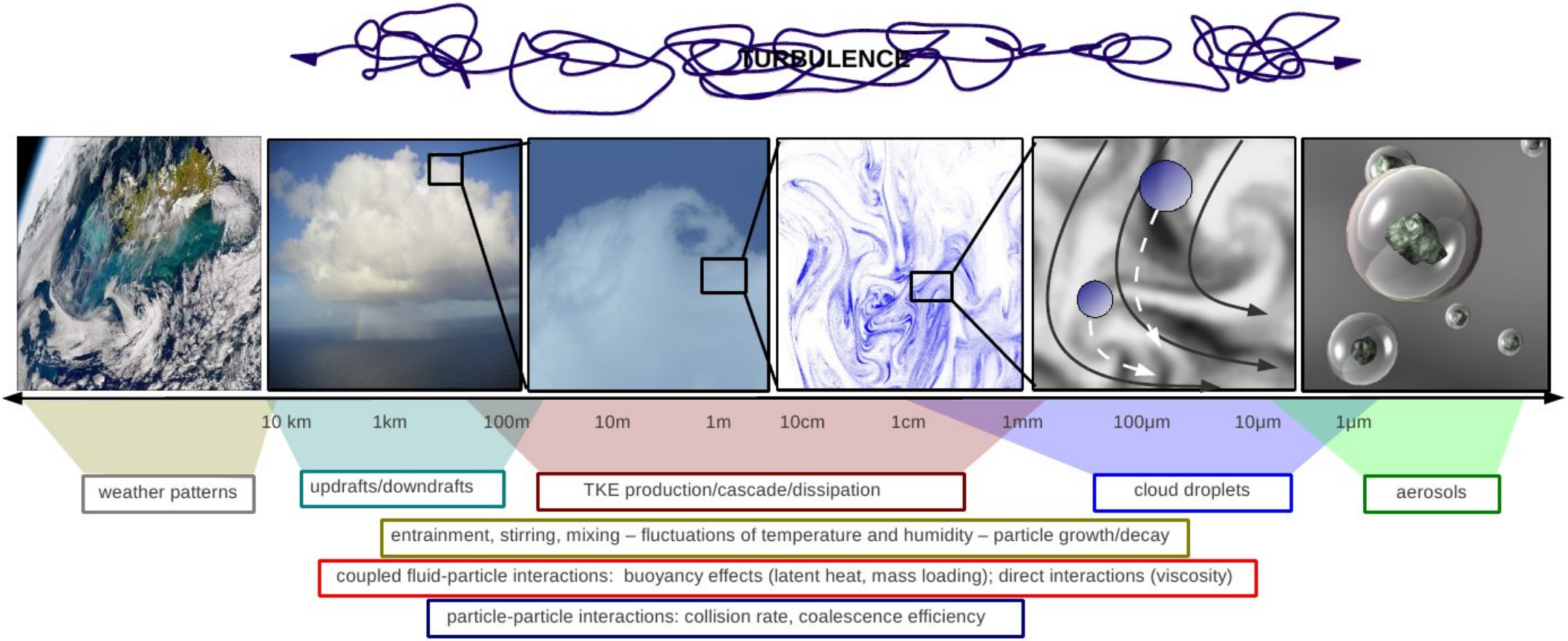

Clouds are dispersions of drops and ice particles embedded in and interacting with a complex turbulent flow. They are highly nonstationary, inhomogeneous, and intermittent, and embody an enormous range of spatial and temporal scales. Strong couplings across those scales between turbulent fluid dynamics and microphysical processes are integral to cloud evolution (see the figure).

Turbulence drives entrainment, stirring, and mixing in clouds, resulting in strong fluctuations in temperature, humidity, aerosol concentration, and cloud particle growth and decay. It couples to phase transition processes (such as nucleation, condensation, and freezing) as well as particle collisions and breakup. All these processes feed back on the turbulent flow by buoyancy and drag forces and affect cloud dynamical processes up to the largest scales.

Bodenschatz et al., Science, 2010.

The last decades have seen the emergence of new views into the "inner workings" of both clouds and turbulent flows.

For example, **high-resolution measurements** of temperature, liquid water content, aerosol physical and chemical properties, and airflow **reveal fascinating small-scale cloud structures,** invisible with earlier technology.

Laboratory experiments and **numerical simulations** are allowing us to study details of cloud microphysics, the **fine structure of turbulence**, turbulent **Lagrangian dynamics**, **interactions and collisions between droplets**.

Scale-resolving simulations merging computational methods from both cloud and turbulence communities are yielding new insights into the wide **variety of circulation regimes**.

These new tools, experimental and computational, have begun to make it possible to explore the full complexity of microphysical and fluid-dynamical interactions within clouds.

We can now begin to address:

- How does **turbulence influence phase transition processes** like condensation, evaporation, activation, and freezing taking place inside clouds?
- How does t**urbulence influence particle-particle interactions** like collisions, coalescence efficiencies, ice aggregation, and drop- or ice-breakup?
- How do **microphysical processes feed back on the turbulence** through latent-heat release, energy injection at small scales, and buoyancy reversal?
- How do **small scale processes propagate to and couple to the larger scales**, such as, cloud dynamics, precipitation formation, and radiative properties?

References:

Andrejczuk M, Grabowski WW, Malinowski SP, Smolarkiewicz PK. 2004.
Numerical simulation of cloud-clear air interfacial mixing. J. Atmos. Sci. 61: 1726-1739.

Andrejczuk M, Grabowski WW, Malinowski SP, Smolarkiewicz PK. 2006.
Numerical simulation of cloud-clear air interfacial mixing: effects of cloud microphysics. J. Atmos. Sci. 63: 3204-3225.

Andrejczuk M, Grabowski WW, Malinowski SP, Smolarkiewicz PK. 2009.
Numerical simulation of cloud-clear air interfacial mixing: homogeneous versus inhomogeneous mixing. J. Atmos. Sci. 66:2493-2500.

Ayala O, Rosa B, Wang L-P, Grabowski WW. 2008a.
Effects of turbulence on the geometric collision rate of sedimenting droplets. Part 1. Results from direct numerical simulation New J.Phys. 10:075015.

Ayala O, Rosa B, Wang L-P. 2008b.
Effects of turbulence on the geometric collision rate of sedimenting droplets. Part 2. Theory and parameterization. NewJ.Phys. 10:075015.

Beard KV. 1976. Terminal velocity and shape of cloud and precipitation drops aloft. J. Atmos. Sci. 33:851-864.

Blyth AM, Cooper WA, Jensen JB. 1988. A study of the source of entrained air in Montana cumuli. J. Atmos. Sci. 45:3944-3964.

Blyth AM. 1993. Entrainment in cumulus clouds. J. Appl. Meteorol. 32:626-641.

Bodenschatz E, Malinowski SP, Shaw RA, Stratmann F. 2010. Can we understand clouds without turbulence? Science 327:970-971.

Brenguier J-L, Chaumat L. 2001a. Droplet spectra broadening in cumulus clouds. Part I: broadening in adiabatic cores. J. Atmos. Sci. 58:628-641.

Celani A, Falkovich G, Mazzino A, Seminara A. 2005. Droplet condensation in turbulent flows. Europhys. Lett. 70:775-781.

Devenish BJ, Bartello P, Brenguier J-L, Collins LR, Grabowski WW, Ijzermans RHA, Malinowski SP, Reeks MW, Vassilicos JC, Wang L-P, Warhaft Z, 2010: Droplet growth in warm turbulent clouds, To be submitted to QJRMS

Falkovich G, Fouxon A, Stepanov MG. 2002. Acceleration of rain initiation by cloud turbulence. Nature 419:151-154.

Gerber H, Frick G, Malinowski SP, Brenguier J-L, Burnet F. 2005. Holes and entrainment in stratocumulus. J. Atmos. Sci. 62:443-459.

Gerber HE, Frick GM, Jensen JB, Hudson JG. 2008. Entrainment, mixing, and microphysics in trade-wind cumulus. J. Met. Soc. Japan 86A:87-106.

Grabowski WW, Clark TL. 1991.
Cloud-environment interface instability: rising thermal calculations in two spatial dimensions. J. Atmos. Sci. 48:527-546.

Grabowski WW, Clark TL. 1993a: Cloud-environment interface instability. Part II: extension to three spatial dimensions. J. Atmos. Sci. 50:555-573.

Grabowski WW, Vaillancourt P. 1999.
Comments on “Preferential concentration of cloud droplets by turbulence: effects on the early evolution of cumulus cloud dro
. J. Atmos. Sci. 56:1433-1436.

Haman KE, Malinowski SP, Kurowski MJ, Gerber H, Brenguier J-L. 2007.
Small-scale mixing processes at the top of a marine stratocumulus – a case-study. Q. J. R. Meteorol. Soc. 133:213-226.

Jaczewski A, Malinowski SP. 2005. Spatial distribution of cloud droplets in a turbulent cloud-chamber flow. Q.J.R. Meteorol. Soc. 131:2047-2062.

Jeffery CA. 2007. Inhomogeneous cloud evaporation, invariance and Damkohler number. J. Geophys. Res. 112:D24S21.

Jonas PR. 1990. Observations of cumulus cloud entrainment. Atmos. Res. 25:105-127.

Kurowski MJ, Malinowski SP, Grabowski WW. 2009.
A numerical investigation of entrain ment and transport within a stratocumulus-topped boundary layer. Q.J.R. Meteorol. Soc. 135:77-92.

Lanotte AS, Seminara A, Toschi F. 2009. Cloud droplet growth by condensation in homogeneous isotropic turbulence. J. Atmos. Sci. 66:1685-1697.

Malinowski SP, Andrejczuk M, Grabowski WW, Korczyk P, Kowalewski TA, Smolarkiewicz PK. 2008.
Laboratory and modeling studies of cloud-clear air interfacial mixing: anisotropy of small-scale turbulence due to evaporative
New J. Phys. 10:075020.

Pawlowska H, Grabowski WW, Brenguier J-L: 2006: Observations of the width of cloud droplet spectra in stratocumulus. Geophys. Res. Lett., 33, L19810

Rauber RM, and Coauthors 2007: Rain in Shallow Cumulus Over the Ocean: The RICO Campaign. Bull. Amer. Meteor. Soc., 88, 1912–1928.

Shaw RA. 2003. Particle-turbulence interactions in atmospheric clouds. Ann. Rev. Fluid.Mech. 35:183-227.

Siebert H, Lehmann K, Wendisch M. 2006.
Observations of small-scale turbulence and energy dissipation rates in the cloudy boundary layer. J. Atmos. Sci. 63:1451-1466.

Siebert H, Shaw RA, Warhaft Z. 2010.
Statistics of small-scale velocity fluctuations and internal intermittency in marine stratocumulus clouds. J. Atmos. Sci. 67:262-273.

Siebert H, S. Gerashchenko, A. Gylfason, K. Lehmann, L.R. Collins, R.A. Shaw, Z. Warhaft, 2010: Towards understanding the role of turbulence on droplets in clouds: In situ and laboratory measurements, Atmos.Res. 97- 4: 426-437.

Stevens B. 2002. Entrainment in stratocumulus-topper mixed layers. Q.J.R. Meteorol. Soc. 128:2663-2690.

Stevens B, Lenschow DH, Vali G, Gerber H, Bandy A, Blomquist B, Brenguier J-L, Bretherton CS, Burnet F, Campos T, Chai S, Faloona I, Friesen D, Haimov S, Laursen K, Lilly DK, Loehrer SM, Malinowski SP, Morley B, Petters MD, Rogers DC, Russell L, Savic-Jovcic V, Snider JR, Straub D, Szumowski MJ, Takagi H, Thornton DC, Tschudi M, Twohy C, Wetzel M, van Zanten MC. 2003. Dynamics and chemistry of marine stratocumulus – DYCOMS-II. Bull. Am. Meteorol. Soc. 84: 579–593.

Stevens B, Moeng C-H, Ackerman AS, Bretherson CS, Chlond A, de Roode S, Edwards J, Golaz J-C, Jiang H, Khairoutdinov M, Kirkpatrick MP, Lewellen DC, Lock A, Mueller F, Stevens DE, Whelan E, Zhu P. 2005. Evaluation of large-eddy simulations via observations of nocturnal marine stratocumulus. Mon. Wea. Rev. 133:1443-1462.

Stevens B, Vali G, Comstock K, Wood R, Van Zanten MC, Austin PH, Bretherton CS, Lenschow DH, 2005: Pockets of open cells and drizzle in marine stratocumulus. Bull. Amer. Meteor. Soc., 86: 51–57.

Stevens B. 2005: Atmospheric moist convection. Annu. Rev. Earth Planet. Sci. 33: 605–643

Stevens, B, Feingold, G. 2009: Untangling aerosol effects on clouds and precipitation in a buffered system, Nature, 461, no. 7264, 607-613.

Vaillancourt PA, Yau MK. 2000. Review of particle-turbulence interactions and consequences for cloud physics. Bull. Am. Meteorol. Soc. 81:285-298.

Vaillancourt PA, Yau MK, Bartello P, Grabowski WW. 2002. Microscopic approach to cloud droplet growth by condensation. Part II: turbulence, clustering and condensational growth. J. Atmos. Sci. 59:3421-3435.

Villermaux E, Bossa B, 2009: Single-drop fragmentation determines size distribution of raindrops, Narure-Physics, 5, 697 - 702

Wang L-P, Grabowski WW. 2009. The role of air turbulence in warm rain initiation. Atmos. Sci. Lett. 10:1-8.

Warhaft Z. 2009. Laboratory studies of droplets in turbulence: towards understanding the formation of clouds. Fluid Dyn. Res. 41:011201.

Warner J. 1970. On steady-state one-dimensional models of cumulus convections. J. Atmos. Sci. 27:1035-1040.

COLOR CODE: Active links Reviews papers Key field campaigns and results from in-situ measurements